The Physiology and Transport of Guanidinium (Gdm^+) and Metformin Metabolites of Bacterial Guanidinium Exporters (Gdx)

by

Rachael Marie Lucero

A dissertation submitted in partial fulfillment
of the requirements for the degree of
Doctor of Philosophy
(Chemical Biology)
in the University of Michigan
2023

Doctoral Committee:

Associate Professor Randy B. Stockbridge, Co-Chair
Professor Matthew R. Chapman, Co-Chair
Associate Professor Tobias Giessen
Associate Professor Nicole Koropatkin
Assistant Professor Jayakrishnan Nandakumar

Rachael Marie Lucero

rlucero@umich.edu

ORCID iD: 0009-0004-7933-4683

Dedication

This dissertation is dedicated to the quietest supporter of my academic journey, my cat Shadow, who has shared every late night and early morning with me during this endeavor. Your unwavering presence, gentle purring, cuddles, and soft nudges have been the moments of joy amidst the challenges. Though you are no longer here to purr by my side, the memories of our time together remain a constant source of warmth and comfort and your legacy lives on in these pages and in my heart. Although you left a few months before this doctorate journey concluded, you deserve this degree just as much as me. Here's to Shadow Marie Lucero-Burata, Ph.D.

Acknowledgements

Thank you, my advisors Randy Stockbridge and Matt Chapman, in guiding me through the past 5 years. Your insights, training, and encouragements have been instrumental in shaping this work. Additionally, thank you to my committee members for listening to my words and investing your time ensuring the quality of this research.

Of course, thank you to the previous and current members of the Stockbridge and Chapman labs for science and non-scientific conversations and coffee runs. These conversations mean a lot especially when I am trying to figure out if I am the insane one in navigating these challenging roads. Some of the friendships I have made with you will last a lifetime (special shout out to Saffron R. Little, Chia-Yu Kang, and my undergrads Kemal Demirer and Ever O'Donnell)! A special thanks to pervious and current Program in Chemical Biology PCB staff, Anna Mapp, Traci Swan, and Laura Howe for being such great people and actively listening to the students of PCB. You guys are one of the main reasons I came to Michigan. You all reminded me to believe in myself and never quit.

This work would not have been possible without the steadfast support and encouragements from my family – my emotional pillars who have always been there to celebrate my successes and help me navigate through my failures. This special thanks goes to my Mom: Suzanne Lucero, my Dad: Don Lucero, and my Grandma: Carlotta Michel. I commend you all for making the effort to understand what it is I do. Your unwavering love, support, sacrifices, and encouragement have made all the difference, especially given that we are not physically in the

same time zone. Grandma, you get extra points for learning how to use and communicate through FaceTime during the COVID-19 times; your adaptability has meant the world to me. Thank you to my previous advisor, Dr. Alberto A. Rascón, Jr., and his wife, Flor for still being there for me when times during my graduate career were challenging and uncertain. Although not blood, you guys are basically my second set of parents guiding, supporting, and motiving me. Whether family by blood or by choice, you all instilled in me the values of hard work, integrity, and compassion. Your faith in me, even when I doubted myself, has been the foundation upon which all my achievements stand. Thank you all for believing that I could become the family's first-generation college graduate, Master's degree holder, and now Ph.D. recipient.

Last but definitely not least, I have to thank my very best friend in this world, who I was lucky enough to marry, Olive E. Burata. I tell you all the time, but I really don't know how I would have been able to keep pushing through the all the challenges over the past five years without you literally by my side. You know when I need something even when I don't admit it. I must thank you a thousand times more than a normal person since you were also going through your own challenges during your own Ph.D. journey as well. When it comes down to it, it's always just you and me, and our new kitten Mochi-Benz-Marie Lucero-Burata! I really can't imagine my life without you between all our fights to all our stupid crying laughing moments. I love you and can't wait to see what our futures have in store for us!

This research was supported by National Institutes of Health (NIH)/National Institutes of General Medical Sciences (NIGMS) Diversity Supplement and Burroughs Wellcome Fund.

Table of Contents

List of Tables

List of Figures

Abstract

Membrane proteins are a crucial interface between the intracellular and extracellular environments and play a vital role in microbial pathogenesis, ranging from dental plaque buildup to complications in medical transplants. The necessity for new antimicrobial strategies to combat persistent microbial infections has never been more urgent. Microbial resistance can be often facilitated by horizontal gene transfer (HGT). Small Multidrug Resistance (SMR) transporters are frequently found in multidrug resistant gene arrays in environments such as wastewater and human-adjacent ecosystems. Recent research implicates certain SMR transporters in metabolism of the pharmaceutical metformin by bacterial consortia. These ~100 residue proteins assemble as antiparallel dimers with four transmembrane helices per monomer that are deeply embedded in the membrane. My thesis focuses on the role of these SMR transporters in evolutionary adaptation and transport of the previously overlooked metabolite, guanidinium (Gdm^+). Therefore, the work presented in each chapter and appendix, involve the study of membrane proteins to gain better insight into how bacteria adapt and evolve to selective pressures through *in vitro* and *in vivo* assays.

Recent evidence has shown that bacteria can sense Gdm^+, use it as a nitrogen source, and export it using guanidinium exporters (SMR_{Gdx}), underlining the importance of Gdm^+ homeostasis in bacterial physiology. In this thesis, I show that both genomic and plasmid-associated SMR transporters export byproducts of microbial metformin metabolism, with particularly high export efficiency for guanylurea. Biochemical, electrophysiological,

biophysical, and structural biological approaches were used to characterize the transport and binding kinetics of four representative SMR_{Gdx} homologues. A guanylurea-bound x-ray crystal structure for Gdx-Clo, a recently characterized SMR homologue, established a functional framework that will inform future mechanistic studies of this model transport protein. Our findings demonstrate how native transport physiologies are co-opted to contend with new selective pressures. This thesis also explores the biological origins and physiological impacts of Gdm^+ on bacteria, revealing that accumulation negatively affects the fitness of *E.coli* strains with a genetic deletion of the guanidinium exporters. Through competition assays between the strains, we exploited the distinct differences in phenotypes to identify metabolic pathways potentially involved in Gdm^+ production. We also investigated the impact of Gdm^+ accumulation on other cellular pathways, particularly those related to virulence, through assays involving planktonic growth, resistance, swimming, and biofilm formation. Our findings suggest a Gdm^+ link to nitrogen availability and virulence, pathways that appear to be particularly sensitive to this metabolite. The sensitivity exposes a potential vulnerability in microbes that could serve as an alternative strategy for combating antimicrobial resistance. Further research is essential to elucidate the exact mechanistic basis for Gdm^+ sensitivity.

Chapter 1 Introduction

1.1 Membrane proteins

Membrane transporters that span the outer and inner membrane are essential for microbial survival in dynamic environments. They act as gatekeepers and bridge the interior of the cell with the external environment and permit the translocation of nutrients, metabolic byproducts, and toxins across the membrane barrier all of which contributes to maintaining basic microbial signaling pathways and homeostasis (Padan, 2009). Not every biological or non-biological compound can or should move across the membrane bilayer making each membrane protein very specific to the type of cell. They can be involved in a multitude of essential functions, ranging from nutrient uptake, signal transduction, and ion channel activity, to molecule transportation (Paulsen, 2003; Peterson & Kaur, 2018). Given their vital roles, any dysfunction in these proteins can be linked to microbial pathogenesis (Bellmann-Sickert et al., 2015; Dias & Nylandsted, 2021; Ng et al., 2012). Studying inner and outer membrane proteins not only offers a deeper understanding of cell biology and the intricacies of cellular communication but also opens avenues for the development of targeted drug therapies and interventions. Delving into the mechanisms, structures, and functions of these proteins can pave the way for innovative treatments, enhancing our ability to address complex health challenges.

1.2 Membrane proteins in microbial pathogenesis

Prokaryotes use the surface of the cell for various virulence pathways. The mechanisms underlying pathogenesis are multifaceted, encompassing a range of virulence factors that enable

bacteria to colonize, invade, attach, and damage host tissues and immune responses. Ultimately, the current strategies to counter the invasive microbial behaviors, have led microbes in becoming resistant to antimicrobial agents in which membrane proteins that span either the inner or outer membrane, serve as key players (Alav et al., 2018; Fleming & Rumbaugh, 2018; Flemming et al., 2016; Gao et al., 2021; Gushchin et al., 2017; McLoon et al., 2011; Paulsen, 2003; Peterson & Kaur, 2018; Soto, 2013). For example, some membrane proteins in prokaryotes are involved in cell signaling mechanisms to establish biofilm formation by sensing external stimuli and enact genetic changes. The two-component regulatory system, is an example of microbes involving a membrane anchored histidine kinase and a response regulator to fulfill pathogenesis (Buschiazzo & Trajtenberg, 2019; Gushchin et al., 2017; Liu et al., 2015; Prindle et al., 2015). Biofilm formation is involved in human disease states ranging from dental plaque to infections from medical implants (Donlan, 2001; Lemon et al., 2008; López et al., 2009; Römling & Balsalobre, 2012). While in the lens of humans, biofilms are a big concern, but for other organisms, such as plants, biofilms are beneficial. The biofilms can provide protection from bacterial or fungal pathogens (Hassanov et al., 2018), from the secreted polysaccharides and functional amyloid fibrils on the extracellular matrix, tightly lock each cell together creating an extremely robust structure (Branda et al., 2005; Haaber et al., 2012; Lemon et al., 2008; McLoon et al., 2011; Van Gerven et al., 2018). The components that assist in complex biofilm development allows the biofilm to be resistant to antibiotics, host defenses, protease digestion and chemical denaturants while allowing biofilms to adhere to surfaces and colonization the host (Cegelski et al., 2009; Evans et al., 2015; Mulcahy et al., 2008; Zhou et al., 2012). Many of these human infections have resulted in the overuse of antibiotic drugs, leading to antibiotic resistance, which has made

it difficult to alleviate common microbial infections (Alav et al., 2018; Cegelski et al., 2009; Mulcahy et al., 2008; Römling & Balsalobre, 2012).

Another example of membrane proteins involved in microbial pathogensis is prokaryotic multidrug efflux pumps, which can be divided into five different mechanistic categories (ATP-Binding Cassette (ABC); Major Facilitator Superfamily (MFS); Resistance/Nodulation/Cell Division (RND); Multidrug and Toxic Compounds Efflux (MATE); Small Multidrug Resistance (SMR) families) (Paulsen, 2003). Multidrug efflux pumps transport a variety of substrates, including anticancer, antifungal and antibacterial drugs. By actively expelling drugs from the bacterial cell, efflux pumps decrease the intracellular concentration of the drug, often below therapeutic levels (Neyfakh, 2002). This broad specificity makes efflux pumps particularly problematic, as they can confer resistance to multiple classes of antibiotics and polyaromatic and quaternary ammonium antimicrobials, simultaneously (Nasie et al., 2012; Paulsen et al., 1996; Saleh et al., 2018; Yerushalmi et al., 1995). The presence of such pumps, combined with other resistance mechanisms, can lead to the emergence of superbugs – microbial strains resistant to most, if not all, clinically available antibiotics (Blair et al., 2014; Christaki et al., 2020; Peterson & Kaur, 2018). Thus, understanding and targeting efflux pump functions are crucial in the fight against multidrug resistance. This thesis will be, specifically, focusing on the study of Small Multidrug Resistance (SMR) family as a model system to understand efflux pump functions.

1.3 Microbial riboswitches control expression of SMR transporters

Riboswitches are found in the non-coding regions of messenger RNAs (mRNAs) that regulate gene expression in response to a specific ligand, such as metabolites or ions (Aghdam et al., 2016; Salvail & Breaker, 2023). RNA structures consist of two domains: an aptamer domain, responsible for ligand recognition, and an expression platform that mediates gene regulation.

Upon ligand binding, riboswitches undergo conformational changes that modulate transcriptional termination, translation initiation, or other downstream regulatory events to adapt to the changing environment conditions (Aghdam et al., 2016; Salvail & Breaker, 2023). There are a diverse repertoire of riboswitch classes, each responsive to distinct ligands, underscoring their significance in fine-tuning metabolic pathways and regulatory networks. Riboswitches give light to how organisms survive and adapt based on the response of the riboswitch-ligand relationship making them an important element in studying bacterial defense and evolutionary mechanisms as well as potential therapeutic targets.

In studying microbial genomes, there have been conserved RNA elements on riboswitches. One of those elements is the *ykkC-yxkD* RNA motif found broadly among bacterial and archaeal phyla (Barrick et al., 2004; Lenkeit et al., 2020; Reiss & Strobel, 2017). The genes that the riboswitch regulated were found to be involved in nitrogen metabolism and multidrug resistance efflux genes, thought to be for detoxification purposes, but the ligand was unknown (Barrick et al., 2004). It was later discovered two more motifs, mini-ykkC, found in primarily proteobacteria, and ykkC-III, almost exclusively found in actinobacteria (Sinn et al., 2021). Although not structurally similar, they regulated similar genes, therefore it was thought the motifs shared a common ligand (Weinberg et al., 2007; Weinberg et al., 2017; Weinberg et al., 2010). It wasn't until almost a decade later that guanidinium ions were discovered as the ligand, which intrigued the field as guanidine is not known to have a biological role, but rather is a metabolic byproduct (Nelson et al., 2017; Sherlock & Breaker, 2017; Sherlock et al., 2017; Sinn et al., 2021). To continue the perplexing matter, out of the thousands of compounds tested, the riboswitch only responses to guanidinium (K_d ~60μM), therefore, their names have been

adjusted to be guanidine-I, -II, -III, and IV riboswitches (Lenkeit et al., 2020; Nelson et al., 2017; Salvail et al., 2020).

The two genes most frequently regulated by all the types of guanidine riboswitches are *sugE* and *emrE* genes, which encode multidrug resistance efflux proteins of the SMR family (Kermani et al., 2018; Sinn et al., 2021). Initially, the *sugE* transporter was misannotated as a "Suppressor of GroEL" suggesting a chaperone-like molecule role (Greener et al., 1993). However, subsequent research led to a reannotation based on the substrate it was found to export. While the gene retains the *sugE* annotation, the protein is now commonly referred to as a **g**uani**d**inium e**x**porters (Gdx) as it exports guanidinium (Kermani et al., 2018). Although these exporter genes represent a significant proportion of those associated with riboswitches, another gene linked to guanidine riboswitches is that of guanidine carboxylases (Kanamori et al., 2004; Schneider et al., 2020; Sinn et al., 2021). Initially named "urea carboxylase" due to its presumed role in urea metabolism, it was subsequently discovered that this enzyme possesses a 40-fold higher catalytic efficiency with guanidinium than urea (Nelson et al., 2017). Notably, certain organisms that encode for guanidine carboxylase genes also contain genes for an ABC transporter, a class of importers (Sinn et al., 2021) (**Figure 1.1**). The distinction in proteins regulated by guanidine riboswitches suggests a mutual exclusivity: organisms possessing an exporter typically lack the associated importer or enzyme. This delineation between utilizer and exporter species demonstrates the importance of maintaining, although different, homeostasis physiology. Although clearly important, it is not clear as to the exact importance of establishing these two opposite processes and how this would be advantageous for the microbes. It is proposed the basis of the difference between exporter and utilization capabilities is centered on the level of nitrogenous environment the microbes can be found. In high nitrogenous

environments, like soil and human gut, more exporter-containing microbes would be found (Sinn et al., 2021). On the other hand, in low nitrogenous environments, like lakes, more importer-containing microbes (utilizers) would be found (Sinn et al., 2021). The riboswitch-ligand discovery along with type of gene regulation, has intriguing implications for the study of SMR proteins and how cells balance the uptake, efflux, and metabolic processing of guanidinium ions, ultimately expanding our knowledge on bacterial homeostasis and potential drug resistance mechanisms.

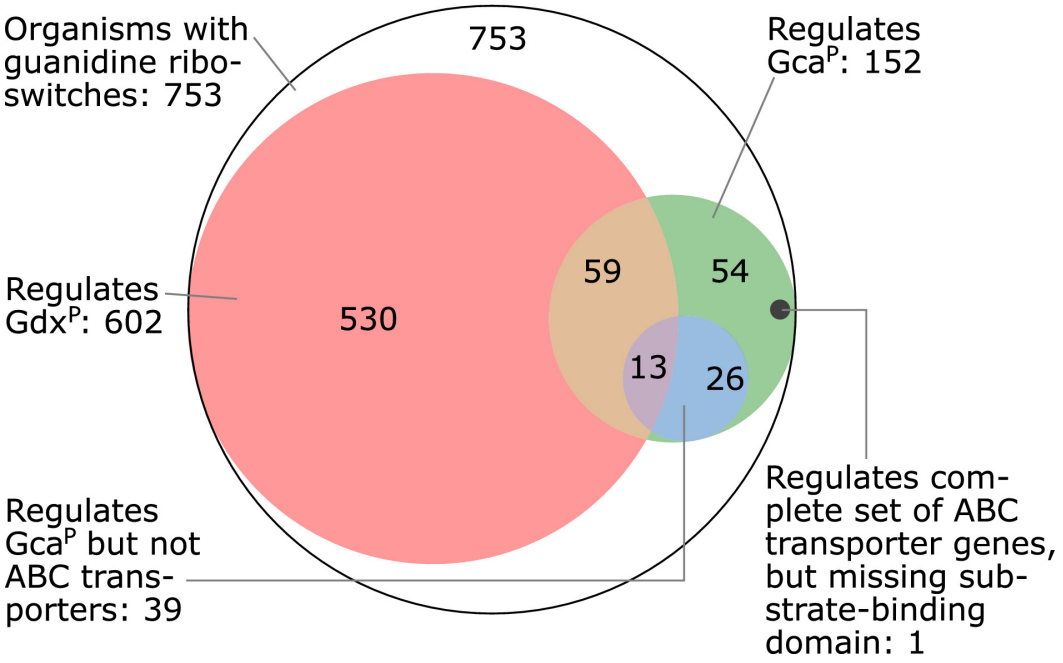

Figure 1.1 Genes regulated by the guanidine riboswitches (I, II, III, and IV) from 753 organisms. Gca^P indicates the genes part of the guanidine carboxylase metabolism pathway (152 organisms). Gdx^P indicates the genes part of the exporter of guanidine (602 organisms). Figure adapted from Sinn et al., 2021.

1.4 General properties of SMR transporters

SMRs are "nature's smallest membrane transport proteins" with ~100 residues. Proteins possess four transmembrane helices per monomer and assemble as antiparallel dimers, almost

completely embedded in the membrane (Fleishman et al., 2006; Kermani et al., 2022; Kermani et al., 2020). These transporters utilize chemical and electrical gradient of a resting cell to carry out proton-substrate antiport. Substrates from this family can range in size and hydrophobicity, but they all are positively charged (Burata et al., 2022; Kermani et al., 2020; Kermani et al., 2018) (**Figure 1.2A**). The SMRs are inserted into the membrane with dual topology, in which they can be inserted in two different ways: one with the N and C termini facing the outside of the cell and the second in which both termini are facing the inside of the cell (Rapp et al., 2006; Stockbridge et al., 2013; Ubarretxena-Belandia et al., 2003; Woodall et al., 2015) (**Figure 1.2B**). The process in which dual topology proteins are inserted into the membrane is still not clear. Previous studies indicate the subunits might be co-translationally folded and assembled (Nicolaus et al., 2021; Woodall et al., 2015). SMRs are frequently inserted into the membrane as antiparallel homodimers. Although less frequent (~30%), SMRs can form heterodimers, which shows their adaptability to form diverse low energy state topologies. SMR homodimers have been more of the focus in the field, therefore not much is known about the heterodimers (Burata et al., 2022).

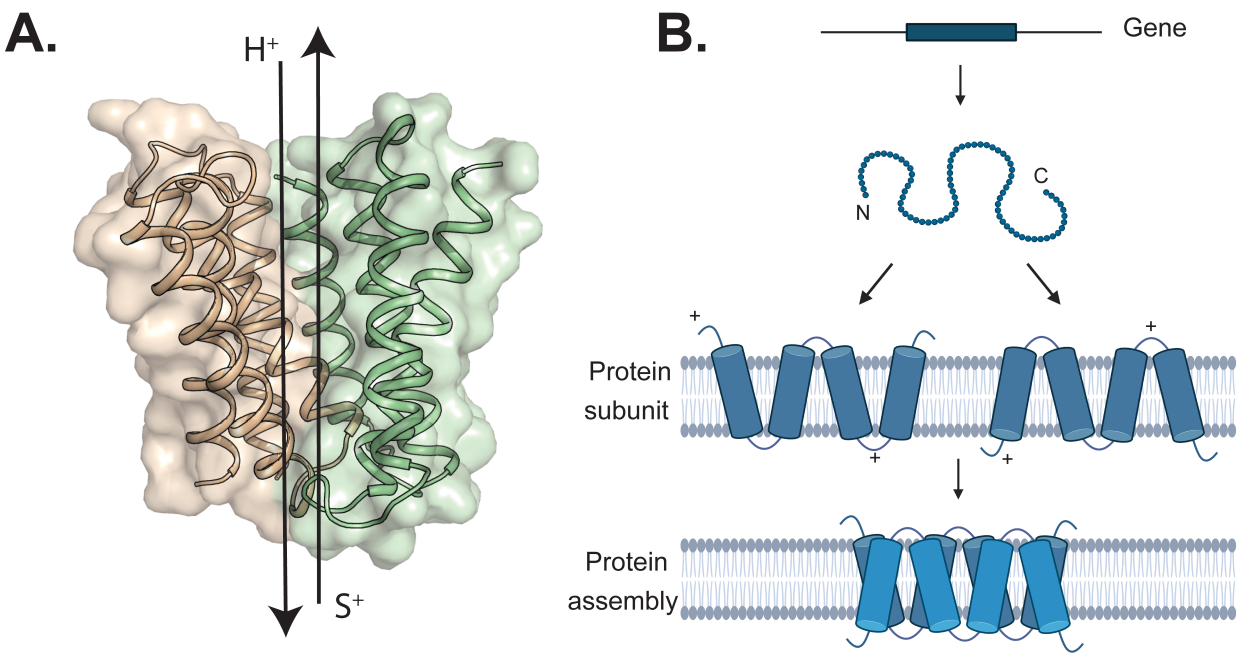

Figure 1.2 SMR transport cycle and topology. A. Gdx crystal structure (PDB: 6WK8) highlighting the antiparallel dimer (subunit A in tan and subunit B in green) structure along with arrows indicating substrate and proton antiport. B. Image made from Biorender. Assembly of dual topology by the SMR gene to protein.

Structures of representative SMRs unveiled several conserved features including central glutamates, the tyrosine switch, and the membrane portal (**Figure 1.3**). In a deep aqueous substrate binding pocket lies a critical pair of glutamate residues (position 13 shown in **Figure 1.3**) at the bottom (Kermani et al., 2022; Kermani et al., 2020). Substrate and protons compete for binding of these conserved glutamates, ensuring the alternating occupancy inherent to antiport mechanisms (Muth & Schuldiner, 2000). Structures with Gdm^+ demonstrate the coordination of the positive head group hydrogen bonding with the essential glutamates (Kermani et al., 2020). The glutamates are also in coordination with surrounding residues (W16, S42, and W62) creating a hydrogen bond network within the binding pocket that has not always been seen to be conserved within the SMR family (Burata et al., 2022; Kermani et al., 2022; Kermani et al., 2020; Saleh et al., 2018). Additionally, the tyrosines (position 59 in **Figure 1.3**) of each subunit will take turns in displacing the substrate from the glutamates in the binding

pocket during confirmational changes in which the GXG motif behaves as the fulcrum, defining the C- and N-lobes (Kermani et al., 2020; Rotem et al., 2006; Vermaas et al., 2018). Lastly, the membrane portal that is defined by transmembrane-2 helices (TM2) is a pocket that is lined with hydrophobic residues thought to allow access for hydrophobic substrates in which the aqueous environment would not be suitable otherwise (Burata et al., 2022).

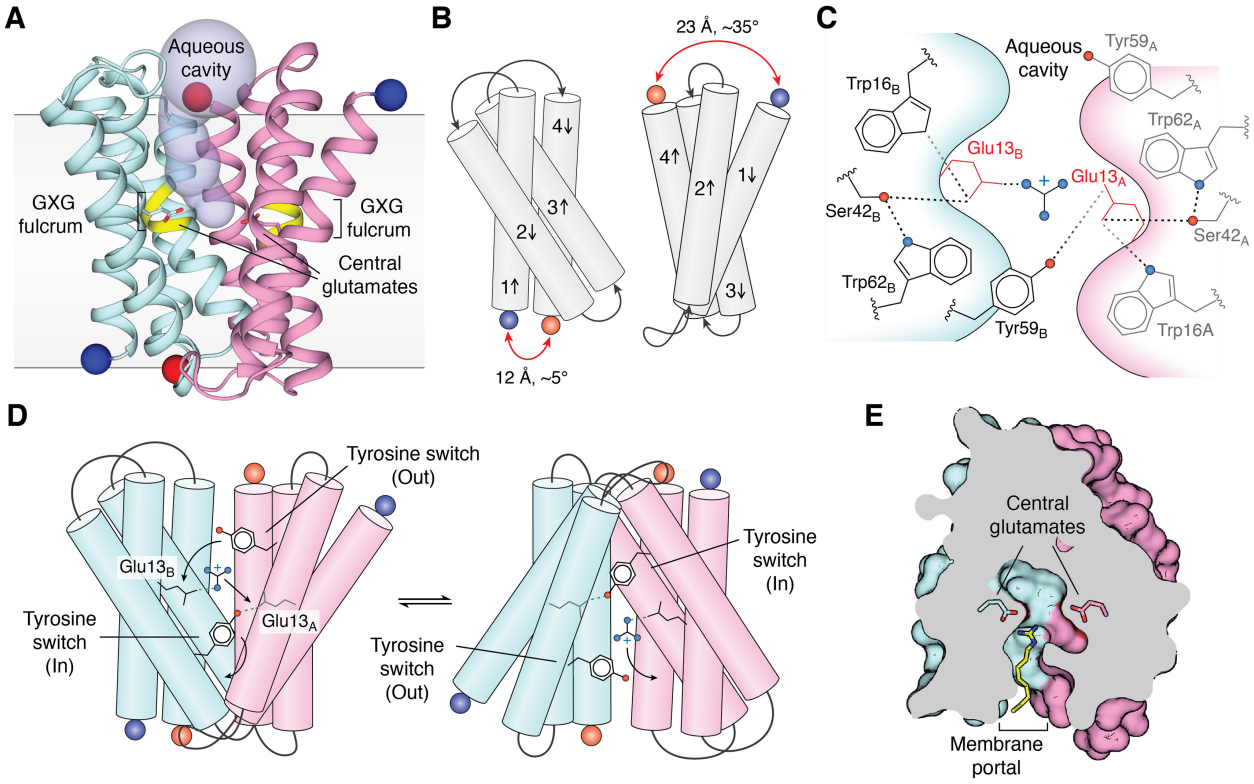

Figure 1.3 SMR structure and transport features. Figure is using a crystal structure of Gdx-Clo (PDB:6WK9) as a representative to highlight conserved mechanistic features: the central glutamates (panel A and C), the tyrosine switch (panel D), and the membrane portal (panel E). Each subunit is colored in blue and pink. Figure adapted from Burata and Yeh, 2022.

There are a total of four major functional subtypes: **G**uani**d**inium e**x**porters (SMR_{Gdx}), **Q**uaternary **a**mmonium **c**ation (SMR_{Qac}), polyamine transporters, and lipid transporters. The first two SMR subtypes, with distinct substrate specificities, are commonly associated with horizontal gene transfer (HGT) (Burata et al., 2022; Kermani et al., 2018; Slipski et al., 2020). Polyamine transporters have been identified to maintain, specifically, cellular levels of polyamine to avoid

toxicity. Additionally, the expression of this subtype has been reported to be low. Lipid transporters are the most distantly related to the rest of the SMR family and have been previously reported to act more like a glycolipid flippases (Burata et al., 2022). For these reasons, this thesis focuses only on representatives from the SMR_{Gdx} and SMR_{Qac} subtypes.

Although the clusters share high structural and sequence identities, their substrate specificities are quite different. A substrate overlap exists between the two clusters which includes small guanidinylated compounds (Kermani et al., 2020). The SMR_{Qac} proteins are promiscuous exporters of polyaromatic and quaternary ammonium antimicrobials, including common household and hospital antiseptics such as benzalkonium (Saleh et al., 2018; Yerushalmi et al., 1995). Quaternary ammonium antiseptics are one of the original modern antimicrobials, commonly used since the 1930s. The SMR_{Qacs} are perhaps the first, and remain among the most common, HGT-associated efflux pumps (Gillings et al., 2009; Zhu et al., 2017). In contrast, the rationale for widespread association between HGT elements and the SMR_{Gdx} is not as obvious. In their major physiological context, SMR_{Gdx} export the nitrogenous waste product guanidinium (Gdm^+) (Kermani et al., 2018; Nelson et al., 2017), a compound that is widespread in microbial metabolism (Breaker et al., 2017; Funck et al., 2022; Schneider et al., 2020; Sinn et al., 2021; Wang et al., 2021). The SMR_{Gdx} do not provide robust resistance to classical antimicrobials or antiseptics (Chung & Saier, 2002; Kermani et al., 2018). This begs the question as to why the SMRs, especially the SMR_{Gdx} cluster that are found so frequently on transferrable elements (Pal et al., 2015), what the fitness advantage do the exporters provide to the microbes. It should be noted that some membrane proteins, including members of the SMR family, have been found to evolve from their native function to adapt to various environmental

pressures. This has lead us to believe the rationale behind the genetic spread of SMR_{Gdx} is due to a new pressure microbes are now exposed to.

1.5 Bacterial evolution to co-opt native physiologies

In bacteria, membrane proteins are the primary defense line, being the first to interact with a vast array of chemical compounds, both native and a variety of xenobiotics, including anthropogenic chemicals (Kim et al., 2021; Paulsen, 2003; Townsend et al., 2012). Prolonged xenobiotic exposure to bacterial membrane proteins can potentially induce alterations in bacterial pathogenesis, impacting their virulence and interaction with host organisms. Within confined environments, the close proximity of different species promotes the exchange of mobile genetic elements like plasmids or transposons (Thomas & Nielsen, 2005). Consequently, advantageous genes (for the microbe) can disseminate rapidly, facilitating swift evolutionary responses (Arber, 2014; Gaze et al., 2005). A major driver behind bacterial adaptability is horizontal gene transfer (HGT) (Alav et al., 2018; Arber, 2014; Christaki et al., 2020; Nakamura et al., 2004). This non-reproductive mechanism allows bacteria to acquire and assimilate foreign genetic material, not just from other bacteria, but also from Archaea and Eukarya (Andersson, 2005; Andersson et al., 2003; Boto, 2010; Gophna et al., 2004; Guljamow et al., 2007; Rest & Mindell, 2003; Watkins & Gray, 2006). In bacteria, HGT can lead to rapid spread of multidrug resistance genes, virulence factor genes, and metabolism genes across populations. Thus, HGT is instrumental in bacterial evolution, equipping them to adapt to fluctuating conditions, resist antimicrobials, and potentially heighten their virulence (Alav et al., 2018; Arber, 2014; Kermani et al., 2018; Martinez-Vaz et al., 2022). The interplay between bacterial pathogenesis and HGT underscores the dynamic nature of bacterial evolution and its profound implications for public health. One reflection of the fitness advantage provided by these exporters is their frequent association with

HGT elements such as integron/integrase sequences and plasmids, which permit useful genes to be shared among bacterial populations. HGT-associated genes encoding drug exporters are especially common among isolates from hospitals, wastewater, agriculture, and other human-adjacent contexts (Pal et al., 2015).

Examples in which membrane transporters have deviated from their original function due to exposure to a xenobiotic are proteins from the ATP-Binding Cassette (ABC) transporters family, the Organic cation transporter (OCT) family, and the Small Multidrug Resistance (SMR) transporter family (reviewed in **Chapter 2**), all at which are suspected from their HGT-associated genes. ABC transporters in rice and various types of weeds exhibit multifunctional roles in plant biology. They function as importers, facilitating the uptake of beneficial flavonoids and anthocyanins, which play important roles in plant defense and pigmentation. Additionally, these same transporters have been observed to act as exporters, pumping out glyphosate, a widely used herbicide, contributing to the development of herbicide resistance in these plants, and posing challenges in weed management and crop protection strategies (Goldberg-Cavalleri et al., 2023; Pan et al., 2021).

Organic cation transporters (OCTs) are a group of membrane transport proteins that have long been naturally present in various organisms, including humans and other mammals, predating the discovery and use of metformin as a medication. These transporters have been extensively studied in the context of normal physiological processes, as they fulfill essential roles in transporting endogenous organic cations, such as neurotransmitters, hormones, and other small molecules, across cell membranes (Boxberger et al., 2014; Chu et al., 1999; Eisenhofer, 2001). It was discovered that OCTs have undergone evolutionary changes over time where certain members of the OCT family have adapted to handle xenobiotics, including drugs, environmental

toxins, and other foreign compounds (Suo et al., 2023). This evolutionary shift in substrate specificity has equipped OCTs to play a crucial role in the elimination of xenobiotics from cells, contributing significantly to the body's defense against harmful substances and the regulation of drug pharmacokinetics.

1.6 General outline of thesis

It may be clear, based on their known function, why some genes would appear not only on the bacterial genome, but also on transferable elements for microbial fitness advantage purposes. On the other hand, representatives of the Small Multidrug Resistance (SMR) family of proton-coupled antiporters are among the most common HGT-associated exporters (Pal et al., 2015). The rationale for widespread association between HGT elements and the SMR_{Gdx} (**g**uani**d**inium e**x**port) is not as obvious. In their major physiological context, SMR_{Gdx} export the nitrogenous waste product guanidinium (Gdm^+) (Kermani et al., 2018; Nelson et al., 2017), a compound that is widespread in microbial metabolism (Breaker et al., 2017; Funck et al., 2022; Schneider et al., 2020; Sinn et al., 2021; Wang et al., 2021). The SMR_{Gdx} do not offer substantial resistance to traditional antimicrobials or antiseptics (Chung & Saier, 2002; Kermani et al., 2018). Given their narrow substrate specificity, it's intriguing and somewhat puzzling why they are so prevalent among an array of microbes.

In chapter 2 we start to uncover evidence suggesting why we see SMR transporter genes on transferable elements in microbes by studying several SMR representatives. The first evidence of SMRs being able to interact with metformin metabolites has led to an in depth biochemical, biophysical, and structural characterization of the SMR representatives with metformin metabolites in chapter 2. In chapter 3, we pivot and tackle to determine origin of the guanidinium (Gdm^+) metabolite in bacterial cells, which has not been elucidated. It opens up the

question of how and why a cell would dedicate various molecular pathways in responding to Gdm^+, just to export the metabolite out of the cell. Additionally, we begin to investigate the cytosolic consequences when the SMR exporter is not present and how this effects virulence pathways such as, biofilm formation. Lastly, in the appendix, we investigated a different model and protein mechanism from the previous chapters. We provide very preliminary data for the investigation of histidine kinase proteins, in attempts to determine their activator ligand for their signaling cascade pathway that ultimately leads to regulation of biofilm formation genes that lead to various resistant bacterial infections. All the chapters encompass the importance of studying membrane proteins to gain better insight how bacteria adapt and evolve to selected pressures in order to revolutionize medical and environmental interventions, ensuring a healthier and more sustainable future.

1.7 References

Aghdam, E. M., Hejazi, M. S., & Barzegar, A. (2016). Riboswitches: From living biosensors to novel targets of antibiotics. *Gene*, *592*(2), 244-259. https://doi.org/10.1016/j.gene.2016.07.035

Alav, I., Sutton, J. M., & Rahman, K. M. (2018). Role of bacterial efflux pumps in biofilm formation. *J Antimicrob Chemother*, *73*(8), 2003-2020. https://doi.org/10.1093/jac/dky042

Andersson, J. O. (2005). Lateral gene transfer in eukaryotes. *Cell Mol Life Sci*, *62*(11), 1182-1197. https://doi.org/10.1007/s00018-005-4539-z

Andersson, J. O., Sjögren, A. M., Davis, L. A., Embley, T. M., & Roger, A. J. (2003). Phylogenetic analyses of diplomonad genes reveal frequent lateral gene transfers affecting eukaryotes. *Curr Biol*, *13*(2), 94-104. https://doi.org/10.1016/s0960-9822(03)00003-4

Arber, W. (2014). Horizontal Gene Transfer among Bacteria and Its Role in Biological Evolution. *Life (Basel)*, *4*(2), 217-224. https://doi.org/10.3390/life4020217

Barrick, J. E., Corbino, K. A., Winkler, W. C., Nahvi, A., Mandal, M., Collins, J., Lee, M., Roth, A., Sudarsan, N., Jona, I., Wickiser, J. K., & Breaker, R. R. (2004). New RNA motifs suggest an expanded scope for riboswitches in bacterial genetic control. *Proc Natl Acad Sci U S A*, *101*(17), 6421-6426. https://doi.org/10.1073/pnas.0308014101

Bellmann-Sickert, K., Stone, T. A., Poulsen, B. E., & Deber, C. M. (2015). Efflux by small multidrug resistance proteins is inhibited by membrane-interactive helix-stapled peptides. *J Biol Chem*, *290*(3), 1752-1759. https://doi.org/10.1074/jbc.M114.616185

Blair, J. M., Richmond, G. E., & Piddock, L. J. (2014). Multidrug efflux pumps in Gram-negative bacteria and their role in antibiotic resistance. *Future Microbiology*, *10*(9), 1165-1177.

Boto, L. (2010). Horizontal gene transfer in evolution: facts and challenges. *Proc Biol Sci*, *277*(1683), 819-827. https://doi.org/10.1098/rspb.2009.1679

Boxberger, K. H., Hagenbuch, B., & Lampe, J. N. (2014). Common drugs inhibit human organic cation transporter 1 (OCT1)-mediated neurotransmitter uptake. *Drug Metab Dispos*, *42*(6), 990-995. https://doi.org/10.1124/dmd.113.055095

Branda, S. S., Vik, S., Friedman, L., & Kolter, R. (2005). Biofilms: the matrix revisited. *Trends Microbiol*, *13*(1), 20-26. https://doi.org/10.1016/j.tim.2004.11.006

Breaker, R. R., Atilho, R. M., Malkowski, S. N., Nelson, J. W., & Sherlock, M. E. (2017). The Biology of Free Guanidine As Revealed by Riboswitches. *Biochemistry*, *56*(2), 345-347. https://doi.org/10.1021/acs.biochem.6b01269

Burata, O. E., Yeh, T. J., Macdonald, C. B., & Stockbridge, R. B. (2022). Still rocking in the structural era: A molecular overview of the small multidrug resistance (SMR) transporter family. *J Biol Chem*, *298*(10), 102482. https://doi.org/10.1016/j.jbc.2022.102482

Buschiazzo, A., & Trajtenberg, F. (2019). Two-Component Sensing and Regulation: How Do Histidine Kinases Talk with Response Regulators at the Molecular Level? *Annu Rev Microbiol*, *73*, 507-528. https://doi.org/10.1146/annurev-micro-091018-054627

Cegelski, L., Pinkner, J. S., Hammer, N. D., Cusumano, C. K., Hung, C. S., Chorell, E., Aberg, V., Walker, J. N., Seed, P. C., Almqvist, F., Chapman, M. R., & Hultgren, S. J. (2009). Small-molecule inhibitors target Escherichia coli amyloid biogenesis and biofilm formation. *Nat Chem Biol*, *5*(12), 913-919. https://doi.org/10.1038/nchembio.242

Christaki, E., Marcou, M., & Tofarides, A. (2020). Antimicrobial Resistance in Bacteria: Mechanisms, Evolution, and Persistence. *J Mol Evol*, *88*(1), 26-40. https://doi.org/10.1007/s00239-019-09914-3

Chu, C. A., Sindelar, D. K., Neal, D. W., & Cherrington, A. D. (1999). Hepatic and gut clearance of catecholamines in the conscious dog. *Metabolism*, *48*(2), 259-263. https://doi.org/10.1016/s0026-0495(99)90044-6

Chung, Y. J., & Saier, M. H., Jr. (2002). Overexpression of the Escherichia coli sugE gene confers resistance to a narrow range of quaternary ammonium compounds. *J Bacteriol*, *184*(9), 2543-2545. https://doi.org/10.1128/jb.184.9.2543-2545.2002

Dias, C., & Nylandsted, J. (2021). Plasma membrane integrity in health and disease: significance and therapeutic potential. *Cell Discov*, *7*(1), 4. https://doi.org/10.1038/s41421-020-00233-2

Donlan, R. M. (2001). Biofilm formation: a clinically relevant microbiological process. *Clin Infect Dis*, *33*(8), 1387-1392. https://doi.org/10.1086/322972

Eisenhofer, G. (2001). The role of neuronal and extraneuronal plasma membrane transporters in the inactivation of peripheral catecholamines. *Pharmacol Ther*, *91*(1), 35-62. https://doi.org/10.1016/s0163-7258(01)00144-9

Evans, M. L., Chorell, E., Taylor, J. D., Åden, J., Götheson, A., Li, F., Koch, M., Sefer, L., Matthews, S. J., Wittung-Stafshede, P., Almqvist, F., & Chapman, M. R. (2015). The bacterial curli system possesses a potent and selective inhibitor of amyloid formation. *Mol Cell*, *57*(3), 445-455. https://doi.org/10.1016/j.molcel.2014.12.025

Fleishman, S. J., Harrington, S. E., Enosh, A., Halperin, D., Tate, C. G., & Ben-Tal, N. (2006). Quasi-symmetry in the cryo-EM structure of EmrE provides the key to modeling its transmembrane domain. *J Mol Biol*, *364*(1), 54-67. https://doi.org/10.1016/j.jmb.2006.08.072

Fleming, D., & Rumbaugh, K. (2018). The Consequences of Biofilm Dispersal on the Host. *Sci Rep*, *8*(1), 10738. https://doi.org/10.1038/s41598-018-29121-2

Flemming, H.-C., Wingender, J., Szewzyk, U., Steinberg, P., Rice, S. A., & Kjelleberg, S. (2016). Biofilms: an emergent form of bacterial life. *Nature Reviews Microbiology*, *14*(9), 563-575. https://doi.org/10.1038/nrmicro.2016.94

Funck, D., Sinn, M., Fleming, J. R., Stanoppi, M., Dietrich, J., López-Igual, R., Mayans, O., & Hartig, J. S. (2022). Discovery of a Ni(2+)-dependent guanidine hydrolase in bacteria. *Nature*, *603*(7901), 515-521. https://doi.org/10.1038/s41586-022-04490-x

Gao, J., Han, Z., Li, P., Zhang, H., Du, X., & Wang, S. (2021). Outer Membrane Protein F Is Involved in Biofilm Formation, Virulence and Antibiotic Resistance in Cronobacter sakazakii. *Microorganisms*, *9*(11). https://doi.org/10.3390/microorganisms9112338

Gaze, W. H., Abdouslam, N., Hawkey, P. M., & Wellington, E. M. (2005). Incidence of class 1 integrons in a quaternary ammonium compound-polluted environment. *Antimicrob Agents Chemother*, *49*(5), 1802-1807. https://doi.org/10.1128/AAC.49.5.1802-1807.2005

Gillings, M. R., Xuejun, D., Hardwick, S. A., Holley, M. P., & Stokes, H. W. (2009). Gene cassettes encoding resistance to quaternary ammonium compounds: a role in the origin of clinical class 1 integrons? *ISME J*, *3*(2), 209-215. https://doi.org/10.1038/ismej.2008.98

Goldberg-Cavalleri, A., Onkokesung, N., Franco-Ortega, S., & Edwards, R. (2023). ABC transporters linked to multiple herbicide resistance in blackgrass (Alopecurus myosuroides). *Front Plant Sci*, *14*, 1082761. https://doi.org/10.3389/fpls.2023.1082761

Gophna, U., Charlebois, R. L., & Doolittle, W. F. (2004). Have archaeal genes contributed to bacterial virulence? *Trends Microbiol*, *12*(5), 213-219. https://doi.org/10.1016/j.tim.2004.03.002

Greener, T., Govezensky, D., & Zamir, A. (1993). A novel multicopy suppressor of a groEL mutation includes two nested open reading frames transcribed from different promoters. *Embo j*, *12*(3), 889-896. https://doi.org/10.1002/j.1460-2075.1993.tb05729.x

Guljamow, A., Jenke-Kodama, H., Saumweber, H., Quillardet, P., Frangeul, L., Castets, A. M., Bouchier, C., Tandeau de Marsac, N., & Dittmann, E. (2007). Horizontal gene transfer of two cytoskeletal elements from a eukaryote to a cyanobacterium. *Curr Biol*, *17*(17), R757-759. https://doi.org/10.1016/j.cub.2007.06.063

Gushchin, I., Melnikov, I., Polovinkin, V., Ishchenko, A., Yuzhakova, A., Buslaev, P., Bourenkov, G., Grudinin, S., Round, E., Balandin, T., Borshchevskiy, V., Willbold, D., Leonard, G., Büldt, G., Popov, A., & Gordeliy, V. (2017). Mechanism of transmembrane signaling by sensor histidine kinases. *Science*, *356*(6342). https://doi.org/10.1126/science.aah6345

Haaber, J., Cohn, M. T., Frees, D., Andersen, T. J., & Ingmer, H. (2012). Planktonic aggregates of Staphylococcus aureus protect against common antibiotics. *PLoS One*, *7*(7), e41075. https://doi.org/10.1371/journal.pone.0041075

Hassanov, T., Karunker, I., Steinberg, N., Erez, A., & Kolodkin-Gal, I. (2018). Novel antibiofilm chemotherapies target nitrogen from glutamate and glutamine. *Scientific Reports*, *8*(1), 7097. https://doi.org/10.1038/s41598-018-25401-z

Kanamori, T., Kanou, N., Atomi, H., & Imanaka, T. (2004). Enzymatic characterization of a prokaryotic urea carboxylase. *J Bacteriol*, *186*(9), 2532-2539. https://doi.org/10.1128/jb.186.9.2532-2539.2004

Kermani, A. A., Burata, O. E., Koff, B. B., Koide, A., Koide, S., & Stockbridge, R. B. (2022). Crystal structures of bacterial small multidrug resistance transporter EmrE in complex with structurally diverse substrates. *Elife*, *11*. https://doi.org/10.7554/eLife.76766

Kermani, A. A., Macdonald, C. B., Burata, O. E., Ben Koff, B., Koide, A., Denbaum, E., Koide, S., & Stockbridge, R. B. (2020). The structural basis of promiscuity in small multidrug resistance transporters. *Nat Commun*, *11*(1), 6064. https://doi.org/10.1038/s41467-020-19820-8

Kermani, A. A., Macdonald, C. B., Gundepudi, R., & Stockbridge, R. B. (2018). Guanidinium export is the primal function of SMR family transporters. *Proc Natl Acad Sci U S A*, *115*(12), 3060-3065. https://doi.org/10.1073/pnas.1719187115

Kim, J., Cater, R. J., Choy, B. C., & Mancia, F. (2021). Structural Insights into Transporter-Mediated Drug Resistance in Infectious Diseases. *J Mol Biol*, *433*(16), 167005. https://doi.org/10.1016/j.jmb.2021.167005

Lemon, K. P., Earl, A. M., Vlamakis, H. C., Aguilar, C., & Kolter, R. (2008). Biofilm development with an emphasis on Bacillus subtilis. *Curr Top Microbiol Immunol*, *322*, 1-16. https://doi.org/10.1007/978-3-540-75418-3_1

Lenkeit, F., Eckert, I., Hartig, J. S., & Weinberg, Z. (2020). Discovery and characterization of a fourth class of guanidine riboswitches. *Nucleic Acids Res*, *48*(22), 12889-12899. https://doi.org/10.1093/nar/gkaa1102

Liu, J., Prindle, A., Humphries, J., Gabalda-Sagarra, M., Asally, M., Lee, D. Y., Ly, S., Garcia-Ojalvo, J., & Süel, G. M. (2015). Metabolic co-dependence gives rise to collective

oscillations within biofilms. *Nature*, *523*(7562), 550-554. https://doi.org/10.1038/nature14660
López, D., Fischbach, M. A., Chu, F., Losick, R., & Kolter, R. (2009). Structurally diverse natural products that cause potassium leakage trigger multicellularity in Bacillus subtilis. *Proc Natl Acad Sci U S A*, *106*(1), 280-285. https://doi.org/10.1073/pnas.0810940106
Martinez-Vaz, B. M., Dodge, A. G., Lucero, R. M., Stockbridge, R. B., Robinson, A. A., Tassoulas, L. J., & Wackett, L. P. (2022). Wastewater bacteria remediating the pharmaceutical metformin: Genomes, plasmids and products. *Front Bioeng Biotechnol*, *10*, 1086261. https://doi.org/10.3389/fbioe.2022.1086261
McLoon, A. L., Kolodkin-Gal, I., Rubinstein, S. M., Kolter, R., & Losick, R. (2011). Spatial regulation of histidine kinases governing biofilm formation in Bacillus subtilis. *J Bacteriol*, *193*(3), 679-685. https://doi.org/10.1128/jb.01186-10
Mulcahy, H., Charron-Mazenod, L., & Lewenza, S. (2008). Extracellular DNA chelates cations and induces antibiotic resistance in Pseudomonas aeruginosa biofilms. *PLoS Pathog*, *4*(11), e1000213. https://doi.org/10.1371/journal.ppat.1000213
Muth, T. R., & Schuldiner, S. (2000). A membrane-embedded glutamate is required for ligand binding to the multidrug transporter EmrE. *Embo j*, *19*(2), 234-240. https://doi.org/10.1093/emboj/19.2.234
Nakamura, Y., Itoh, T., Matsuda, H., & Gojobori, T. (2004). Biased biological functions of horizontally transferred genes in prokaryotic genomes. *Nat Genet*, *36*(7), 760-766. https://doi.org/10.1038/ng1381
Nasie, I., Steiner-Mordoch, S., & Schuldiner, S. (2012). New substrates on the block: clinically relevant resistances for EmrE and homologues. *J Bacteriol*, *194*(24), 6766-6770. https://doi.org/10.1128/jb.01318-12
Nelson, J. W., Atilho, R. M., Sherlock, M. E., Stockbridge, R. B., & Breaker, R. R. (2017). Metabolism of Free Guanidine in Bacteria Is Regulated by a Widespread Riboswitch Class. *Mol Cell*, *65*(2), 220-230. https://doi.org/10.1016/j.molcel.2016.11.019
Neyfakh, A. A. (2002). Mystery of multidrug transporters: the answer can be simple. *Molecular Microbiology*, *44*(5), 1123-1130. https://doi.org/https://doi.org/10.1046/j.1365-2958.2002.02965.x
Ng, D. P., Poulsen, B. E., & Deber, C. M. (2012). Membrane protein misassembly in disease. *Biochim Biophys Acta*, *1818*(4), 1115-1122. https://doi.org/10.1016/j.bbamem.2011.07.046
Nicolaus, F., Metola, A., Mermans, D., Liljenström, A., Krč, A., Abdullahi, S. M., Zimmer, M., Miller Iii, T. F., & von Heijne, G. (2021). Residue-by-residue analysis of cotranslational membrane protein integration in vivo. *Elife*, *10*, e64302. https://doi.org/10.7554/eLife.64302
Padan, E. (2009). Bacterial Membrane Transport: Superfamilies of Transport Proteins. In *Encyclopedia of Life Sciences*. https://doi.org/https://doi.org/10.1002/9780470015902.a0003743.pub2
Pal, C., Bengtsson-Palme, J., Kristiansson, E., & Larsson, D. G. (2015). Co-occurrence of resistance genes to antibiotics, biocides and metals reveals novel insights into their co-selection potential. *BMC Genomics*, *16*, 964. https://doi.org/10.1186/s12864-015-2153-5
Pan, L., Yu, Q., Wang, J., Han, H., Mao, L., Nyporko, A., Maguza, A., Fan, L., Bai, L., & Powles, S. (2021). An ABCC-type transporter endowing glyphosate resistance in plants. *Proc Natl Acad Sci U S A*, *118*(16). https://doi.org/10.1073/pnas.2100136118

Paulsen, I. T. (2003). Multidrug efflux pumps and resistance: regulation and evolution. *Curr Opin Microbiol*, *6*(5), 446-451. https://doi.org/10.1016/j.mib.2003.08.005
Paulsen, I. T., Skurray, R. A., Tam, R., Saier, M. H., Jr., Turner, R. J., Weiner, J. H., Goldberg, E. B., & Grinius, L. L. (1996). The SMR family: a novel family of multidrug efflux proteins involved with the efflux of lipophilic drugs. *Mol Microbiol*, *19*(6), 1167-1175. https://doi.org/10.1111/j.1365-2958.1996.tb02462.x
Peterson, E., & Kaur, P. (2018). Antibiotic Resistance Mechanisms in Bacteria: Relationships Between Resistance Determinants of Antibiotic Producers, Environmental Bacteria, and Clinical Pathogens. *Front Microbiol*, *9*, 2928. https://doi.org/10.3389/fmicb.2018.02928
Prindle, A., Liu, J., Asally, M., Ly, S., Garcia-Ojalvo, J., & Süel, G. M. (2015). Ion channels enable electrical communication in bacterial communities. *Nature*, *527*(7576), 59-63. https://doi.org/10.1038/nature15709
Rapp, M., Granseth, E., Seppälä, S., & von Heijne, G. (2006). Identification and evolution of dual-topology membrane proteins. *Nat Struct Mol Biol*, *13*(2), 112-116. https://doi.org/10.1038/nsmb1057
Reiss, C. W., & Strobel, S. A. (2017). Structural basis for ligand binding to the guanidine-II riboswitch. *Rna*, *23*(9), 1338-1343. https://doi.org/10.1261/rna.061804.117
Rest, J. S., & Mindell, D. P. (2003). Retroids in archaea: phylogeny and lateral origins. *Mol Biol Evol*, *20*(7), 1134-1142. https://doi.org/10.1093/molbev/msg135
Römling, U., & Balsalobre, C. (2012). Biofilm infections, their resilience to therapy and innovative treatment strategies. *J Intern Med*, *272*(6), 541-561. https://doi.org/10.1111/joim.12004
Rotem, D., Steiner-Mordoch, S., & Schuldiner, S. (2006). Identification of Tyrosine Residues Critical for the Function of an Ion-coupled Multidrug Transporter*. *Journal of Biological Chemistry*, *281*(27), 18715-18722. https://doi.org/https://doi.org/10.1074/jbc.M602088200
Saleh, M., Bay, D. C., & Turner, R. J. (2018). Few Conserved Amino Acids in the Small Multidrug Resistance Transporter EmrE Influence Drug Polyselectivity. *Antimicrob Agents Chemother*, *62*(8). https://doi.org/10.1128/aac.00461-18
Salvail, H., Balaji, A., Yu, D., Roth, A., & Breaker, R. R. (2020). Biochemical Validation of a Fourth Guanidine Riboswitch Class in Bacteria. *Biochemistry*, *59*(49), 4654-4662. https://doi.org/10.1021/acs.biochem.0c00793
Salvail, H., & Breaker, R. R. (2023). Riboswitches. *Curr Biol*, *33*(9), R343-r348. https://doi.org/10.1016/j.cub.2023.03.069
Schneider, N. O., Tassoulas, L. J., Zeng, D., Laseke, A. J., Reiter, N. J., Wackett, L. P., & Maurice, M. S. (2020). Solving the Conundrum: Widespread Proteins Annotated for Urea Metabolism in Bacteria Are Carboxyguanidine Deiminases Mediating Nitrogen Assimilation from Guanidine. *Biochemistry*, *59*(35), 3258-3270. https://doi.org/10.1021/acs.biochem.0c00537
Sherlock, M. E., & Breaker, R. R. (2017). Biochemical Validation of a Third Guanidine Riboswitch Class in Bacteria. *Biochemistry*, *56*(2), 359-363. https://doi.org/10.1021/acs.biochem.6b01271
Sherlock, M. E., Malkowski, S. N., & Breaker, R. R. (2017). Biochemical Validation of a Second Guanidine Riboswitch Class in Bacteria. *Biochemistry*, *56*(2), 352-358. https://doi.org/10.1021/acs.biochem.6b01270

Sinn, M., Hauth, F., Lenkeit, F., Weinberg, Z., & Hartig, J. S. (2021). Widespread bacterial utilization of guanidine as nitrogen source. *Mol Microbiol*, *116*(1), 200-210. https://doi.org/10.1111/mmi.14702

Slipski, C. J., Jamieson, T. R., Zhanel, G. G., & Bay, D. C. (2020). Riboswitch-Associated Guanidinium-Selective Efflux Pumps Frequently Transmitted on Proteobacterial Plasmids Increase Escherichia coli Biofilm Tolerance to Disinfectants. *J Bacteriol*, *202*(23). https://doi.org/10.1128/JB.00104-20

Soto, S. M. (2013). Role of efflux pumps in the antibiotic resistance of bacteria embedded in a biofilm. *Virulence*, *4*(3), 223-229. https://doi.org/10.4161/viru.23724

Stockbridge, R. B., Robertson, J. L., Kolmakova-Partensky, L., & Miller, C. (2013). A family of fluoride-specific ion channels with dual-topology architecture. *Elife*, *2*, e01084. https://doi.org/10.7554/eLife.01084

Suo, Y., Wright, N. J., Guterres, H., Fedor, J. G., Butay, K. J., Borgnia, M. J., Im, W., & Lee, S. Y. (2023). Molecular basis of polyspecific drug and xenobiotic recognition by OCT1 and OCT2. *Nat Struct Mol Biol*, *30*(7), 1001-1011. https://doi.org/10.1038/s41594-023-01017-4

Thomas, C. M., & Nielsen, K. M. (2005). Mechanisms of, and barriers to, horizontal gene transfer between bacteria. *Nat Rev Microbiol*, *3*(9), 711-721. https://doi.org/10.1038/nrmicro1234

Townsend, J. P., Bøhn, T., & Nielsen, K. M. (2012). Assessing the probability of detection of horizontal gene transfer events in bacterial populations. *Front Microbiol*, *3*, 27. https://doi.org/10.3389/fmicb.2012.00027

Ubarretxena-Belandia, I., Baldwin, J. M., Schuldiner, S., & Tate, C. G. (2003). Three-dimensional structure of the bacterial multidrug transporter EmrE shows it is an asymmetric homodimer. *Embo j*, *22*(23), 6175-6181. https://doi.org/10.1093/emboj/cdg611

Van Gerven, N., Van der Verren, S. E., Reiter, D. M., & Remaut, H. (2018). The Role of Functional Amyloids in Bacterial Virulence. *J Mol Biol*, *430*(20), 3657-3684. https://doi.org/10.1016/j.jmb.2018.07.010

Vermaas, J. V., Rempe, S. B., & Tajkhorshid, E. (2018). Electrostatic lock in the transport cycle of the multidrug resistance transporter EmrE. *Proc Natl Acad Sci U S A*, *115*(32), E7502-e7511. https://doi.org/10.1073/pnas.1722399115

Wang, B., Xu, Y., Wang, X., Yuan, J. S., Johnson, C. H., Young, J. D., & Yu, J. (2021). A guanidine-degrading enzyme controls genomic stability of ethylene-producing cyanobacteria. *Nature Communications*, *12*(1), 5150. https://doi.org/10.1038/s41467-021-25369-x

Watkins, R. F., & Gray, M. W. (2006). The frequency of eubacterium-to-eukaryote lateral gene transfers shows significant cross-taxa variation within amoebozoa. *J Mol Evol*, *63*(6), 801-814. https://doi.org/10.1007/s00239-006-0031-0

Weinberg, Z., Barrick, J. E., Yao, Z., Roth, A., Kim, J. N., Gore, J., Wang, J. X., Lee, E. R., Block, K. F., Sudarsan, N., Neph, S., Tompa, M., Ruzzo, W. L., & Breaker, R. R. (2007). Identification of 22 candidate structured RNAs in bacteria using the CMfinder comparative genomics pipeline. *Nucleic Acids Res*, *35*(14), 4809-4819. https://doi.org/10.1093/nar/gkm487

Weinberg, Z., Lünse, C. E., Corbino, K. A., Ames, T. D., Nelson, J. W., Roth, A., Perkins, K. R., Sherlock, M. E., & Breaker, R. R. (2017). Detection of 224 candidate structured RNAs

by comparative analysis of specific subsets of intergenic regions. *Nucleic Acids Res*, *45*(18), 10811-10823. https://doi.org/10.1093/nar/gkx699

Weinberg, Z., Wang, J. X., Bogue, J., Yang, J., Corbino, K., Moy, R. H., & Breaker, R. R. (2010). Comparative genomics reveals 104 candidate structured RNAs from bacteria, archaea, and their metagenomes. *Genome Biol*, *11*(3), R31. https://doi.org/10.1186/gb-2010-11-3-r31

Woodall, N. B., Yin, Y., & Bowie, J. U. (2015). Dual-topology insertion of a dual-topology membrane protein. *Nature Communications*, *6*(1), 8099. https://doi.org/10.1038/ncomms9099

Yerushalmi, H., Lebendiker, M., & Schuldiner, S. (1995). EmrE, an Escherichia coli 12-kDa multidrug transporter, exchanges toxic cations and H+ and is soluble in organic solvents. *J Biol Chem*, *270*(12), 6856-6863. https://doi.org/10.1074/jbc.270.12.6856

Zhou, Y., Blanco, L. P., Smith, D. R., & Chapman, M. R. (2012). Bacterial amyloids. *Methods Mol Biol*, *849*, 303-320. https://doi.org/10.1007/978-1-61779-551-0_21

Zhu, Y. G., Zhao, Y., Li, B., Huang, C. L., Zhang, S. Y., Yu, S., Chen, Y. S., Zhang, T., Gillings, M. R., & Su, J. Q. (2017). Continental-scale pollution of estuaries with antibiotic resistance genes. *Nat Microbiol*, *2*, 16270. https://doi.org/10.1038/nmicrobiol.2016.270

Chapter 2 The Transport of Metformin Metabolites in Small Multidrug Resistance (SMR) Proteins

This chapter is adapted from the following published articles:

Martinez-Vaz, B.M., A.G. Dodge, R.M. Lucero, R.B. Stockbridge, A.A. Robinson, L.J. Tassoulas, and L.P. Wackett. 2022. Wastewater bacteria remediating the pharmaceutical metformin: genomes, plasmids, and products. Frontiers in Bioengineering and Biotechnology. 10:1086261.

Author contribution: LW and BM-V conceived and planned the experiments presented on the paper. BM-V isolated, characterized and analyzed the genome sequence of Pseudomonas mendocina MET. AD purified the GuuH enzyme, isolated the Aminobacter pure culture and carried out the growth experiments, and identification of metabolic of products by HPLC. RS and RL conceived, planned and conducted the cloning and purification of the Gdx genes and the transport experiments to study their function. AR worked on the isolation and initial characterization of Aminobacter sp. MET. LT helped with bioinformatics analyses and the GuuH protein purification.

Lucero, R.M., Demirer, K., Yeh, T.J., Stockbridge, R.B. 2023. Transport of metformin metabolites by guanidinium exporters of the small multidrug resistance family. Journal of General Physiology (Under revisions). BioRxiv doi: https://doi.org/10.1101/2023.08.10.552832

Author contribution: Rachael M. Lucero: Conceptualization, investigation, writing – original draft, visualization; Kemal Demirer: Conceptualization, investigation, validation, writing – original draft, visualization; Trevor Justin Yeh: Conceptualization, investigation, methodology, writing – review and editing, visualization; Randy B. Stockbridge: Conceptualization, investigation, writing – original draft, writing – review and editing, funding acquisition, project administration.

2.1 Abstract

Proteins from the SMR family are frequently associated with horizontally transferred multidrug resistance gene arrays found in bacteria from wastewater and the human-adjacent biosphere, and recent studies suggest that a subset of SMR transporters might participate in metabolism of the common pharmaceutical metformin by bacterial consortia. Here, we show that both genomic and plasmid-associated transporters of the SMR_{Gdx} functional subtype export byproducts of microbial metformin metabolism, with particularly high export efficiency for guanylurea. We use solid supported membrane electrophysiology to evaluate the transport kinetics for guanylurea and native substrate guanidinium by four representative SMR_{Gdx} homologues. Using an internal reference to normalize independent electrophysiology experiments, we show that transport rates are comparable for genomic and plasmid-associated SMR_{Gdx} homologues, and using a proteoliposome-based transport assay, we show that 2 proton:1 substrate transport stoichiometry is maintained. Additional characterization of guanidinium and guanylurea export properties focuses on the structurally characterized homologue, Gdx-Clo, for which we examined the pH dependence and thermodynamics of substrate binding and solved an x-ray crystal structure with guanylurea bound. Together, these experiments contribute in two main ways. First, by providing the first detailed kinetic examination of the structurally characterized SMR_{Gdx} homologue Gdx-Clo, they provide a functional framework that will inform future mechanistic studies of this model transport protein. Second, this study casts light on a potential role for SMR_{Gdx} transporters in microbial handling of metformin and its microbial metabolic byproducts, providing insight into how native transport physiologies are co-opted to contend with new selective pressures. Using biochemical, electrophysiological and structural biology techniques, we show that metformin metabolites that are ubiquitous in wastewater are

transported by SMR_{Gdx} homologues and that metformin metabolism by bacteria might rationalize the horizonal spread of SMR_{Gdx}-encoding genes among bacterial populations.

2.2 Bacterial consortia rationalizing HGT of SMR genes

2.2.1 Consequences of metformin

An emerging body of literature suggests that even pharmaceuticals that are not used explicitly as antimicrobials also shape bacterial communities in the human microbiome and other human-associated environments (Maier et al., 2018). One such pharmaceutical is the biguanide antidiabetic metformin. The most frequently prescribed drug worldwide, over 150 million patients are prescribed metformin annually to manage type II diabetes (Lunger et al., 2017). The prevalence of Type 2 diabetes has surpassed 500 million individuals globally, with the CDC highlighting a doubling of these cases over the last two decades. In addition to metformin's effective treatment on hyperglycemia, metformin has efficacy in treating obesity, polycystic ovarian syndrome, COVID-19 symptoms while also exhibiting anti-cancer properties (Bramante et al., 2021; Lv & Guo, 2020; Nasri & Rafieian-Kopaei, 2014; Sam & Ehrmann, 2017; Scheen, 2020; Top et al., 2022). The surge underscores the critical role of effective medications. Metformin is typically dosed in gram quantities daily, and is excreted in an unaltered form ultimately accumulating in wastewater sources (Corcoran & Jacobs, 2023; Gong et al., 2012) (**Figure 2.1**). The metabolic process of metformin begins with oral ingestion. Metformin can be uptaken by intestinal transporters, which in turn allows for the gut's microbiome to be exposed to the drug. Although it is not well understood, it has been observed in type 2 diabetics, their gut-microbiome composition is very different compared to those who are not taking the antidiabetic drug (Larsen et al., 2012; Wu et al., 2017; Zhang et al., 2020). Furthermore, metformin-induced changes in bacterial gene expression profiles may contribute to the development of cross-

resistance between metformin and antibiotics. Despite metformin's passage through the intestines, it remains unmetabolized and is then uptaken by hepatic cells resulting in excretion of its unaltered form through urine leading to its accumulation in the wastewater system (Balakrishnan et al., 2022; Gong et al., 2012).

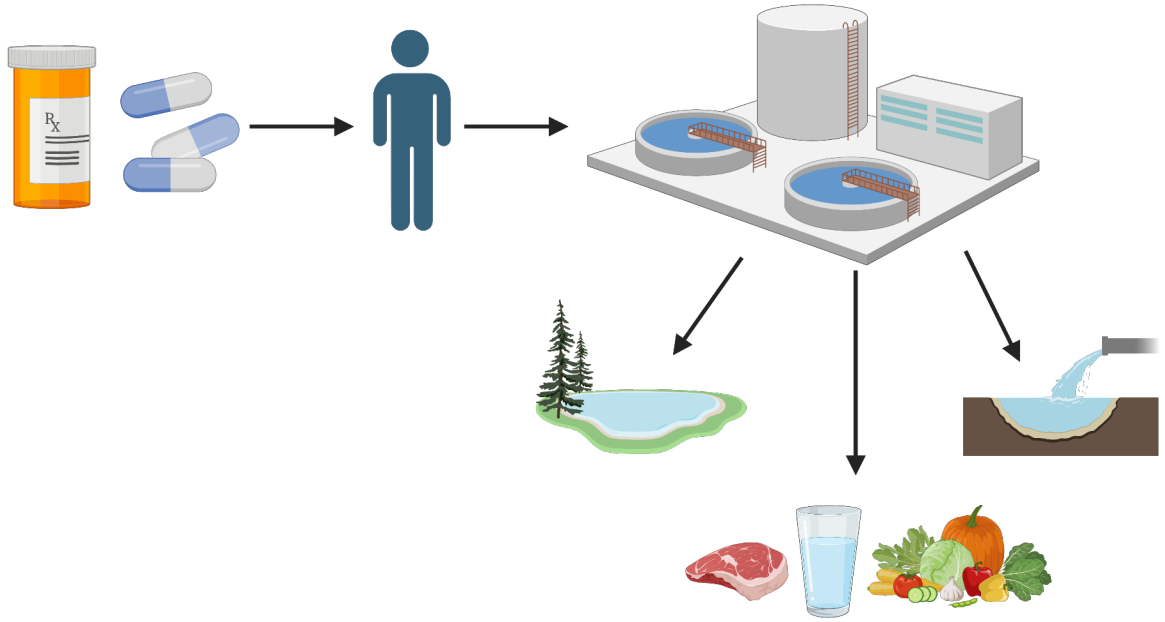

Figure 2.1 Route of metformin from the human body to water sources. Metformin is taken by humans and excreted as an unaltered form in urine. This compound cannot be fully removed from the wastewater treatment plant, ultimately contaminating water sources. Made with BioRender.

Metformin and its associated degradation product guanylurea are the most prevalent anthropogenic chemicals in wastewater globally (Balakrishnan et al., 2022; Elizalde-Velázquez & Gómez-Oliván, 2020; Scheurer et al., 2012). Concentrations of metformin and its degradation product guanylurea have been measured up to the low µM range in sampled waste and surface waters, and these compounds are not removed through typical wastewater treatment protocols (Briones et al., 2016; Golovko et al., 2021). There have been numerous efforts to address the most prevalent anthropogenic environmental pollutant with very little success. Metformin accumulation has been seen as a threat towards ecosystems, wildlife, aquatic life, plants, and humans (Balakrishnan et al., 2022; Li et al., 2023). Additionally, metformin is also associated

with changes in the composition of microbial communities including the gut microbiome (Vich Vila et al., 2020; Wu et al., 2017) and in wastewater treatment plants (Briones et al., 2016). In some cases, metformin may act as a co-selective agent, enhancing the survival of antibiotic-resistant bacteria in the presence of antibiotics (Wei et al., 2022). As a result, these compounds have accumulated to levels of environmental concern in surface water worldwide (Balakrishnan et al., 2022; Briones et al., 2016; Elizalde-Velázquez & Gómez-Oliván, 2020; Scheurer et al., 2012). The widespread presence of metformin in wastewater systems has raised concerns about its ecological consequences, particularly with respect to the wastewater microbiome.

2.2.2 SMR genes found on the same plasmid as metformin degradation genes

Recent studies have isolated bacteria that utilize metformin as a nitrogen and/or carbon source (Chaignaud et al., 2022; Li et al., 2023; Martinez-Vaz et al., 2022), suggesting that biodegradation of metformin and guanylurea may be a viable strategy for remediation of these compounds. *Aminobacter* sp. MET grew to a final OD_{600nm} of 2.3 with metformin as the sole nitrogen source and to OD_{600nm} of 2.8 with methylamine or dimethylamine as sole nitrogen after three days. There was no substantial growth ($OD_{600nm} \leq 0.2$) with 1-N- methylbiguanide, biguanide, guanylurea or guanidine supplied as the nitrogen source, even after incubation for seven days. *Aminobacter* sp. MET also grew on metformin as a sole carbon source. Metformin was shown by HPLC to be consumed and guanylurea increased concomitantly. In nitrogen deficient minimal media to which metformin was provided, *Aminobacter* sp. MET supported the growth of *Pseudomonas mendocina* GU. Previously, *Pseudomonas mendocina* GU was demonstrated to use guanylurea as a nitrogen source, but it was unable to metabolize metformin (Martinez-Vaz et al., 2022).

Studies on metformin degradation by microbial communities suggests that SMR transporters might have an emerging role in metformin biodegradation. For example, two identical, adjacent open reading frames encoding an SMR_{Gdx} protein were identified on the same plasmid as other genes that contribute to metformin degradation by a wastewater treatment plant isolate (**Figure 2.2A**). We found this protein possesses guanylurea transport activity (**Figure 2.2B**). In the physiological context, the proton gradient maintained by bacteria would favor export of guanylurea. These transport data are consistent with the HPLC determination of guanylurea produced by *Aminobacter* sp. MET that also was shown to support growth of *Pseudomonas mendocina* GU that grows on guanylurea but not metformin. Our observations here are also consistent with multiple earlier reports that metformin is metabolized to guanylurea as a "dead-end" product in some wastewater treatment systems (Trautwein et al., 2014; Trautwein & Kümmerer, 2011). In an independent study, a transcriptional analysis of a metformin-degrading *Aminobacter* strain showed a 30-fold increase in gene expression of an SMR_{Gdx} transporter in metformin-grown cells (Li et al., 2023). In contrast, the other species isolated, *Pseudomonas mendocina*, possesses genes important for metformin degradation pathways, on the chromosome and its plasmid. Notably, the plasmid houses the gene for guanylurea hydrolase, an enzyme responsible for breaking down guanylurea to guanidinium. The placement of this gene on the plasmid suggests potential adaptation advantages facilitated by HGT (Arber, 2014; Gaze et al., 2005). On the basis of these studies, pathways for the full breakdown of metformin by bacterial consortia have been proposed. In such pathways, SMR_{Gdx} transporters would provide a key step in the process, export of the intermediate guanylurea (**Figure 2.3**).

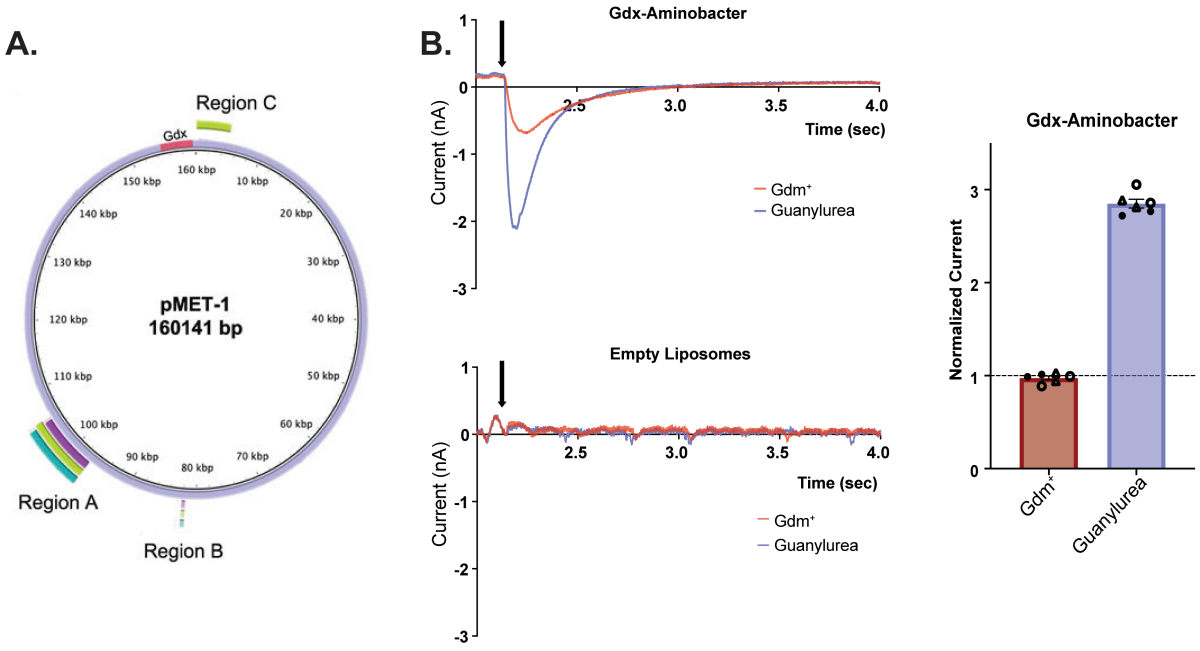

Figure 2.2 *Aminobacter* sp. MET (pMET-1) plasmid and substrate transport by Gdx. A. Segments A, B, and C represent plasmid DNA fragments containing genes shared by all metformin-degrading bacteria studied (*Aminobacter* sp MET, *Pseudomonas mendocina* MET, *Pseudomonas mendocina* GU, *Pseudomonas* sp. KHPS1, *Pseudomonas hydrolytica* KHPS2). Gdx denotes the guanylurea transporters found in Aminobacter sp.MET. B. Representative SSM electrophysiology traces for Gdx-Aminobacter (pAmi) proteoliposomes (top) and protein free liposomes (bottom) upon perfusion indicated y arrow with 2 mM Gdm^+ (red) and guanylurea (purple). Relative amplitude of Gdx-pAmi peak currents evoked by Gdm^+ and gunaylurea (right). Duplicate substrate perfusions were performed for each of three independent sensor preps (independent sensor preps represented by open circles, closed circles, and triangles). Currents were normalized against the first Gdm^+ trace collected on the same sensor. Error bars represent the mean and SEM of replicate measurements. Figure adapted from Martinez-Vaz et al., 2022.

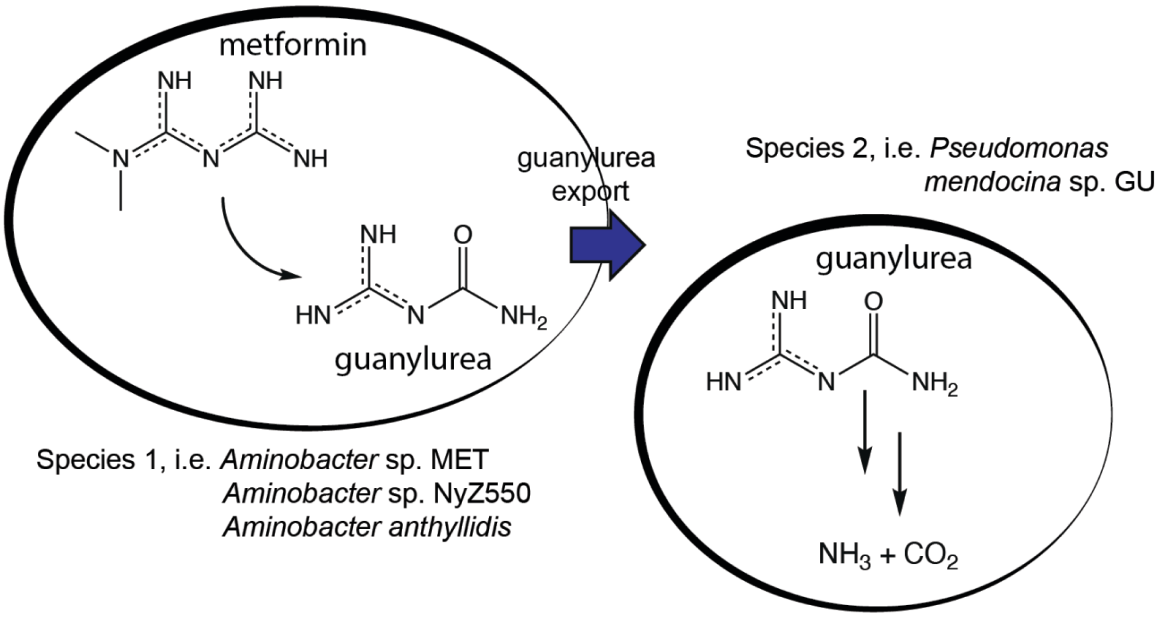

Figure 2.3 SMR_{Gdx} role in bacterial consortia. Schematic showing hypothesized role for horizontally transferred SMR_{Gdx} homologues in biodegradation of metformin by bacterial consortia. Figure adapted from (Lucero et al., 2023)

Bacterial consortia are assemblies of diverse bacterial species coexisting in a shared environment. In environments with limited nutrients, these consortia can efficiently utilize resources by exploiting complementary metabolic pathways from various bacterial members (Cao et al., 2022). Such diversity enhances resilience against environmental stresses. While one species might be vulnerable to a particular challenge, another within the consortium, may thrive, ensuring collective survival. These consortia not only foster ecological collaboration but also serve as hubs for genetic innovation through horizontal gene transfer, introducing novel functionalities that might not be achievable by a singular species. In regards to the SMR family, the clear division between utilizer and exporter species highlights the importance of distinct homeostatic and evolutionary xenobiotic physiologies. It might explain the observed specialization in species for exporting and utilizing Gdm^+ and metformin metabolites and provide insight into the prevalence of SMR_{Gdx} genes found on HGT elements.

2.2.3 Chapter outline

In this chapter we investigate whether several genomic and plasmid-associated SMRs (**Figure 2.4, Table 2.5**) transport metformin or other byproducts of microbial metformin metabolism. For our initial screen, we examined four SMR_{Gdx} homologues and two SMR_{Qac} homologues. The SMR_{Gdx} homologues we examined include 1) the structurally characterized genomic protein from *Clostridales* oral taxon 876, Gdx-Clo (Kermani et al., 2020); 2) the genomic *Escherichia coli* homologue Gdx-Eco (Kermani et al., 2018); 3) a common plasmid-borne variant isolated from multiple species of γ-Proteobacteria, Gdx-pPro (Slipski et al., 2020), which shares 81% sequence identity with Gdx-Eco; and 4) a plasmid-borne variant isolated from *Aminobacter* sp. MET, which uses metformin as a sole nitrogen source, Gdx-pAmi (Martinez-Vaz et al., 2022). We also selected two representatives of the SMR_{Qac} subtype; exemplar EmrE from *E. coli;* and QacE, the most common integron- and plasmid-associated sequence (Burata et al., 2022). We show that efficient guanylurea transport is a general property of the SMR_{Gdx} subtype, but not of SMR_{Qac}, and that other metformin degradation products are also transported by SMR_{Gdx}. We characterize the transport kinetics and proton-coupling stoichiometry of a representative plasmid-borne and genomic SMR_{Gdx}, and determine a structure of a representative SMR_{Gdx} with guanylurea bound. This work provides a case study into bacterial co-option of existing metabolic transporters to deal with novel xenobiotics. Furthermore, this study provides foundational biochemical characterization of the SMR_{Gdx} subtype, which will support future efforts to understand detailed molecular mechanisms of substrate transport by this family of proteins.

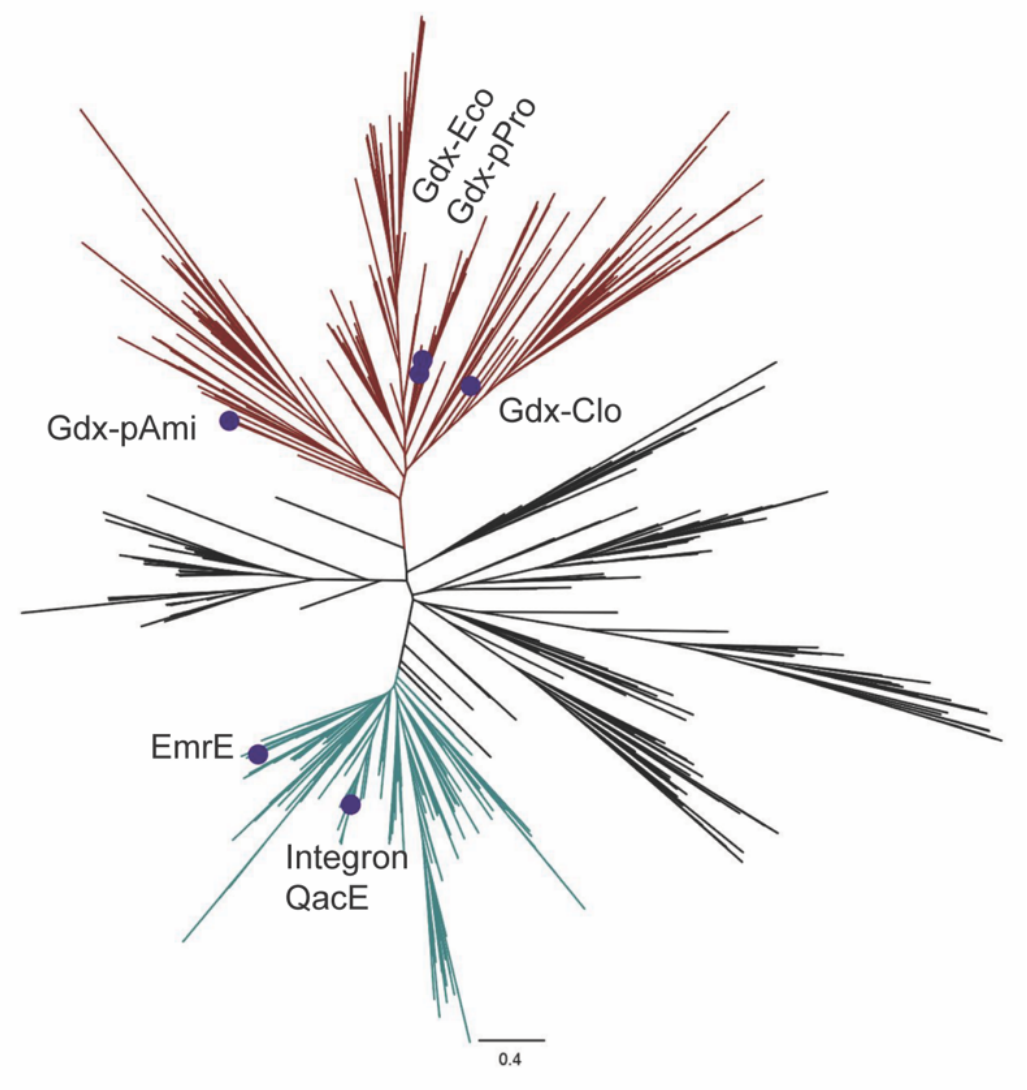

Figure 2.4 Phylogenetic distribution of SMR representatives. Phylogeny of the SMR family. SMR_{Gdx} are shown in rust and SMR_{Qac} in teal. Proteins examined in this chapter are indicated. Figure adapted from Lucero 2023

2.3 Results

2.3.1 Guanylurea transport is general among SMR_{Gdx} homologues

We first sought to determine whether transport of guanylurea is widespread among SMR homologues, and whether other metformin metabolites might also be exported by transporters from this family. We selected several SMRs that could be purified with monodispersed size exclusion chromatograms (**Figure 2.14**), including both genomic and plasmid- associated

SMR_{Qac} and SMR_{Gdx} representatives (see **Figure 2.4)**. We screened a series of metformin metabolites for transport using solid-supported membrane (SSM) electrophysiology (**Figure 2.5**). For these experiments, purified proteins are reconstituted into proteoliposomes, which are then capacitively coupled to an electrode to monitor charge movement across the liposome membrane (Bazzone et al., 2023). Because of their antiparallel topology, homodimeric SMR transporters possess two-fold symmetry with identical inward- and outward-facing structures (Morrison et al., 2012) thus, in contrast to most transporters, orienting the proteins in the reconstituted liposome system is not necessary. All compounds were tested for transport at 2 mM, and for each substrate, we confirmed that protein-free liposomes did not exhibit pronounced currents (**Figure 2.6**). Since the efficiency of proteoliposome fusion to the sensors is variable, we included a positive control compound to benchmark the currents for test substrates evaluated on the same sensor: Gdm^+ for SMR_{Gdx} proteins, and tetrapropylammonium (TPA^+) for SMR_{Qac} proteins. For all SMR_{Gdx} homologs, we observed negative capacitive currents for both Gdm^+ and guanylurea, consistent with electrogenic proton-coupled substrate antiport (**Figure 2.6**). The best characterized SMR_{Gdx} homologue, Gdx-Clo, transported only Gdm^+ and guanylurea. However, the other three SMR_{Gdx} homologues tested also transported singly-substituted biguanides, including the metformin degradation product methylbiguanide and the related antidiabetic drug buformin. Metformin, a doubly-substituted biguanide, exhibited currents barely above the detectable limit by SMR_{Gdx} proteins. These observations are congruent with prior observations that guanidinium ions with single hydrophobic substitutions are transported by SMR_{Gdx}, but that doubly-substituted guanidiniums are not (Kermani and MacDonald et al., 2020). The SMR_{Qacs} examined, EmrE and integron-associated QacE, did not exhibit transport currents for this series of compounds.

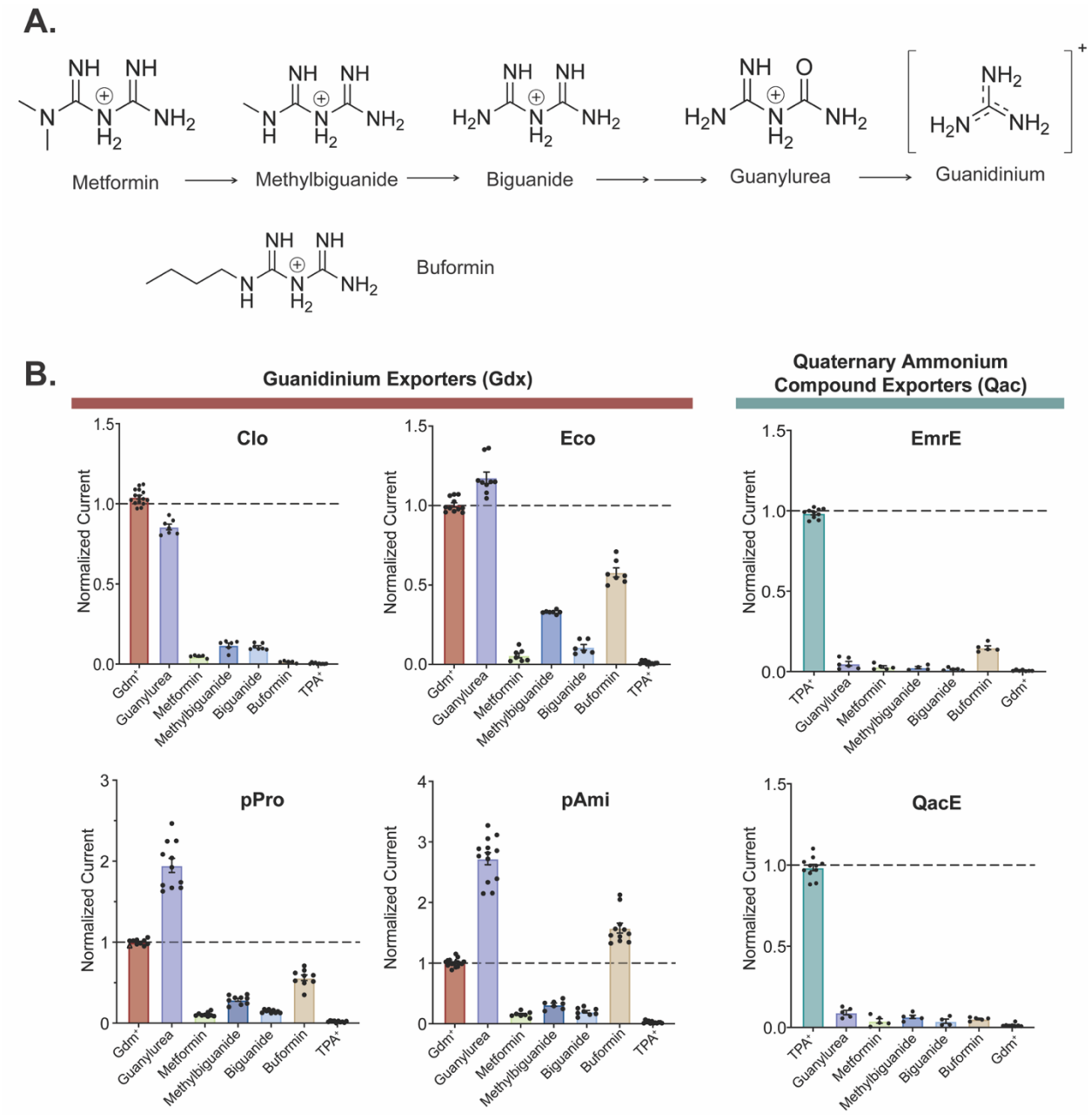

Figure 2.5 Screen for transport of metformin metabolites by SMR homologues. A. Chemical structures of metformin metabolites and metformin analog buformin. B. Amplitude of transport current evoked by perfusion with 2 mM substrate. Current amplitudes are normalized to a positive control (Gdm^+ for SMR_{Gdx} and TPA^+ for SMR_{Qac}) collected on the same sensor. Datapoints represent at least three independent sensor preparations from at least two independent biochemical purifications. Figure adapted from Lucero et al., 2023.

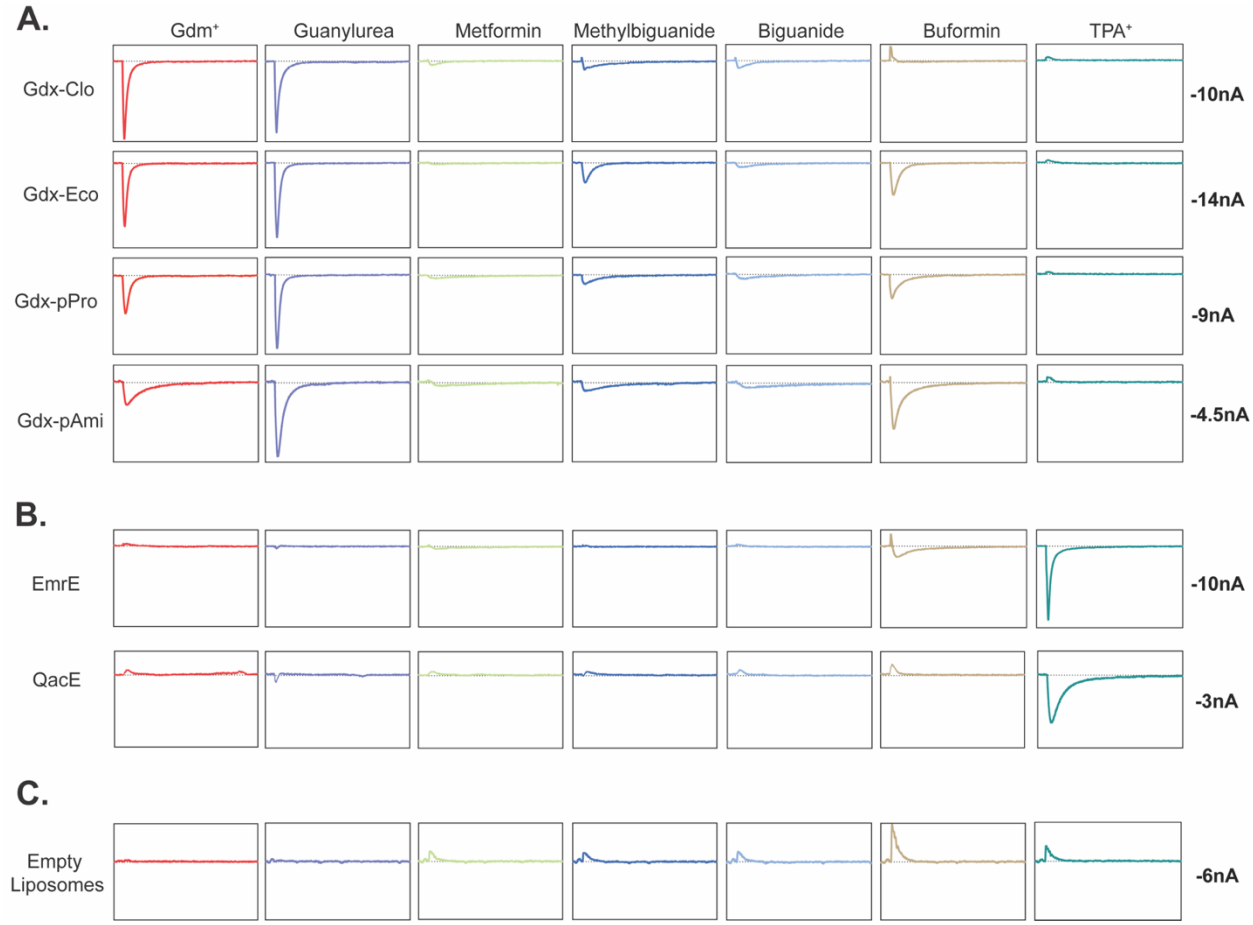

Figure 2.6 Representative current traces for substrates and transporters summarized in **Figure 2.4**, and no-protein controls. Traces for a substrate series are from the same sensor. Box height is equal to current values shown at the right. Figure adapted from Lucero et al., 2023.

2.3.2 Kinetics and proton coupling for Gdm^+ and guanylurea transport

To compare the kinetic properties for transport of guanylurea and the physiological substrate Gdm^+, we measured the peak amplitudes of the capacitive currents for the four SMR_{Gdx} homologues as a function of substrate concentration. The current amplitudes reflect the initial rate of transport (Bazzone et al., 2017), and their concentration dependence follows Michaelis-Menten kinetics (**Figure 2.7, Table 2.1**). For all four homologues, the K_m value for guanylurea was ~2-fold lower than that of Gdm^+. However, the absolute K_m values varied over a factor of

~50 among these proteins. The genomic Gdx-Clo exhibited the lowest K_m values (500 µM for Gdm^+ and 220 µM for guanylurea), and the plasmid-associated Gdx-pAmi exhibited the highest K_m values (16 mM for Gdm^+ and 5 mM for guanylurea). We verified that protein-free liposomes did not exhibit currents at all substrate concentrations tested (**Figure 2.15**).

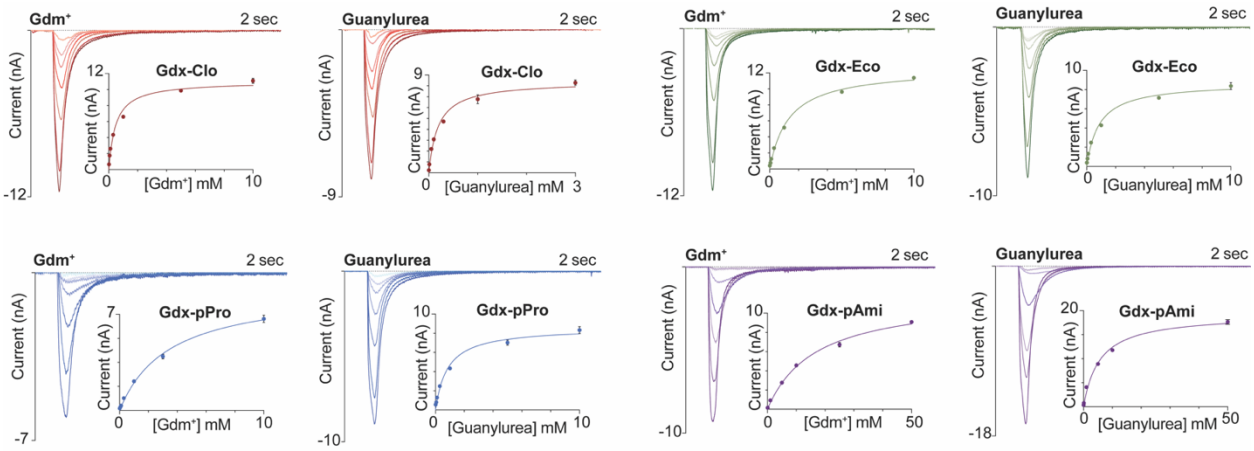

Figure 2.7 Maximal current amplitudes as a function of Gdm^+ or guanylurea concentration. Representative transport currents for concentration series of the indicated substrates. Inset: maximum current amplitude as a function of substrate concentration. Solid line represents a fit to the Michaelis-Menten equation. Each of these representative plots was obtained on a single sensor, and error bars represent the SEM for triplicate measurements on that single sensor. K_m values reported in **Table 2.1** represent averages from at least three independent sensor prepared from 2-3 independent protein preparations. Figures adapted from Lucero et al., 2023.

Table 2.1 K_m values determined using SSM electrophysiology at pH 7.5. Table adapted from Lucero et al., 2023.

	Gdm^+ (mM)	**Guanylurea (mM)**
Gdx-Clo	0.5 ± 0.1	0.22 ± 0.06
Gdx-Eco	1.7 ± 0.5	0.85 ± 0.1
Gdx-pPro	2.9 ± 0.5	0.9 ± 0.2
Gdx-pAmi	15.7 ± 3.3	5.2 ± 2.0

Our experiments thus far do not allow comparison of transport rates among SMR homologues. As with other measurements that rely on liposome fusion to a lipid bilayer (Stockbridge & Tsai, 2015), the absorption of proteoliposomes to the sensor is subject to considerable variability from experiment to experiment, so that current measurements from different sensors cannot be quantitatively compared (Barthmes et al., 2016). Fusion efficiency

can vary from day-to-day, by experimenter, or by sensor batch. In order to normalize maximal currents obtained on different sensors, and thus evaluate differences in transport rate among different proteins (or different mutants of the same protein), we co-reconstituted each SMR_{Gdx} homologue with an internal reference, the fluoride channel Fluc-Bpe (Stockbridge et al., 2013; Stockbridge & Tsai, 2015), so that both the test protein and the reference protein would be absorbed to the sensor in a prescribed molar ratio **(Figure 2.8A)**. We selected Fluc-Bpe as an internal reference because its extremely high selectivity for fluoride (McIlwain, Gundepudi, et al., 2021) prevents cross-reactivity with other substrates or common buffer components. Moreover, its fast fluoride permeation rate and channel mechanism (McIlwain, Ruprecht, & Stockbridge, 2021) yield high sensitivity with small amounts of protein and low concentrations of fluoride. Control experiments with individually reconstituted Fluc-Bpe and SMR_{Gdx} confirm that the SMR_{Gdx} substrates guanidinium and guanylurea do not elicit a response from Fluc-Bpe, and that the SMR_{Gdx} are similarly insensitive to fluoride perfusion (**Figure 2.8B, Figure 2.16**). By normalizing with respect to the peak fluoride current amplitudes, we obtain good sensor-to-sensor reproducibility (**Figure 2.8C**). At high protein concentrations or ion fluxes, the maximal currents can be limited by a number of factors such as internal volume, membrane potential, or membrane crowding. However, at the low protein concentrations used in these experiments (2.5 μg Gdx-Clo and 1 μg Fluc-Bpe per mg lipid), the normalized current amplitudes are reasonably linear with respect to the SMR_{Gdx} concentration (**Figure 2.8D**), indicating that in the concentration regime of these experiments, using Fluc-Bpe as a reference provides a linear readout of transport velocity (**Figure 2.8D**).

To assess the relative maximal transport velocities of the four SMR_{Gdx} homologues, we evaluated the maximal (initial rate) capacitive currents upon perfusion with substrate at a

concentration 5-fold higher than the K_m values reported in **Figure 2.7**. Using peak fluoride current amplitudes as an internal reference, these experiments show that the transport rates are comparable (within a factor of 3) among the four SMR_{Gdx}. For Gdx-Clo, Gdx-Eco, and Gdx-pPro, the maximal velocity for Gdm^+ is ~2-fold higher than for guanylurea, whereas for Gdx-pAmi, the turnover rates of guanylurea and Gdm^+ are comparable (**Figure 2.8E**).

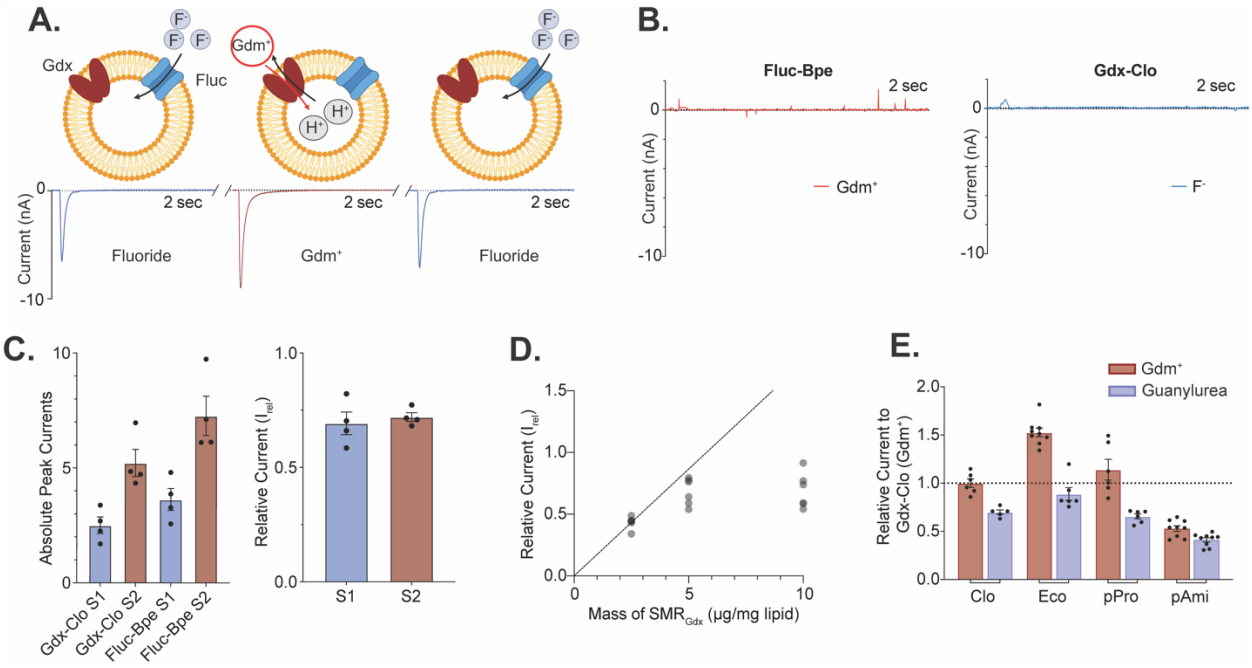

Figure 2.8 Comparison of maximal velocities for different SMR homologues using an internal reference. A. Schematic showing experimental strategy of co-reconstitution of target transporter and fluoride channel Fluc-Bpe with alternating substrate perfusions. Cartoon made using Biorender. B. Current traces for Gdx-Clo and Fluc-Bpe reconstituted individually do not show substrate cross-reactivity. Tests for cross-reactivity by guanylurea and other SMR_{Gdx} homologues are shown in **Figure 2.16**. Left, peak current amplitude for Gdm^+ and fluoride currents for two examples of independent sensor preparations. Right, relative Gdm^+/fluoride current (I_{rel}) for the sensors shown in the left panel. Error bars represent the SEM of individual replicates shown as points in D. I_{rel} as a function of increasing SMR_{Gdx} (Bpe-Fluc held constant at 1 µg/ml lipid). The dashed line represents expected peak current amplitude for a linear response. E. Currents for Gdm^+ and gunaylurea transport by four SMR_{Gdx} homologues normalized against internal Fluc-Bpe reference currents. Each substrate was perfused at a concentration of five-fold higher than the K_d values measured in **Figure 2.7** in order to compare maximal turnover velocities among the different transporters. Error bars represent the SEM of individual replicates shown as points. Figure adapted from Lucero et al., 2023

The negative capacitive currents observed in the SSM electrophysiology experiments presented thus far are in accord with electrogenic transport of >1 H^+ per substrate, but they do

not reveal the precise transport stoichiometry. Prior studies have shown Gdx-Eco possesses a well-coupled 2 H^+: 1 Gdm^+ stoichiometry (Kermani et al., 2018; Thomas et al., 2021). However, for SMR_{Qac} EmrE, it has been reported that the transport stoichiometry differs among transported substrates (Robinson et al., 2017). We therefore employed a proteoliposome assay to experimentally assess coupling stoichiometry of Gdx-Clo and plasmid-associated Gdx-pAmi. In these experiments, a 10-fold Gdm^+ or guanylurea concentration gradient is applied, and the direction of substrate movement is monitored as a function of membrane potential (Fitzgerald et al., 2017; Kermani et al., 2018). When no voltage is applied, substrate is transported down its chemical gradient, coupled to proton efflux. Application of increasingly negative membrane potentials thermodynamically pushes back against the 10-fold substrate gradient; the electrochemical equilibrium point at which no substrate movement occurs is the reversal potential, from which the transport stoichiometry can be calculated using Eq. 2.2.

In our setup, the membrane potential is established using a potassium gradient and the potassium ionophore valinomycin, and substrate-coupled proton movement is monitored using pyranine, a pH sensitive fluorescent dye, encapsulated inside the liposomes. For coupled 2 H^+ to 1 substrate transport, electrochemical equilibrium is expected at -60 mV under a 10-fold substrate concentration gradient. We confirmed this value for Gdm^+ transport by Gdx-Clo (**Figure 2.9A**), and our experiments show that guanylurea export is carried out with the same stoichiometry by both Gdx-Clo and Gdx-pAmi (**Figure 2.9B, C**).

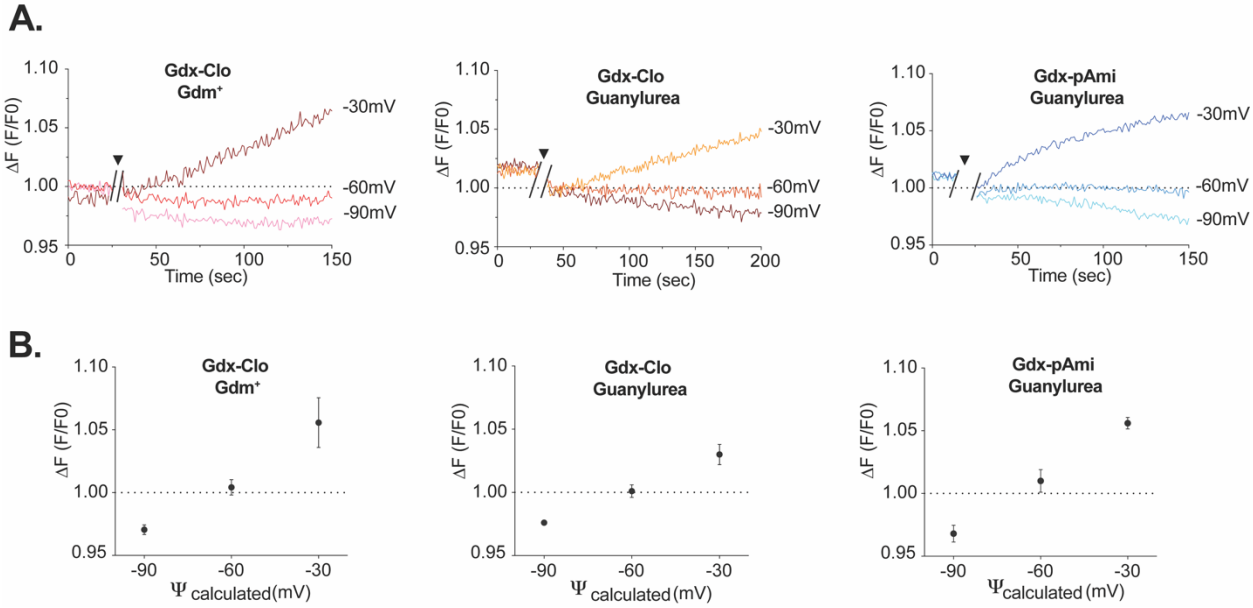

Figure 2.9 Proton coupling stoichiometry for substrate transport by Gdx-Clo and Gdx-pAmi. A. Change in pyranine fluorescence over time for substrate transport at applied membrane potentials of -30, -60, and -90 mV. After ~20 seconds of baseline collection, external substrate was added together with valinomycin to establish the 10-fold substrate gradient and membrane potential (indicated by break in trace and triangle). B. Change in pyranine fluorescence as a function of membrane potential for replicate experiments. Error bars represent the SEM for three replicates (-90 and -30 mV) or four replicates (-60 mV). The dashed line represents the equilibrium condition where no proton transport occurs. Figure adapted from Lucero et al., 2023

2.3.3 Gdm^+ and guanylurea binding in Gdx-Clo

To further characterize the pH dependence and thermodynamic properties of Gdm^+ and guanylurea binding by SMR_{Gdx}, we selected the homologue with the best biochemical stability, Gdx-Clo. Although we initially sought to examine substrate binding by Gdx-pAmi as well, the protein requires high salt concentrations for purification and, in detergent, was prone to aggregate over long titrations or at more physiological salt concentrations.

We first exploited intrinsic changes in tryptophan fluorescence to monitor substrate binding at pH values between pH 6 and pH 9 (**Figure 2.10A**). Gdm^+ titration induces an increase in tryptophan fluorescence that can be fit with a single site binding isotherm described by Eq. 2.3 (**Figure 2.11**); separate control experiments showed that binding kinetics are fast and the binding

reaction achieved equilibrium prior to measurement. As expected for a model where protons and Gdm^+ compete for binding to the central glutamates, the apparent binding affinity increases with pH as the central glutamates become increasingly deprotonated (**Table 2.2, Figure 2.10B**). Although careful NMR experiments with SMR homologue EmrE have shown that the pKa values of the two central glutamates differ (Li et al., 2021; Morrison et al., 2015), the current binding assays do not have the resolution to distinguish independent K_a values and report on the averaged behavior of the binding site residues. Using the approximation that the glutamates have equal K_a values, the relationship between apparent K_d and pH can be fit using Eq. 2.5, yielding an average pKa for the glutamates of 6.7 and a K_d for Gdm^+ of 600 μM.

Analogous binding experiments were also performed for guanylurea (**Figure 2.10**, lower panels). In contrast to the tryptophan fluorescence trend observed for Gdm^+ binding, titration with guanylurea quenched the tryptophan fluorescence signal. Binding data also suggested there was also a low affinity, non-specific component to substrate binding, which became more apparent at high guanylurea concentrations. Fitting the data to a binding model with a linear non-specific component (Eq. 2.4) yields apparent K_d values of the same order as the K_m value determined previously. A fit to Eq. 2.5 indicates that the pKa value of the glutamates is 6.9, in reassuring agreement with the pKa determined in the Gdm^+ binding experiment, and yields a guanylurea K_d of 70 μM. For both substrates, the K_d values are similar to the transport K_m values, suggesting that the kinetics of substrate binding are fast relative to the conformational change during substrate transport.

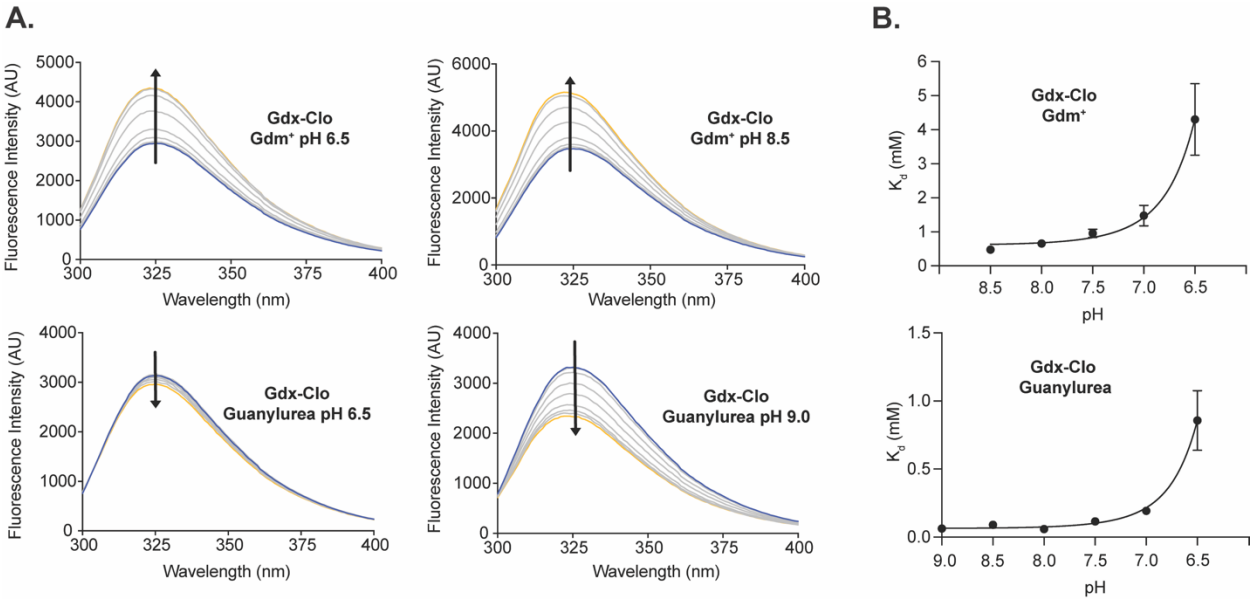

Figure 2.10 pH dependence of equilibrium substrate binding for Gdx-Clo. A. tryptophan fluorescence spectra measured at increasing concentrations of Gdm^+ (top panels) or guanylurea (lower panels) at representative low and high pH values. Arrows denote direction of change in fluorescence intensity with increasing substrate concentration. B. Plot of apparent K_d values measure for Gdm^+ (top) or guanylurea (bottom) as a function of pH. Apparent K_d values were determined by fitting tryptophan fluorescence titration isotherms. Fluorescence spectra and fits for all pH values are shown in **Figure 2.11**. The solid lines represent fits to Equation 2.5, with a K_d value of 600 µM and a pK_a of 6.7 for Gdm^+ titrations, and a K_d value of 70 µM and a pK_a of 6.9 for the guanylurea titrations. Error bars represent the SEM of values from 3-4 independent titrations from two independent protein preps. Figure adapted from Lucero et al., 2023

Table 2.2 K_d values measured using tryptophan fluorescence titrations as a function of pH. Table adapted from Lucero et al., 2023.

pH	**Gdm^+ (mM)** ±SEM	**Guanylurea (mM)** ±SEM
6.5	4.3 ± 1.0	0.86 ± 0.22
7.0	1.5 ± 0.3	0.19 ± 0.02
7.5	0.96 ± 0.12	0.12 ± 0.02
8.0	0.66 ± 0.08	0.059 ± 0.001
8.5	0.48 ± 0.10	0.091 ± 0.016
9.0	Not determined	0.063 ± 0.005

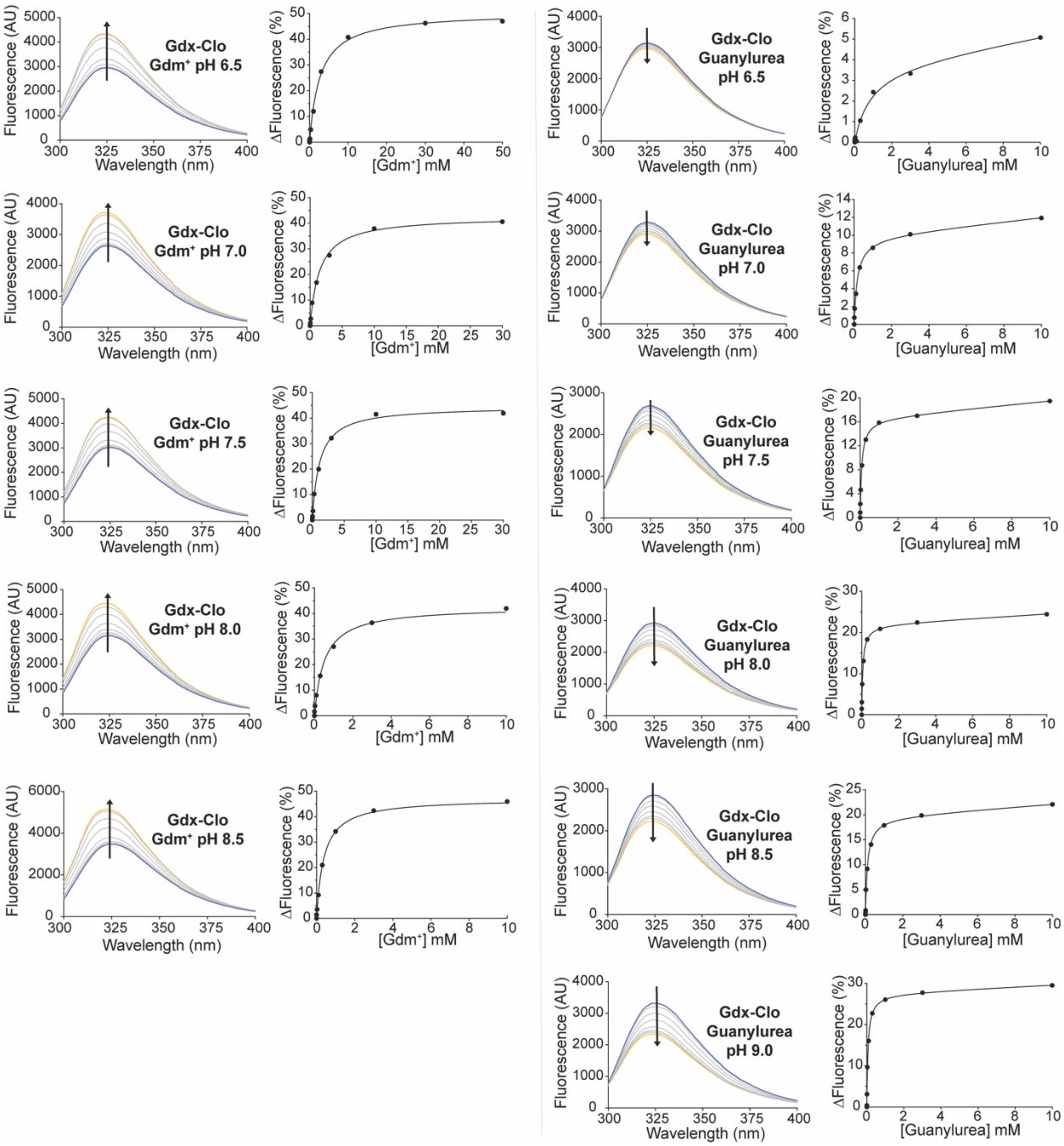

Figure 2.11 Tryptophan fluorescence spectra and fits to binding isotherms for all data reported in **Figure 2.10** and **Table 2.2**. Figure adapted from Lucero et al., 2023.

Because tryptophan fluorescence is an indirect measurement of binding (made additionally mysterious by the opposite effects of Gdm^+ and guanylurea on the fluorescence intensity), and to gain additional information on the thermodynamics of substrate binding, we

also sought to reproduce our binding measurements using isothermal titration calorimetry (ITC). At pH 8.5, where proton binding to the glutamates is minimized, we observed an exothermic binding reaction for both Gdm^+ and guanylurea. Gdm^+ binds with the expected stoichiometry of 1 substrate per protein dimer (**Figure 2.12 left, Table 2.3**). For guanylurea, we also observed a weak endothermic reaction after saturation of the first high-affinity binding site (**Figure 2.12 right**). We did not observe this endothermic contribution in control titrations into buffer, suggesting that it is protein-dependent. We assume that the endothermic reaction represents the non-specific binding observed at high guanylurea concentrations in our tryptophan fluorescence titrations. Subtraction of this component, and setting the binding stoichiometry to one substrate per dimer, yields a fittable binding isotherm. For both substrates, the K_d value measured using ITC was in good agreement with the K_d value obtained using tryptophan fluorescence, validating the tryptophan fluorescence approach to monitor substrate binding. The ~4-fold increase in affinity for guanylurea relative to Gdm^+ was due to increased entropy of the binding reaction. Thermodynamic parameters derived from the ITC data are reported in **Table 2.3**.

Table 2.3 Equilibrium binding parameters derived from isothermal titration calorimetry. Table adapted from Lucero et al., 2023.

	Gdm^+	**Guanylurea**
K_d	490 μM	230 μM
ΔG	-4.5	-5.0
ΔH	-3.4	-3.4
TΔS	1.1	1.6
n	0.49 (from fit)	0.5 (fixed)

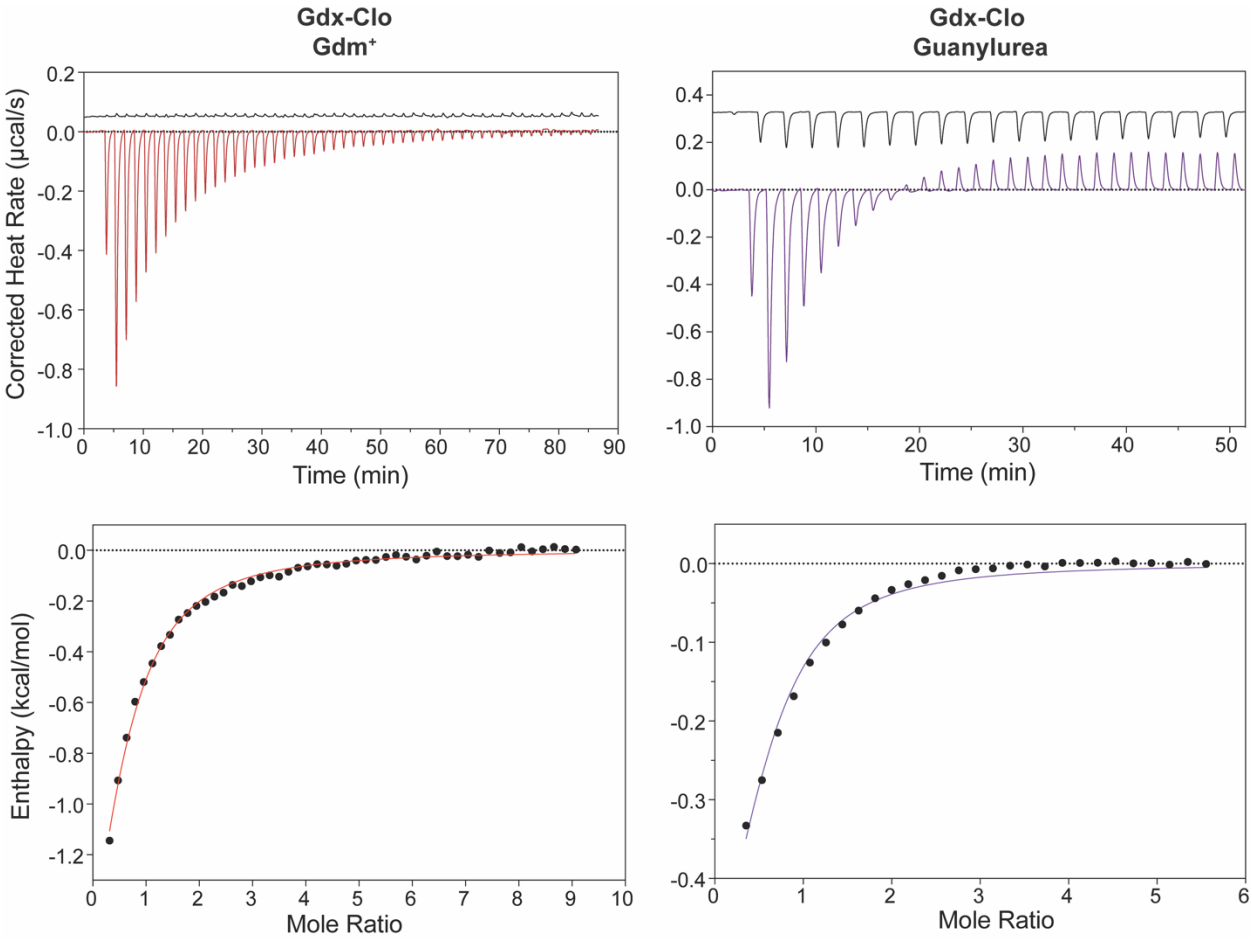

Figure 2.12 Isothermal titration calorimetry of Gdm^+ and guanylurea binding to Gdx-Clo. Top panels: Thermograms for Gdm^+ titrations (left) and guanylurea titrations (right). Lower panels: datapoints show heat absorbed as a function of substrate concentration, fit to equilibrium binding isotherms (solid lines). Equilibrium binding parameters are shown in **Table 2.3**. Figure adapted from Lucero et al., 2023

Finally, to determine whether guanylurea occupies the same binding pocket as guanidinium in Gdx-Clo, we solved a crystal structure of Gdx-Clo in the presence of 10 mM guanylurea (**Figure 2.13, Table 2.4**). Crystals were prepared as in previous studies (Kermani et al., 2022; Kermani et al., 2020), and diffracted to 2.1Å. Two transporters are present in the unit cell, and the maps showed clearly resolved guanylurea density nestled in the binding pocket of one of these transporters (**Figure 2.13A**). The guanidinium group is poised between the central glutamates, within hydrogen bonding distance, in the same binding mode as observed for

phenylguanidinium (Kermani et al., 2020). The carbonyl of guanylurea faces the cleft between helices 2_A and 2_B (termed the hydrophobic portal (Kermani et al., 2020)), but is just small enough to fit in the binding pocket without requiring a rearrangement of the sidechains lining the portal, in contrast to the slightly larger phenylguanidinium (Kermani et al., 2020). The carbonyl of the guanylurea is twisted slightly out of plane with respect to the guanidinyl group, and is positioned ~3Å from the electropositive ring edge of portal sidechain F43. There are no other residues within coordination distance of guanylurea, recapitulating the undercoordination of the native substrate Gdm^+. Other key binding pocket residues (W16, S42, Y59, and W62) contribute to a H- bond network that stabilize the central E13 residues, in the same orientation as seen in other structures (**Figure 2.13B**) (Kermani et al., 2022; Kermani et al., 2020).

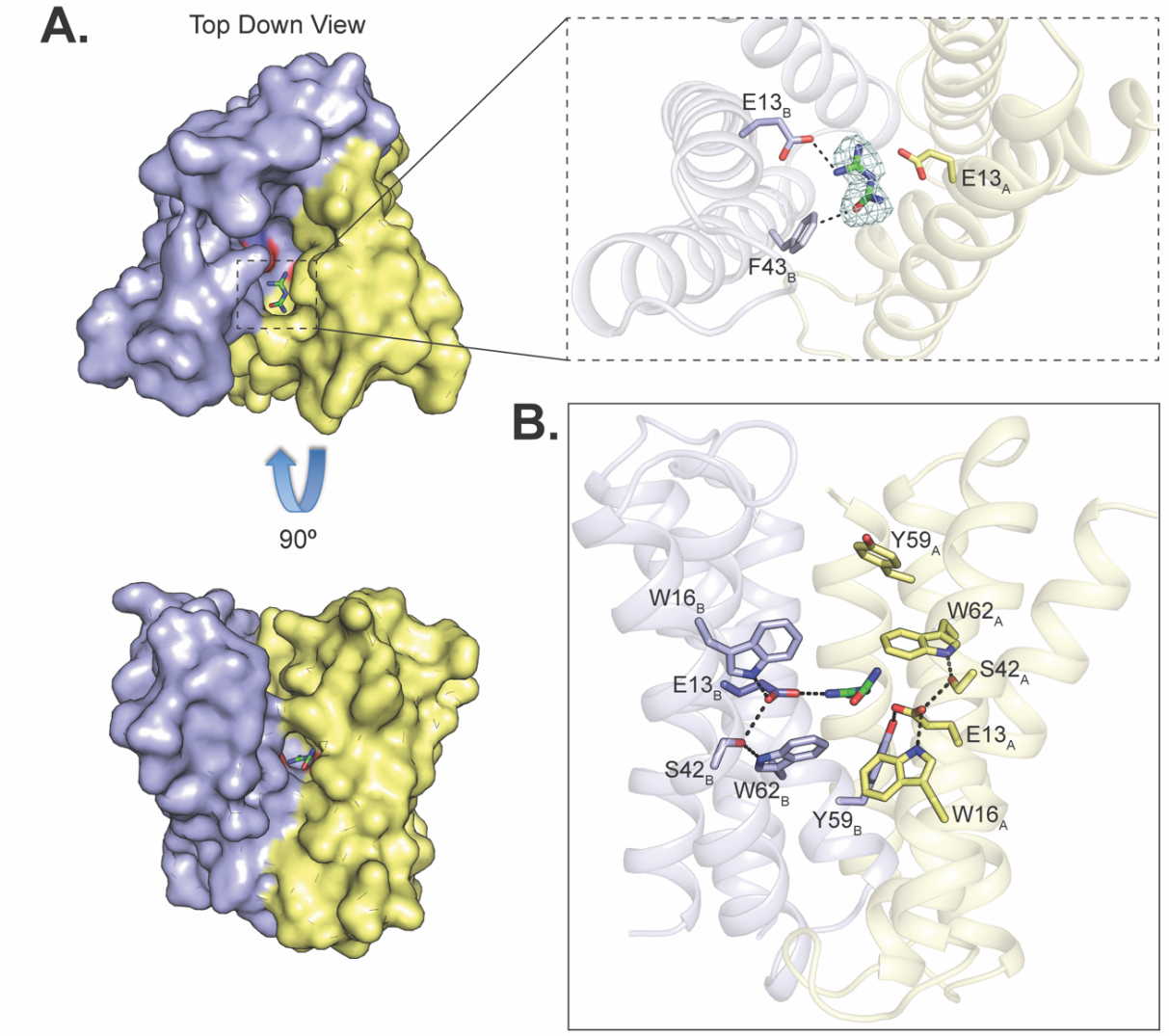

Figure 2.13 Crystal structure of Gdx-Clo in complex with guanylurea. A. A and B subunits are shown in yellow and blue, respectively, with central glutamates shown as sticks and guanylurea as green sticks. The right upper panel shows F_o-F_c omit map for guanlurea contoured at a 3.5σ. B. Putative polar interactions among binding site residues are indicated with dashed lines. Figure adapted from Lucero et al., 2023.

Table 2.4 Data collection and refinement statistics for crystal structure of Gdx-Clo in complex with guanylurea. Table adapted from Lucero et al., 2023

Data Collection	
Space Group	P1
Cell dimensions *a*, *b*, *c*, (Å)	49.91, 74.37, 107.21
α, β, *γ* (°)	86.76, 90.01, 70.26
Resolution (Å)	107-2.185
Ellipsoidal Resolution Limit (best/worst)	2.185/3.665
% Spherical Data Completeness	39.0 (5.6)
% Ellipsoidal Data Completeness	81.1 (69.8)
R_{merge}	0.099 (0.600)
R_{meas}	0.122 (0.698)
Mn $I/\sigma I$	18.1 (2.8)
Multiplicity	3.3 (3.8)
Refinement	
Resolution (Å)	35.66 – 2.18
No. reflections	27,820
R_{work} / R_{free}	28.0/30.9
Ramachandran Favored	94.7
Ramachandran Outliers	1.8
Clashscore	11.2
R.m.s. deviations	
Bond lengths (A)	0.002
Bond angles (°)	0.480
Coordinates in Protein Databank	8TGY

2.4 Discussion

Microbes are constantly evolving to contend with new environmental pressures, including the recent introduction of anthropogenic chemicals. Major routes for the acquisition of new traits by a microbial population include the gain of new genes via HGT transfer events, and the co-option of native proteins' cryptic functions (functions not under natural selection) to fulfill novel functional roles. Here, we examine a family of transporters, the SMRs, that are associated with both evolutionary processes. In particular, we focus on the SMR_{Gdx}, which undergo frequent HGT, despite playing little role in bacterial resistance to classical antimicrobials or antiseptics

(Kermani et al., 2020; Slipski et al., 2020). Based on genetic evidence (Li et al., 2023; Martinez-Vaz et al., 2022), we hypothesized a role for the SMR_{Gdx} in transport of metformin metabolites, which structurally resemble the native substrate Gdm^+, and have accumulated to high levels in waste and surface waters. Our previous work provided preliminary support for this possibility (Martinez-Vaz et al., 2022).

In this chapter, we investigate whether export of guanylurea or other metformin metabolites is a general property of SMR_{Gdx}, and we functionally characterize this activity across multiple plasmid-associated and genomic transporters. We show robust transport of guanylurea, with the same transport stoichiometry, and transport kinetics on the same order as that of the physiological substrate Gdm^+. Structures of the guanylurea-bound transporter Gdx-Clo show how guanylurea binding exploits the protein's undercoordination of the native substrate, Gdm^+ (Kermani et al., 2020), fulfilling all of the hydrogen bonds seen for the native substrate without interference from the substrate's urea group.

It was surprising on its face that the homologue with the most explicit connection to metformin degradation, Gdx-pAmi, had the lowest affinity for guanylurea (5 mM). But for bacteria actively metabolizing metformin as a nitrogen source, very high concentrations of guanylurea are likely to be produced. A prior study measured metformin degradation by an *Aminobacter* culture at a rate of ~0.7 mM/hour (Li et al., 2023). Considering the culture density and approximating a ~fL volume for each cell, each bacterium will produce nearly 16 mM internal guanylurea per minute. This back-of-the-envelope calculation illustrates the need for an efflux pathway, and also suggests that bacteria that occupy this niche might be adapted to handle high steady state guanylurea concentrations. It is a truism that an enzyme only needs to be good

enough, and apparently, high substrate affinity is not essential for Gdx-pAmi to contribute a selective advantage in the context of metformin degradation.

In summary, this work has functionally characterized an emerging physiological role of the SMR_{Gdx} transporters, export of metformin metabolites. Such a function rationalizes their genetic occurrence with wastewater-associated plasmids and may also have implications for species distribution or horizontal gene transfer in the gut microbiome of patients treated with metformin. Moreover, understanding how bacteria co-opt native physiologies to contend with novel xenobiotics yields insights into microbial adaptation to an increasingly human-impacted biosphere. Our current study highlights a role for active transport in the full microbial degradation pathway for a chemical pollutant, and may inform effective multispecies bioremediation strategies for metformin and other pharmaceuticals in the environment.

2.5 Methods

2.5.1 Phylogeny

SMR sequences from representative genomes and from Integrall (Moura et al., 2009), a database of integron-associated genes, were aligned using MUSCLE (Edgar, 2004). A phylogeny was constructed using PhyMl3.0 (Guindon et al., 2010) and visualized using FigTree (http://tree.bio.ed.ac.uk/software/figtree).

2.5.2 Transporter expression, purification, and reconstitution

Gdx-Clo (Kermani et al., 2018), Gdx-Eco (Kermani et al., 2018), EmrE (Kermani et al., 2022), and Gdx-pAmi (Martinez-Vaz et al., 2022) construct design and purification have been described previously. For QacE and Gdx-pPro, synthetic geneblocks (Integrated DNA Technologies, Coralville, IA) were cloned into a pET21b vector with an N-terminal

hexahistidine tag and LysC and thrombin recognition sequences. Proteins were overexpressed in C41(DE3). Expression was induced by addition of 0.2 mM IPTG for 3 hours. Cells were lysed and extracted with 2% n- decyl-b-D-maltoside (DM) for 2 hours. After pelleting insoluble cell debris, proteins were purified using cobalt affinity resin. Wash buffer contained 25 mM Tris, pH 8.5, 150 mM NaCl, 5 mM DM. For Gdx-pAmi, NaCl concentration was increased to 500 mM NaCl. The affinity column was washed with wash buffer, then wash buffer with 10 mM imidazole, prior to elution with wash buffer with 400 mM imidazole. For Gdx-Clo and Gdx-Eco, histidine tags were cleaved with LysC (200 ng/mg of protein; two hours at room temperature; New England Biolabs), and for all others, histidine tags were cleaved with thrombin (1 U per mg of protein, overnight at room temperature; MilliporeSigma, Burlington, MA, United States). Proteins were further purified using a gel filtration Superdex200 column (Cytiva, Marlborough, MA) equilibrated with 100 mM NaCl, 10 mM N-2-hydroxyethylpiperazine-N'-2-ethanesulfonic acid (HEPES) pH 7.5, 5 mM DM. Purified proteins were stored at 4° C for up to five days before detergent binding assays. To prepare proteoliposomes for electrophysiology assays, purified protein was mixed with *E. coli* polar lipid extract (10 mg/mL; Avanti Polar Lipids, Alabaster, AL) solubilized with 35 mM 3-[(3-cholamidopropyl)dimethylammonio]-1-propanesulfonate (CHAPS) at a protein to lipid ratio of 40 μg SMR transporter: mg lipid (1:370 protein:lipid molar ratio) prior to detergent removal by dialysis. For preparations that included Fluc-Bpe, liposomes were reconstituted with a molar ratio of 0.3 Fluc-Bpe:1 SMR_{Gdx}: 5920 lipid (1 μg Fluc-Bpe and ~2.5 μg SMR_{Gdx} per mg lipid). For liposome transport assays, proteoliposomes were prepared similarly, except that a 2:1 mixture of 1-palmitoyl, 2-oleoylphosphatidylethanolamine (POPE) and 1-palmitoyl, 2-oleoylphosphatidylglycerol (POPG) (10 mg/mL; Avanti Polar Lipids) was used with 0.2μg protein/mg lipid. Proteoliposomes were stored at -80° C until use.

2.5.3 Solid Supported Membrane (SSM) electrophysiology

SSM experiments were performed using SURFE^{2}R N1 instrument (Nanion Technologies, Munich, Germany). Sensors were prepared with a 1,2-diphytanoyl-sn-glycero-3-phosphocholine (DPhPC) lipid monolayer according to published protocols (Bazzone et al., 2017). Each sensor's capacitance and conductance were verified before use (<80 nF capacitance, <50 nS conductance) using Nanion software protocols. Proteoliposome stock was diluted 1:25 in assay buffer (100 mM KCl, 100 mM KPO_4 pH 7.5) prior to fusion with the DPhPC monolayer. For substrate screening experiments, positive reference samples were checked periodically; if the current amplitude of the reference compound differed by more than 10% on one sensor, this indicated bilayer instability, and the sensor was not used for further experiments.

2.5.4 Pyranine stoichiometry

Proteoliposomes were reconstituted with an internal buffer of 25 mM HEPES, pH 7.53, 100 mM NaCl, 100 mM KCl and pre-loaded with 0.4 mM substrate (Gdm^+ or guanylurea) and 1mM pyranine (trisodium 8-hydroxypyrene-1, 3, 6-trisulfonate; Sigma-Aldrich) using three freeze/thaw cycles. Unilamellar liposomes were formed by extrusion through a 400 nm membrane filter and the external pyranine was removed by passing liposomes through a Sephadex G-50 column spin column equilibrated in internal buffer with substrate. The external assay buffers contained 25 mM HEPES, pH 7.53, 0.4 mM substrate, and varying KCl concentration (3-46 mM) to establish the membrane potential, with NaCl to bring the total salt concentration to 200 mM. Proteoliposomes were diluted 200-fold into the external buffer, and after ~30 s. to establish a baseline, valinomycin (final concentration 0.2 ng/mL) was added together with substrate (final concentration 4 mM). Fluorescence spectra were monitored (λ_{ex} =

455 nm; (λ_{ex} = 515 nm) for ~300 s. The membrane potential was calculated using the Nernst potential for K^+:

Equation 2.1 $$\psi_{calc} = \frac{RT}{F} \ln \frac{[K^+]_{out}}{[K^+]_{in}}$$

Fluorescence emission timecourses were corrected for baseline drift measured prior to substrate and valinomycin addition. The stoichiometry was determined from the voltage at which electrochemical equilibrium occurred (no change in fluorescence) using the following equation:

Equation 2.2 $$\mathrm{E}_{rev} = \left(\frac{n}{-n+m} \frac{RT}{F} ln \frac{[substrate^+]_{in}}{[substrate^+]_{out}}\right)$$

where *n* and *m* represent the stoichiometric coefficients of protons and substrate, respectively.

2.5.5 Tryptophan fluorescence

Fluorescence emission spectra (λ_{ex} = 280 nm, λ_{em} = 300-400 nm) were collected for 1μM purified protein in assay buffer containing 200 mM NaCl, 10 mM HEPES, 10 mM bicine, 10 mM $NaPO_4$, 5mM DM, with pH adjusted from 6.5-9.0. Substrate was added from a stock solution prepared in assay buffer. For Gdm^+ titrations, the change in fluorescence, *F*, as a function of substrate fit to a single site binding isotherm,

Equation 2.3 $$\Delta F = \left(\frac{F_{max}[S]}{K_d + [S]}\right)$$

For guanylurea titration, binding data fit to a single site binding isotherm with a correction for a linear, non-specific binding component, *c*:

Equation 2.4 $$\Delta F = \left(\frac{F_{max}[S]}{K_d + [S]}\right) + c[S]$$

To derive the K_a values and K_d values from the apparent K_d measured as a function of pH, we used the following equation, which uses the approximation that the protonatable E13 sidechains have equal K_a values:

Equation 2.5 $$K_{d,app} = (K_d) * \left(1 + \left(\frac{[H^+]}{K_a}\right)\right) * \left(1 + \left(\frac{[H^+]}{K_a}\right)\right)$$

2.5.6 Isothermal titration calorimetry (ITC)

ITC experiments were conducted using a low volume Nano ITC instrument (TA Instruments, New Castle, DE). Freshly purified protein (650 μM) in 10 mM 4-(2-Hydroxyethyl)-1-piperazinepropanesulfonic acid (EPPS), pH 8.53, 100 mM NaCl, 4 mM DM was titrated with 20 mM Gdm^+ or 10 mM guanylurea prepared in the same buffer. Data was analyzed using NanoAnalyze software.

2.5.7 Structure of Gdx-Clo in complex with guanylurea

The crystallization chaperone monobody L10 was prepared as described previously (Kermani et al., 2022; Kermani et al., 2020). Freshly purified Gdx-Clo (10mg/mL) and L10 monobody (10mg/mL, supplemented with 4 mM DM) were mixed at a 1:1 ratio. Guanylurea and lauryldimethylamine-N-Oxide (LDAO, Anatrace) were added to a final concentration of 10 mM and 6.6 mM, respectively, and combined in a 1:1 ratio with crystallization solution. Crystals formed at room temperature after ~ 7 days in 0.1 M HEPES pH 7.0, 0.1 M calcium acetate, 31% PEG600. Data was collected at the Life Sciences Collaborative Access Team at the Advanced Photon Source, Argonne National Laboratory. Data was processed using DIALS (Winter et al., 2018) software and subjected to anisotropic truncation using Staraniso (Tickle et al., 2018). Phaser (McCoy et al., 2007) was used for molecular replacement with Gdx-Clo and L10 monobodies (PDB:6WK9) as search models. Coot (Emsley et al., 2010) and Phenix (Liebschner et al., 2019) were used for iterative rounds of model building and refinement.

2.6 Appendix

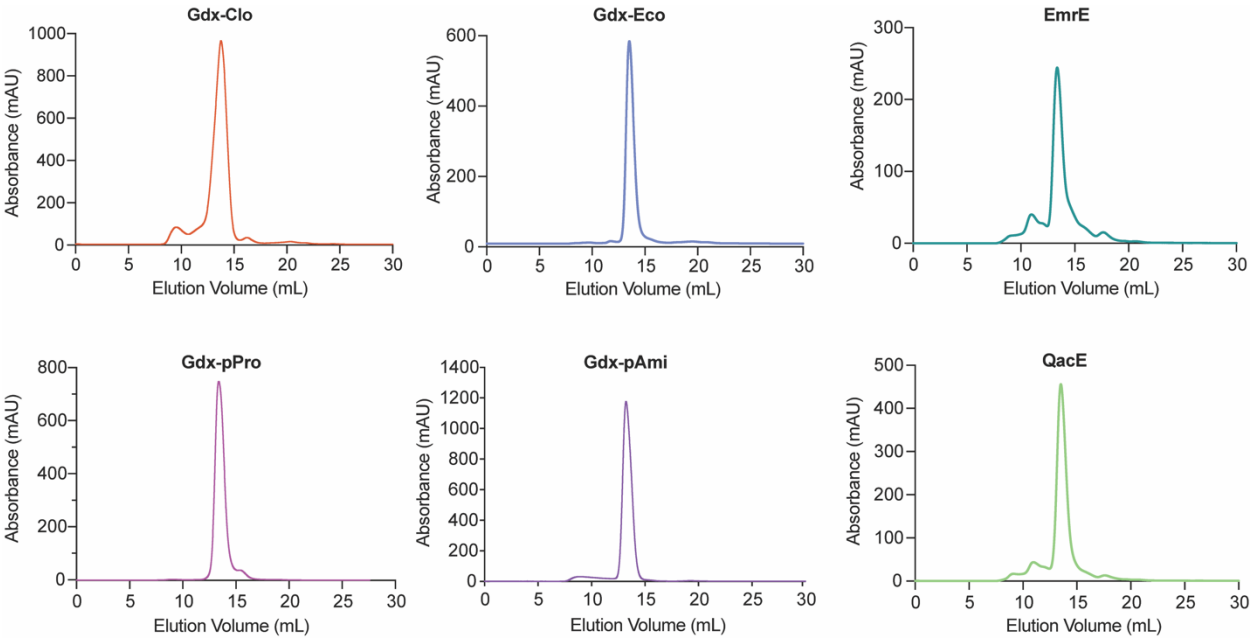

Figure 2.14 Size exclusion chromatograms for six proteins studied in chapter 2

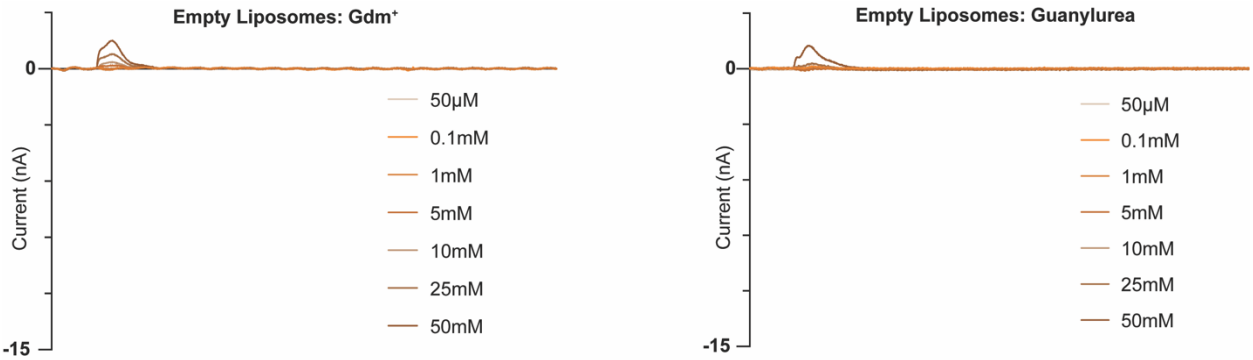

Figure 2.15 Representative current traces for Gdm^+ and guanylurea titrations of protein-free liposomes.

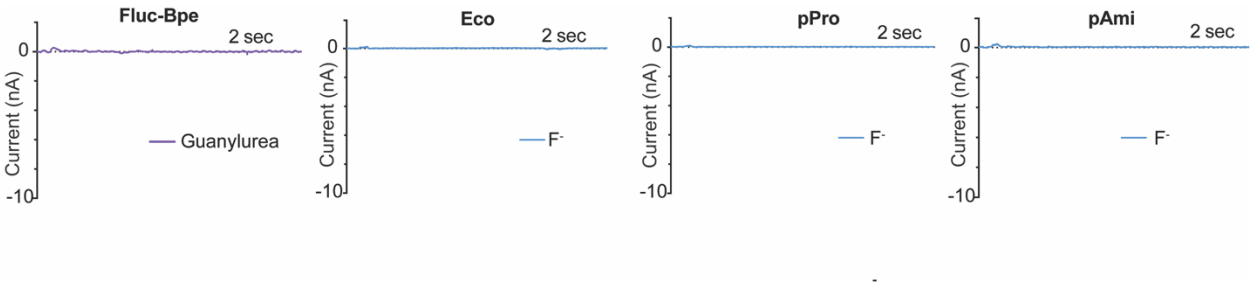

Figure 2.16 Representative current traces for guanylurea perfusion of Fluc-Bpe and fluoiride perfusions of Gdx-Eco, Gdx-pPro, and Gdx-pAmi.

Table 2.5 Coding sequences for transporters examined in chapter 3. Bolded sequences are the gene, His_6-tag is in red, and the cleavage site is indicated in green.

Construct	Coding Sequence
Gdx-Clo	**ATGGCGTGGCTGATCCTGATCATTGCGGGTATTTTCGAGGTGGTTTGGGCGAT CGCGCTGAAGTACAGCAACGGTTTTACCCGTCTGATCCCGAGCATGATCACCC TGATTGGCATGCTGATTAGCTTCTACCTGCTGAGCCAAGCGACCAAGACCCTG CCGATTGGTACCGCGTATGCGATCTGGACCGGTATTGGCGCGCTGGGTGCGGT GATTTGCGGCATCATTTTCTTTAAAGAACCGCTGACCGCGCTGCGTATCGTTTT TATGATTCTGCTGCTGACCGGTATCATTGGCCTGAAAGCGACCAGCAGC**GGTG GCACCGCGAAAGCGAGCCTGGTGCCGCGTGGTAGCGGTGGCCACCACCACCACCAC CACTG
Gdx-Eco	**ATGAGCTGGATCATTCTGGTGATCGCGGGCCTGCTGGAAGTGGTTTGGGCGGT TGGCCTGAAGTACACCCACGGTTTCAGCCGTCTGACCCCGAGCGTGATTACCG TTACCGCGATGGTGGTTAGCATGGCGCTGCTGGCGTGGGCGATGAAAAGCCTG CCGGTGGGTACCGCGTATGCGGTTTGGACCGGTATTGGTGCGGTGGGTGCGG CGATCACCGGCATTGTTCTGTTTGGTGAAAGCGCGAACCCGATGCGTCTGGCG AGCCTGGCGCTGATTGTGCTGGGTATCATTGGCCTGAAGCTGAGCACCCATGG** TGGCACCGCGAAAGCGAGCCTGGTTCCGCGTGGCAGCGGTGGCCACCACCACCACC ACCACTGA
Gdx-pPro	ATGGGCAGCAGCCATCACCATCATCATCACAGCAGCGGCCTGGTGCCGCGCGGCAG CGGTGGCACCGCGAAAGCGAGC**TCCTGGATCGTTCTGTTGATCGCGGGCTTGTT AGAGGTTGTATGGGCCATCGGACTTAAATACACTCACGGTTTCACACGCTTGA CCCCAAGTATTATTACAATCGCTGCTATGATCGTGTCAATCGCCATGCTTTCGT GGGCAATGCGCACCCTTCCAGTCGGGACGGCATACGCAGTGTGGACCGGGATT GGCGCTGTTGGAGCGGCGATCACCGGCATCCTTCTTCTGGGTGAAAGTGCGTC ACCGGCTCGTTTGTTGAGTCTTGGACTGATTGTGGCCGGGATTATCGGCTTAA AACTTAGCACTCATTAA**
Gdx-pAmi	ATGGGCAGCAGCCATCACCATCATCATCACAGCAGCGGCCTGGTGCCGCGCGGCAG CGGTGGCACCGCGAAAGCGAGC**GCTTGGATCTATTTACTGCTTGCTGGTCTTTTC GAGATTGGTTGGCCGGTCGGACTGAAGATGGCTCAAGAGCCTGACACGCGTTG GAGTGGGATTGGTGTCGCAGTGGTATTTATGGGAATTAGCGGGGCGTTGCTTT TCCTTGCTCAGCGCACCATTCCCATTGGCACTGCTTACGCTATCTGGACCGGAA TTGGAGCCGCCGGAACCTTTTTAGTTGGAGTTATGTACTACGGCGACCCCACT AGCTTCTTTCGTTATTTGGGTGTCGCACTTATCGTTGCTGGAGTGGCGACACTG AAGTTAGCGCACTAA**
EmrE	ATGGGCAGCAGCCATCACCATCATCATCACAGCAGCGGCCTGGTGCCGCGCGGCAG CCAT**ATGAACCCTTATATTTATCTTGGTGGTGCAATACTTGCAGAGGTCATTGG TACAACCTTAATGAAGTTTTCAGAAGGTTTTACACGGTTATGGCCATCTGTTGG TACAATTATTTGTTATTGTGCATCATTCTGGTTATTAGCTCAGACGCTGGCTTA TATTCCTACAGGGATTGCTTATGCTATCTGGTCAGGAGTCGGTATTGTCCTGAT TAGCTTACTGTCATGGGGATTTTTCGGCCAACGGCTGGACCTGCCAGCCATTAT AGGCATGATGTTGATTTGTGCCGGTGTGTTGATTATTAATTTATTGTCACGAAG CACACCACATTAA**
QacE	ATGGGCAGCAGCCATCACCATCATCATCACAGCAGCGGCCTGGTGCCGCGCGGCAG CAAAGGTTGGCTTTTTCTTGTAATTGCTATCGTAGGTGAAGTAATCGCTACCTC GGCCTTAAAATCAAGCGAAGGTTTTACCAAACTTGCGCCCTCGGCTGTCGTCAT TATCGGATACGGAATTGCGTTCTATTTCCTGTCATTAGTGATGAAGTCTATTCC GGTGGGGGTTGCTTATGCGGTATGGAGTGGGCTTGGAGTTGTAATTATTACCG CAATCGCTTGGCTTCTTCACGGTCAGAAGTTGGACGCCTGGGGCTTCGTAGGT ATGGGCCTTATTGTCAGTGGAGTCGTCGTTTTAAATTTGCTGTCCAAAGCGTCG GCACATTAA**

2.7 References

Arber, W. (2014). Horizontal Gene Transfer among Bacteria and Its Role in Biological Evolution. *Life (Basel)*, *4*(2), 217-224. https://doi.org/10.3390/life4020217

Balakrishnan, A., Sillanpää, M., Jacob, M. M., & Vo, D. N. (2022). Metformin as an emerging concern in wastewater: Occurrence, analysis and treatment methods. *Environ Res*, *213*, 113613. https://doi.org/10.1016/j.envres.2022.113613

Barthmes, M., Liao, J., Jiang, Y., Brüggemann, A., & Wahl-Schott, C. (2016). Electrophysiological characterization of the archaeal transporter NCX_Mj using solid supported membrane technology. *J Gen Physiol*, *147*(6), 485-496. https://doi.org/10.1085/jgp.201611587

Bazzone, A., Barthmes, M., & Fendler, K. (2017). SSM-Based Electrophysiology for Transporter Research. *Methods Enzymol*, *594*, 31-83. https://doi.org/10.1016/bs.mie.2017.05.008

Bazzone, A., Zerlotti, R., Barthmes, M., & Fertig, N. (2023). Functional characterization of SGLT1 using SSM-based electrophysiology: Kinetics of sugar binding and translocation [Original Research]. *Frontiers in Physiology*, *14*. https://doi.org/10.3389/fphys.2023.1058583

Bramante, C. T., Ingraham, N. E., Murray, T. A., Marmor, S., Hovertsen, S., Gronski, J., McNeil, C., Feng, R., Guzman, G., Abdelwahab, N., King, S., Tamariz, L., Meehan, T., Pendleton, K. M., Benson, B., Vojta, D., & Tignanelli, C. J. (2021). Metformin and risk of mortality in patients hospitalised with COVID-19: a retrospective cohort analysis. *Lancet Healthy Longev*, *2*(1), e34-e41. https://doi.org/10.1016/s2666-7568(20)30033-7

Briones, R. M., Sarmah, A. K., & Padhye, L. P. (2016). A global perspective on the use, occurrence, fate and effects of anti-diabetic drug metformin in natural and engineered ecosystems. *Environ Pollut*, *219*, 1007-1020. https://doi.org/10.1016/j.envpol.2016.07.040

Burata, O. E., Yeh, T. J., Macdonald, C. B., & Stockbridge, R. B. (2022). Still rocking in the structural era: A molecular overview of the small multidrug resistance (SMR) transporter family. *J Biol Chem*, *298*(10), 102482. https://doi.org/10.1016/j.jbc.2022.102482

Cao, Z., Yan, W., Ding, M., & Yuan, Y. (2022). Construction of microbial consortia for microbial degradation of complex compounds. *Front Bioeng Biotechnol*, *10*, 1051233. https://doi.org/10.3389/fbioe.2022.1051233

Chaignaud, P., Gruffaz, C., Borreca, A., Fouteau, S., Kuhn, L., Masbou, J., Rouy, Z., Hammann, P., Imfeld, G., Roche, D., & Vuilleumier, S. (2022). A Methylotrophic Bacterium Growing with the Antidiabetic Drug Metformin as Its Sole Carbon, Nitrogen and Energy Source. *Microorganisms*, *10*(11). https://doi.org/10.3390/microorganisms10112302

Corcoran, C., & Jacobs, T. F. (2023). Metformin. In *StatPearls*. https://www.ncbi.nlm.nih.gov/pubmed/30085525

Edgar, R. C. (2004). MUSCLE: multiple sequence alignment with high accuracy and high throughput. *Nucleic Acids Res*, *32*(5), 1792-1797. https://doi.org/10.1093/nar/gkh340

Elizalde-Velázquez, G. A., & Gómez-Oliván, L. M. (2020). Occurrence, toxic effects and removal of metformin in the aquatic environments in the world: Recent trends and perspectives. *Sci Total Environ*, *702*, 134924. https://doi.org/10.1016/j.scitotenv.2019.134924

Emsley, P., Lohkamp, B., Scott, W. G., & Cowtan, K. (2010). Features and development of Coot. *Acta Crystallogr D Biol Crystallogr*, *66*(Pt 4), 486-501. https://doi.org/10.1107/s0907444910007493

Fitzgerald, G. A., Mulligan, C., & Mindell, J. A. (2017). A general method for determining secondary active transporter substrate stoichiometry. *Elife*, *6*. https://doi.org/10.7554/eLife.21016

Gaze, W. H., Abdouslam, N., Hawkey, P. M., & Wellington, E. M. (2005). Incidence of class 1 integrons in a quaternary ammonium compound-polluted environment. *Antimicrob Agents Chemother*, *49*(5), 1802-1807. https://doi.org/10.1128/AAC.49.5.1802-1807.2005

Golovko, O., Örn, S., Sörengård, M., Frieberg, K., Nassazzi, W., Lai, F. Y., & Ahrens, L. (2021). Occurrence and removal of chemicals of emerging concern in wastewater treatment plants and their impact on receiving water systems. *Sci Total Environ*, *754*, 142122. https://doi.org/10.1016/j.scitotenv.2020.142122

Gong, L., Goswami, S., Giacomini, K. M., Altman, R. B., & Klein, T. E. (2012). Metformin pathways: pharmacokinetics and pharmacodynamics. *Pharmacogenet Genomics*, *22*(11), 820-827. https://doi.org/10.1097/FPC.0b013e3283559b22

Guindon, S., Dufayard, J. F., Lefort, V., Anisimova, M., Hordijk, W., & Gascuel, O. (2010). New algorithms and methods to estimate maximum-likelihood phylogenies: assessing the performance of PhyML 3.0. *Syst Biol*, *59*(3), 307-321. https://doi.org/10.1093/sysbio/syq010

Kermani, A. A., Burata, O. E., Koff, B. B., Koide, A., Koide, S., & Stockbridge, R. B. (2022). Crystal structures of bacterial small multidrug resistance transporter EmrE in complex with structurally diverse substrates. *Elife*, *11*. https://doi.org/10.7554/eLife.76766

Kermani, A. A., Macdonald, C. B., Burata, O. E., Ben Koff, B., Koide, A., Denbaum, E., Koide, S., & Stockbridge, R. B. (2020). The structural basis of promiscuity in small multidrug resistance transporters. *Nat Commun*, *11*(1), 6064. https://doi.org/10.1038/s41467-020-19820-8

Kermani, A. A., Macdonald, C. B., Gundepudi, R., & Stockbridge, R. B. (2018). Guanidinium export is the primal function of SMR family transporters. *Proc Natl Acad Sci U S A*, *115*(12), 3060-3065. https://doi.org/10.1073/pnas.1719187115

Larsen, S., Rabøl, R., Hansen, C. N., Madsbad, S., Helge, J. W., & Dela, F. (2012). Metformin-treated patients with type 2 diabetes have normal mitochondrial complex I respiration. *Diabetologia*, *55*(2), 443-449. https://doi.org/10.1007/s00125-011-2340-0

Li, J., Sae Her, A., & Traaseth, N. J. (2021). Asymmetric protonation of glutamate residues drives a preferred transport pathway in EmrE. *Proceedings of the National Academy of Sciences*, *118*(41), e2110790118. https://doi.org/doi:10.1073/pnas.2110790118

Li, T., Xu, Z. J., & Zhou, N. Y. (2023). Aerobic Degradation of the Antidiabetic Drug Metformin by Aminobacter sp. Strain NyZ550. *Environ Sci Technol*. https://doi.org/10.1021/acs.est.2c07669

Liebschner, D., Afonine, P. V., Baker, M. L., Bunkóczi, G., Chen, V. B., Croll, T. I., Hintze, B., Hung, L. W., Jain, S., McCoy, A. J., Moriarty, N. W., Oeffner, R. D., Poon, B. K., Prisant, M. G., Read, R. J., Richardson, J. S., Richardson, D. C., Sammito, M. D., Sobolev, O. V., . . . Adams, P. D. (2019). Macromolecular structure determination using X-rays, neutrons and electrons: recent developments in Phenix. *Acta Crystallogr D Struct Biol*, *75*(Pt 10), 861-877. https://doi.org/10.1107/s2059798319011471

Lucero, R., M., Demirer, K., Yeh, T. J., & Stockbridge, R. B. (2023). Transport of metformin metabolites by guanidinium exporters of the Small Multidrug Resistance family. *bioRxiv*, 2023.2008.2010.552832. https://doi.org/10.1101/2023.08.10.552832

Lunger, L., Melmer, A., Oberaigner, W., Leo, M., Juchum, M., Pölzl, K., Gänzer, J., Innerebner, M., Eisendle, E., Beck, G., Kathrein, H., Heindl, B., Schönherr, H. R., Lechleitner, M., Tilg, H., & Ebenbichler, C. (2017). Prescription of oral antidiabetic drugs in Tyrol - Data from the Tyrol diabetes registry 2012-2015. *Wien Klin Wochenschr*, *129*(1-2), 46-51. https://doi.org/10.1007/s00508-016-1135-1

Lv, Z., & Guo, Y. (2020). Metformin and Its Benefits for Various Diseases. *Front Endocrinol (Lausanne)*, *11*, 191. https://doi.org/10.3389/fendo.2020.00191

Maier, L., Pruteanu, M., Kuhn, M., Zeller, G., Telzerow, A., Anderson, E. E., Brochado, A. R., Fernandez, K. C., Dose, H., Mori, H., Patil, K. R., Bork, P., & Typas, A. (2018). Extensive impact of non-antibiotic drugs on human gut bacteria. *Nature*, *555*(7698), 623-628. https://doi.org/10.1038/nature25979

Martinez-Vaz, B. M., Dodge, A. G., Lucero, R. M., Stockbridge, R. B., Robinson, A. A., Tassoulas, L. J., & Wackett, L. P. (2022). Wastewater bacteria remediating the pharmaceutical metformin: Genomes, plasmids and products. *Front Bioeng Biotechnol*, *10*, 1086261. https://doi.org/10.3389/fbioe.2022.1086261

McCoy, A. J., Grosse-Kunstleve, R. W., Adams, P. D., Winn, M. D., Storoni, L. C., & Read, R. J. (2007). Phaser crystallographic software. *J Appl Crystallogr*, *40*(Pt 4), 658-674. https://doi.org/10.1107/s0021889807021206

McIlwain, B. C., Gundepudi, R., Koff, B. B., & Stockbridge, R. B. (2021). The fluoride permeation pathway and anion recognition in Fluc family fluoride channels. *Elife*, *10*. https://doi.org/10.7554/eLife.69482

McIlwain, B. C., Ruprecht, M. T., & Stockbridge, R. B. (2021). Membrane Exporters of Fluoride Ion. *Annu Rev Biochem*, *90*, 559-579. https://doi.org/10.1146/annurev-biochem-071520-112507

Morrison, E. A., DeKoster, G. T., Dutta, S., Vafabakhsh, R., Clarkson, M. W., Bahl, A., Kern, D., Ha, T., & Henzler-Wildman, K. A. (2012). Antiparallel EmrE exports drugs by exchanging between asymmetric structures. *Nature*, *481*(7379), 45-50. https://doi.org/10.1038/nature10703

Morrison, E. A., Robinson, A. E., Liu, Y., & Henzler-Wildman, K. A. (2015). Asymmetric protonation of EmrE. *Journal of General Physiology*, *146*(6), 445-461. https://doi.org/10.1085/jgp.201511404

Moura, A., Soares, M., Pereira, C., Leitão, N., Henriques, I., & Correia, A. (2009). INTEGRALL: a database and search engine for integrons, integrases and gene cassettes. *Bioinformatics*, *25*(8), 1096-1098. https://doi.org/10.1093/bioinformatics/btp105

Nasri, H., & Rafieian-Kopaei, M. (2014). Metformin: Current knowledge. *J Res Med Sci*, *19*(7), 658-664.

Robinson, A. E., Thomas, N. E., Morrison, E. A., Balthazor, B. M., & Henzler-Wildman, K. A. (2017). New free-exchange model of EmrE transport. *Proc Natl Acad Sci U S A*, *114*(47), E10083-e10091. https://doi.org/10.1073/pnas.1708671114

Sam, S., & Ehrmann, D. A. (2017). Metformin therapy for the reproductive and metabolic consequences of polycystic ovary syndrome. *Diabetologia*, *60*(9), 1656-1661. https://doi.org/10.1007/s00125-017-4306-3

Scheen, A. J. (2020). Metformin and COVID-19: From cellular mechanisms to reduced mortality. *Diabetes Metab*, *46*(6), 423-426. https://doi.org/10.1016/j.diabet.2020.07.006
Scheurer, M., Michel, A., Brauch, H. J., Ruck, W., & Sacher, F. (2012). Occurrence and fate of the antidiabetic drug metformin and its metabolite guanylurea in the environment and during drinking water treatment. *Water Res*, *46*(15), 4790-4802. https://doi.org/10.1016/j.watres.2012.06.019
Slipski, C. J., Jamieson, T. R., Zhanel, G. G., & Bay, D. C. (2020). Riboswitch-Associated Guanidinium-Selective Efflux Pumps Frequently Transmitted on Proteobacterial Plasmids Increase Escherichia coli Biofilm Tolerance to Disinfectants. *J Bacteriol*, *202*(23). https://doi.org/10.1128/JB.00104-20
Stockbridge, R. B., Robertson, J. L., Kolmakova-Partensky, L., & Miller, C. (2013). A family of fluoride-specific ion channels with dual-topology architecture. *Elife*, *2*, e01084. https://doi.org/10.7554/eLife.01084
Stockbridge, R. B., & Tsai, M. F. (2015). Lipid reconstitution and recording of recombinant ion channels. *Methods Enzymol*, *556*, 385-404. https://doi.org/10.1016/bs.mie.2014.12.028
Thomas, N. E., Feng, W., & Henzler-Wildman, K. A. (2021). A solid-supported membrane electrophysiology assay for efficient characterization of ion-coupled transport. *J Biol Chem*, *297*(4), 101220. https://doi.org/10.1016/j.jbc.2021.101220
Tickle, I. J., Flensburg, C., Keller, P., Paciorek, W., Sharff, A., Vonrhein, C., & Bricogne, G. (2018). STARANISO. *Cambridge, United Kingdom: Global Phasing Ltd.*
Top, W. M. C., Kooy, A., & Stehouwer, C. D. A. (2022). Metformin: A Narrative Review of Its Potential Benefits for Cardiovascular Disease, Cancer and Dementia. *Pharmaceuticals (Basel)*, *15*(3). https://doi.org/10.3390/ph15030312
Trautwein, C., Berset, J. D., Wolschke, H., & Kümmerer, K. (2014). Occurrence of the antidiabetic drug Metformin and its ultimate transformation product Guanylurea in several compartments of the aquatic cycle. *Environ Int*, *70*, 203-212. https://doi.org/10.1016/j.envint.2014.05.008
Trautwein, C., & Kümmerer, K. (2011). Incomplete aerobic degradation of the antidiabetic drug Metformin and identification of the bacterial dead-end transformation product Guanylurea. *Chemosphere*, *85*(5), 765-773. https://doi.org/10.1016/j.chemosphere.2011.06.057
Vich Vila, A., Collij, V., Sanna, S., Sinha, T., Imhann, F., Bourgonje, A. R., Mujagic, Z., Jonkers, D., Masclee, A. A. M., Fu, J., Kurilshikov, A., Wijmenga, C., Zhernakova, A., & Weersma, R. K. (2020). Impact of commonly used drugs on the composition and metabolic function of the gut microbiota. *Nat Commun*, *11*(1), 362. https://doi.org/10.1038/s41467-019-14177-z
Wei, Z., Wei, Y., Li, H., Shi, D., Yang, D., Yin, J., Zhou, S., Chen, T., Li, J., & Jin, M. (2022). Emerging pollutant metformin in water promotes the development of multiple-antibiotic resistance in Escherichia coli via chromosome mutagenesis. *J Hazard Mater*, *430*, 128474. https://doi.org/10.1016/j.jhazmat.2022.128474
Winter, G., Waterman, D. G., Parkhurst, J. M., Brewster, A. S., Gildea, R. J., Gerstel, M., Fuentes-Montero, L., Vollmar, M., Michels-Clark, T., Young, I. D., Sauter, N. K., & Evans, G. (2018). DIALS: implementation and evaluation of a new integration package. *Acta Crystallogr D Struct Biol*, *74*(Pt 2), 85-97. https://doi.org/10.1107/s2059798317017235

Wu, H., Esteve, E., Tremaroli, V., Khan, M. T., Caesar, R., Mannerås-Holm, L., Ståhlman, M., Olsson, L. M., Serino, M., Planas-Fèlix, M., Xifra, G., Mercader, J. M., Torrents, D., Burcelin, R., Ricart, W., Perkins, R., Fernàndez-Real, J. M., & Bäckhed, F. (2017). Metformin alters the gut microbiome of individuals with treatment-naive type 2 diabetes, contributing to the therapeutic effects of the drug. *Nat Med*, *23*(7), 850-858. https://doi.org/10.1038/nm.4345

Zhang, Y., Gu, Y., Ren, H., Wang, S., Zhong, H., Zhao, X., Ma, J., Gu, X., Xue, Y., Huang, S., Yang, J., Chen, L., Chen, G., Qu, S., Liang, J., Qin, L., Huang, Q., Peng, Y., Li, Q., . . . Wang, W. (2020). Gut microbiome-related effects of berberine and probiotics on type 2 diabetes (the PREMOTE study). *Nature Communications*, *11*(1), 5015. https://doi.org/10.1038/s41467-020-18414-8

Chapter 3 The Molecular Consequences of Cytosolic Accumulation of Guanidinium (Gdm^+) on Bacterial Fitness and Biofilm Formation

3.1 Introduction

Until recently, guanidinium (Gdm^+) was not known to be physiologically relevant in bacteria. Gdm^+ is most commonly known for industrial purposes in production of explosives, rubber, plastics and as a chaotropic agent for protein denaturation (Güthner et al., 2006; Qasim & Taha, 2013). However, bacteria have specialized mechanisms in managing guanidinium (Gdm^+). These mechanisms can be categorized into three primary areas: the capability of riboswitches to sense Gdm^+, the metabolism, or utilization, of Gdm^+ as a nitrogen source, and the active export of Gdm^+ (Kermani et al., 2018; Nelson et al., 2017; Sherlock & Breaker, 2017; Sherlock et al., 2017; Sinn et al., 2021). Given these intricate systems for Gdm^+ management, it's evident that maintaining Gdm^+ homeostasis is an important theme of bacterial physiology. While the metabolic pathways involving Gdm^+ have been well studied, the broader understanding of this metabolite's significance is still evolving. There is still a gap in knowledge particularly concerning the mechanisms driving its production and the cellular consequences of cytosolic accumulation in bacterial cells. It would be important to understand the metabolism pathways leading to Gdm^+ production, offering insights into the specific bacterial strategies for managing this metabolite. Doing so could uncover molecular vulnerabilities that could be a potential therapeutic targets against multidrug resistance. Lastly, this could illuminate why there is an observed mechanistic divide in the handling of Gdm^+ and highlight the propensity of the Small Multidrug Resistance (SMR) protein family's linkage to horizontal gene transfer (HGT) events.

In this chapter we start the investigation of the following three main questions: (1) What is the biological role of Gdm^+? (2) Which bacterial metabolism pathways yield Gdm^+? (3) How does accumulation of Gdm^+ affect the cell and its pathogenesis pathways? To investigate the production of the metabolite, a non-pathogenic *Escherichia coli* (*E.coli*) model was used to assess fitness during various growth conditions yielding Gdm^+. A variety of pathogenic bacterial strains were used to used to determine Gdm^+ affects on virulence pathways including biofilm formation and swimming mechanisms. I have shown that preventing guanidinium export impairs bacterial fitness, and that the fitness costs are greater for biofilm formation relative to planktonic growth.

3.2 Results

3.2.1 Exogenous Gdm^+ decreases fitness when exporter is not present

Using non-pathogenic (Keio Collection (Baba et al., 2006)) and pathogenic (UTI89) *Escherichia coli* (*E.coli*) strains as our bacterial model, the knockout of the guanidinium exporter (Gdx) was used (and created in UTI89 strain) to understand how accumulation of guanidinium ions (Gdm^+) impacts bacterial fitness and biofilm formation. Additionally, to understand how bacterial metabolism influences guanidinium productions, an assay was developed to utilize the fitness differences when competing the wild-type and knockout strains (**Figure 3.1C, Figure 3.8**). The ongoing hypothesis about the role of the SMR_{Gdx} is that it prevents Gdm^+ toxicity (Kermani et al., 2018; Nelson et al., 2017). Therefore, the phenotype of bacterial cells that do not possess the export (knockout strain annotated as Δ*sugE*) was examined with additions of exogenous Gdm^+ during planktonic growth curve assays and resistance assays (**Figure 3.1A** and **B**). Growth curves and spotting assays between isogenic strains WT, Δ*emrE* (SMR_{Qac}: drug exporter knock out), and Δ*sugE* (SMR_{Gdx}: Gdx knocked out) demonstrated a phenotype of

inverse correlation between growth as the amount of Gdm^+, but specific to only the Gdx. The very closely related drug exporter, EmrE did not exhibit the same effect and behaved like wildtype (**Figure 3.1A** and **B**). For the SMR_{Gdx}, the growth defects begin at 3 mM Gdm^+ and is profound at the higher concentrations tested, 10 and 30 mM Gdm^+. The phenotype lost in the Δ*sugE* strain with Gdm^+-containing liquid and agar cultures can be rescued with the insertion of an inducible pET plasmid containing the SMR_{Gdx} gene from *E.coli*, annotated as "SugE" (Kermani et al., 2018).

To quantify the fitness differences observed between the wildtype and SMR_{Gdx} knockout strains, a competition assay between these two strains was performed. Fluorescent bacterial culture samples were analyzed through flow cytometry where each sample analyzed contained ~100,000 cells. We would expect that during growth conditions yielding Gdm^+, wildtype (labeled with Cyan Fluorescent Protein (CFP)) would outcompete, or would be more fit, than the Δ*sugE* strain (labeled with Yellow Fluorescent Protein (YFP)). The expected observation of the wildtype strain outcompeting the other strain was observed while using a variety of different media compositions with and without the addition of exogenous Gdm^+. This fitness defect could be rescued by inserting the SMR_{Gdx} containing plasmid into the knockout strain (**Figure 3.1C**). Quantifying the flow cytometry data allowed us to statistically analyze any significant differences between the strains.

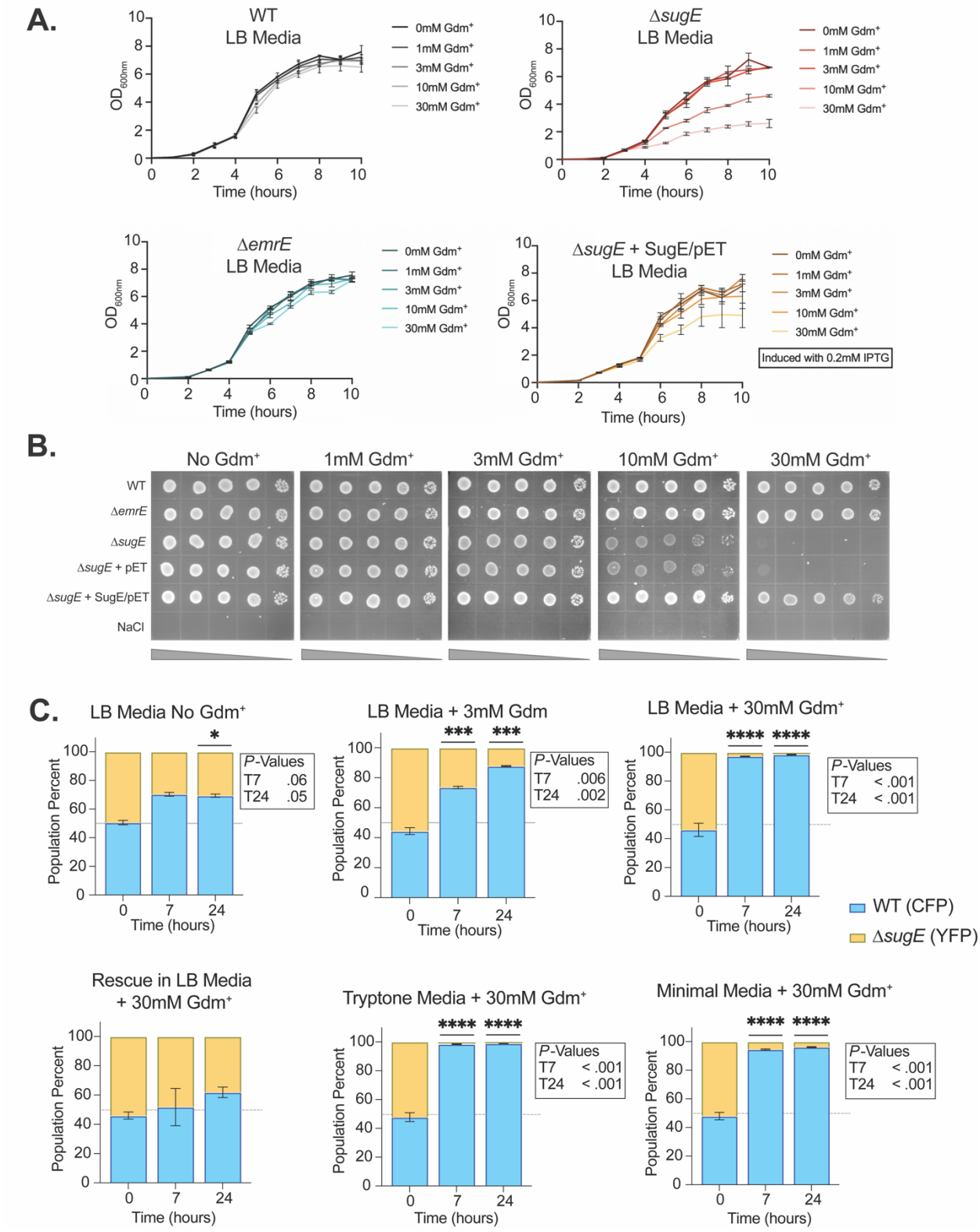

Figure 3.1 Consequences of exogenous Gdm^+ addition in the Keio Collection cell line. A. Liquid growth curves, B. Resistance spotting assay, C. Flow cytometry competition assay demonstrating SugE conferring resistance to Gdm^+. Inserting a plasmid containing Gdx can rescue the knockout's decreased fitness. Note that non-fluorescent species (~10%) were neglected in the analysis in the competition assay.

3.2.2 Virulence mechanisms are sensitive to Gdm^+

In several types of media compositions, when Gdm^+ is present, wildtype possesses enhanced fitness compared to the Gdx knockout strain. Given this observed disparity in fitness, it becomes imperative to probe further how the accumulation of guanidinium ions influences other cellular pathways, especially those related to virulence. To investigate virulence, some bacteria employ flagella-driven swimming mechanisms to navigate their environment, moving towards favorable conditions and away from harmful ones through chemotaxis (Brown & Berg, 1974; Miller et al., 2021; Mulcahy et al., 2008; Naaz et al., 2021). The favorable or harmful conditions can be based on pH, nutrient availability, temperature, toxic compounds, osmotic pressure, oxygen levels, and chemical gradients that play pivotal roles in bacterial behavior to ensure they find the most suitable environments for growth, reproduction, and survival (Andrews et al., 2010; Cegelski et al., 2009; Evans et al., 2015; Hung et al., 2013). When the environment is suitable for bacteria to thrive, bacteria take on a different survival strategy, biofilm formation. In biofilms, bacteria adhere to surfaces and develop complex, structured communities encased in a self-produced matrix of extracellular polymeric substances providing protection (Cegelski et al., 2009; Evans et al., 2015; Hung et al., 2013; Zhou et al., 2012). It has been reported that biofilms are dependent on the use of glutamate and glutamine as a nitrogen source for successful biofilm formation (Hassanov et al., 2018) motivating investigation about Gdm^+ and its effects on biofilms. Robust biofilms protect and are resistant to environmental stresses, including antibiotics, and often plays a significant role in persistent infections and antimicrobial resistance, making them a good target for novel therapeutics. Pathogenic UTI89 *E.coli* strain was used to monitor the effects of Gdm^+ on biofilm formation, while both pathogenic and non-pathogenic strains were used to monitor swimming phenotypes.

Two different types of biofilms were tested: solid surface biofilms (rugose) and air-liquid interface biofilms (pellicles) (**Figure 3.2**). The formed pellicle biofilms could be quantified by using a crystal violet dye that binds the components of biofilms (**Figure 3.2 C** and **D**). Curli and cellulose producing biofilms will be stained red from the binding of Congo Red (Evans et al., 2018). Without any exogenous Gdm^+ added to the media, there did not appear to be any differences in the wildtype and knockout morphology of pellicle or rugose biofilms nor when the pellicle biofilms were quantified. For the Gdx knockout strain, the difficulties to form a robust biofilm (indicated by the decrease in wrinkle texture, color, and thinness of the biofilm) begin to have an effect starting at 1 mM Gdm^+ and is very profound at the higher concentrations tested, 3, 10 and 30 mM Gdm^+. The biofilm morphology lost in the Δ*sugE* UTI89 strain with Gdm^+-containing media can be rescued with the insertion of a plasmid containing either the *sugE* gene from the UTI89 strain (**Figure 3.2B** and **3.9 - bottom**) or the Keio collection (**Figure 3.2A, C, D** and **3.9 - top**). The plasmid construct with the pathogenic Gdx gene did not need to be induced for successful rescue. The use of the Gdx gene from the Keio collection for rescue was rationalized as it shares a 97.1-percent amino acid sequence identity with the Gdx gene in UTI89 cells.

Controls using Δ*bscA* (cellulose gene knocked out) and Δ*csgBA* (curli genes knocked out) for pellicle and rugose biofilms was used as a reference to determine which biofilm composition process is affected with exogenous Gdm^+ (data not shown). Curli expression levels in the rugose biofilms were determined quantitatively by a Western Blot (data not shown) and did not provide any evidence that Gdm^+ alters expression levels. Planktonic growth curves and spotting assays using the same yeast extract-Casamino acid (YESCA) media between the wildtype and Δ*sugE* strains demonstrated similar results as seen with the Keio collection strains (**Figure 3.9**). UTI89

strain is slightly more sensitive than Keio, but the observation that the liquid culture is less sensitive than the biofilms remains.

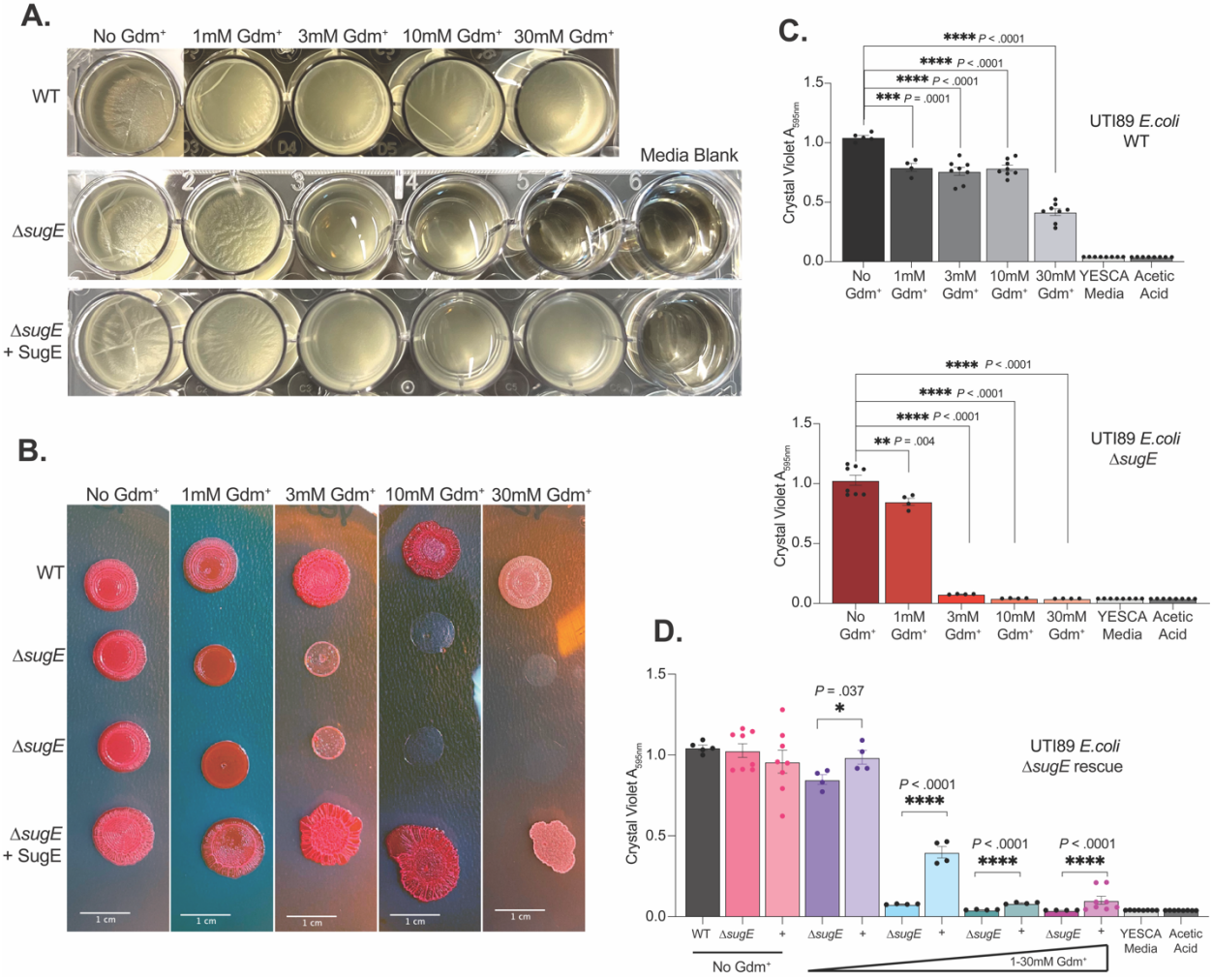

Figure 3.2 Biofilms are sensitive to Gdm^+. A. Pellicle biofilms and B, rugose biofilms after two days of incubation with a gradient of Gdm^+ are more sensitive. C. Pellicle biofilms were stained with crystal violet stain and quantified at 595nm. D. Pellicle biofilm partial rescue. All error bars represent the SEM replicate measurement. One way ANOVA and unpaired t-test analysis was used to determine statistical significance.

Biofilm formation and bacterial motility are interrelated behaviors, intricately linked to bacterial survival and adaptation (Cho et al., 2020; Miller et al., 2021; Yan et al., 2019). Swimming allows for bacteria to forage for nutrients by "swimming", facilitated by flagella movement, through the water filled channels in agar. In turn these non-ATP driven mechanisms are sensitive to metabolic metabolites and ions (Adler, 1969; Berg & Anderson, 1973; Biquet-

Bisquert et al., 2021; Naaz et al., 2021). The flagellar movement is driven by translocation of protons motivated by the proton motor force (Biquet-Bisquert et al., 2021; Yan et al., 2019). First, swimming was monitored between isogenic strains WT, Δ*emrE*, and Δ*sugE* from the Keio collection by measuring the concentric zones from the midpoint over time. The Δ*emrE* strain mimicked that of wildtype which took a longer time to reach the designated end point of the assay. The Gdx knockout strain swam significantly faster on rich media, low percentage agar plates (Miller et al., 2021; Morales-Soto et al., 2015) without any addition of exogenous Gdm^+ (**Figure 3.3A** and **B**). The rescue with transformed plasmid encoding with the Gdx gene was not complete. However, overexpression of membrane proteins can become toxic to cells, potentially a reason for only partial swimming rescue. An alternative that could be used is a low expression plasmid, so it is not overwhelming to the cell. As the Δ*emrE* mimicked wildtype, this unique phenotype is specific to only the SMR_{Gdx}. The swimming behavior is sensitive to endogenous levels of Gdm^+ accumulated in the knockout strain. The accumulation may directly or indirectly cause the cells to move more from this chemical stimulus.

If the swimming mechanism is sensitive to the accumulation of Gdm^+, leading to a faster swimming phenotype, we added exogenous Gdm^+ to the swimming plates. Observations revealed that both wildtype and Δ*emrE* exhibited a faster swimming pace, comparable to the Gdx knockout (**Figure 3.3C**). Using pathogenic strains (UTI89 *E.coli* cells and *Pseudomonas aeruginosa*) the same faster swimming phenotype was observed with accumulation of Gdm^+ (**Figure 3.10**). To further explore the consequences Gdm^+ accumulation on swimming behavior, it is important to note that one key cellular factor influencing swimming pace is the membrane potential. At constant swimming speed, it has been reported to be at -100 to -130mV. The rotation speed of the flagella is governed by ion movement through stator units on the membrane

and is influenced by pH changes, which consequently fluctuates the membrane potential (Biquet-Bisquert et al., 2021; Naaz et al., 2021). Increased flagellar movement is a result of increased proton influx. This influx of protons decreases the membrane potential, initiating compensary mechanisms to return back to baseline potential (Minamino et al., 2016). Using a membrane potential detection kit, growth samples were analyzed at the log-phase through flow cytometry to monitor shifts in a fluorescent dye (3,3'-diethyloxacarbocyanine iodide (DiOC2(3))). When the cell is healthy and maintaining cell membrane potential the dye will enter the cell and aggregate causing a shift in fluorescence to red (Thomas et al., 2011). Preliminary membrane potential data indicates the Gdx knockout strain exhibited a different fluorescence than wildtype and Δ*emrE* in the Keio collection strains (**Figure 3.11**). The accumulation of Gdm^+ was predicted to initiate compensation mechanisms to maintain the cell membrane potential (indicative to a higher red:green fluorescence ratio). However, our results were opposite of what we expected. This experiment was conducted with LB media which has a slightly different nutrient composition compared to the media which was used for the swimming assays. Tryptone media, which was used for the swimming assays, displayed the result we expected (data not shown and has not been completed in replicates). The fluorescence increased in the knockout cells, which we hypothesize is due to the cell's need to compensate and counter the accumulated positive charges inside the cell from Gdm^+. The precise mechanisms by which Gdm^+ accumulation affects swimming (and biofilms) behavior remain unclear. Although virulence behaviors appear to be more sensitive to this metabolite, additional research is essential to elucidate the exact mechanistic consequences.

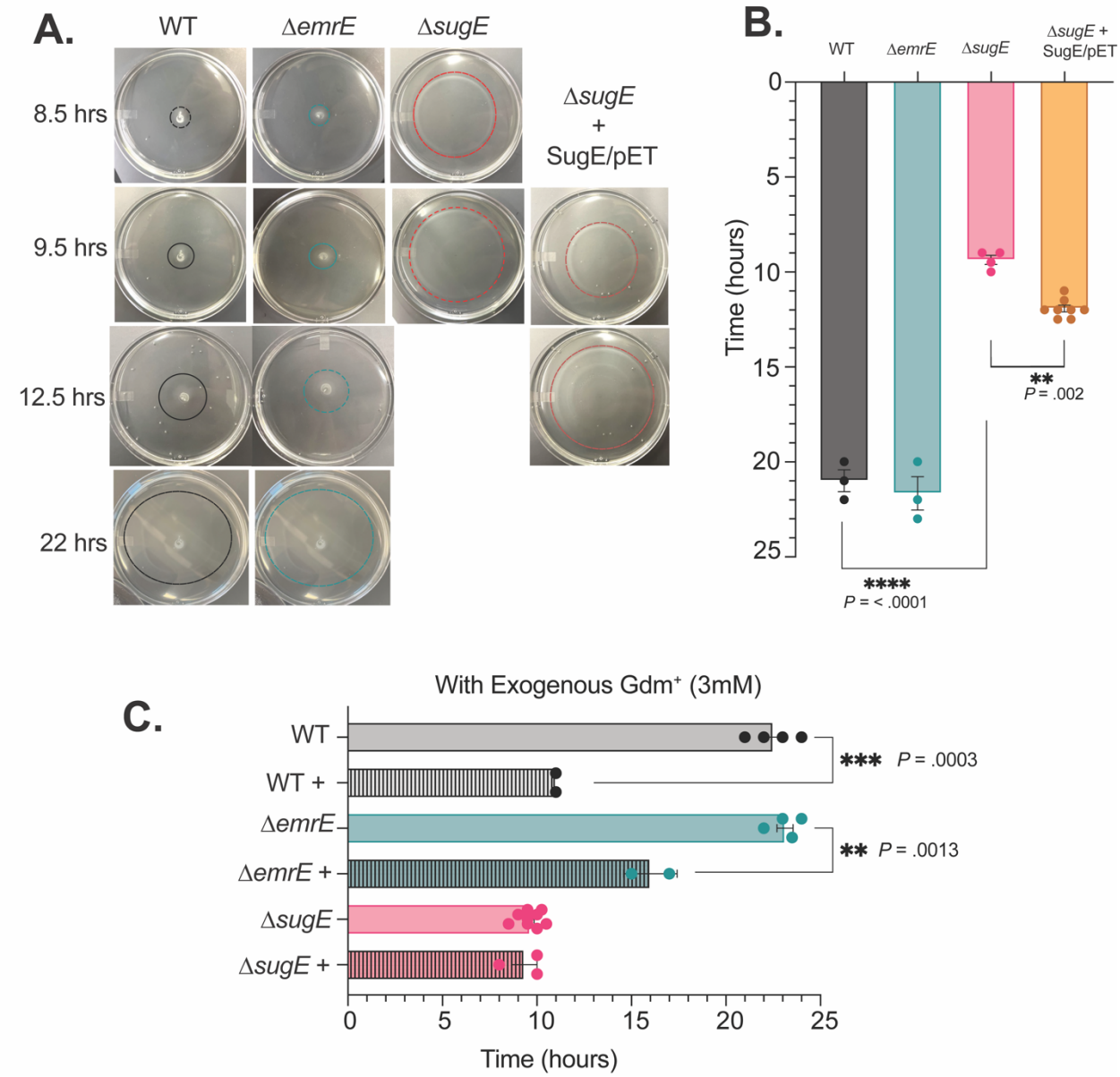

Figure 3.3 Faster swimming in SMR_{Gdx} knockout. A. Images of swimming monitored by measuring the diameter from inoculation point in the middle of the plate which can be rescued and graphed in B against time. C. Swimming rates when 3 mM of Gdm^+ was added to the LB agar plates. Error bars represent the SEM replicate measurement. One-way ANOVA and unpaired t-test analysis was used to determine statistical significance.

3.2.3 Relative fitness of WT and ΔsugE as a function of carbon/nitrogen budget

We have established at this point that exogenous Gdm^+ exhibits a negative effect upon the fitness of the Gdx knockout strain. This distinction was exploited as a tool to ascertain

growth conditions for Gdm^+ production through quantitative analysis through flow cytometry through investigation of various growth conditions that yield guanidine production. First, we tried to use a plasmid to express fluorescence protein for each strain, which the cells containing the plasmid would be selected for ampicillin resistance resulting from the plasmid. There was inconsistent plasmid expression throughout the entirety of the assay (**Figure 3.6**). Unlike chromosomal DNA, plasmids are not equally divided during cells proliferation and can be energetically more favorable for cells to lose the plasmid over time (Bumann et al., 2000; Grozdanov et al., 2002; McKenzie & Craig, 2006). The loss of fluorophore over time will create bias by potentially incorrectly representing a strain in the flow cytometry sorting read-out. Chromosomal expression, on the other hand, provides a single copy and inherent stability (Bumann et al., 2000; Grozdanov et al., 2002; McKenzie & Craig, 2006). To ensure the cell's fitness is not sacrificed with insertion of the fluorophore, the fluorophore gene was inserted downstream of the *glmS* gene, a conserved, cell wall synthesis enzyme for bacteria. It has been reported insertion at this position does not disrupt cell fitness (Craig, 1996; Crépin et al., 2012; Peters & Craig, 2001). To avoid any potential skewed cell population read-outs, each fluorophore (green fluorescent protein (GFP), cyan fluorescent protein (CFP) and yellow fluorescent protein (YFP)) was inserted into the bacterial genome of each strain. One labeled genomic strain was grown with the other non-labeled and observed over time through plating on agar plates and flow cytometry (**Figure 3.7**). There was not any indication of fluorescence loss over time even when the fluorophores were switched between strains. Competition between two genomic labeled strains was tested to further ensure there was not any deviations from previous competition results with high concentrations of exogenous Gdm^+ (**Figure 3.8 and 3.12**).

Genomic labeling was further confirmed stable with competitive growths using different media compositions **(Figure 3.1**, **3.8**, **3.13**, and **3.14).**

Rich media like Luria Broth (LB) (**Figure 3.1** and **3.8**) and tryptone (**Figure 3.13**) were examined first to determine the origin of Gdm^+ production. The knockout was less fit compared to wildtype, but it is difficult to determine the source of Gdm^+ in highly supplemented media. To narrow in, a limited ingredient media (minimal media) was used to control each ingredient in the media. If the exporter is involved in nitrogen metabolism and a detoxification role, the first hypothesis would indicate the metabolite is produced from breakdown of a nitrogen source or from the utilization of amino acid building blocks for various metabolism pathways. Varying the nitrogen and carbon source in minimal media was first targeted (**Figure 3.14**) to see if a nitrogen source, in bacterial nutrients, is the origin of Gdm^+ production in the cell. As we varied the sources in minimal media, there was not a clear distinction in which nitrogen or carbon source is the origin of Gdm^+, therefore both would need to be further unraveled.

Focus on changing the nitrogen source, as Gdm^+ is thought to be involved in nitrogen metabolism, various amino acids that take part in important metabolism pathways were investigated. In addition to amino acids shown in **Figure 3.4**, arginine, arginine and glutamate, ammonium, creatine, creatinine, agmatine, guanylurea, and urea as the nitrogen source did not yield significant fitness differences between the wildtype and knockout that would indicate Gdm^+ production (data not shown). During the amino acid screening the only set of amino acids that yielding a fitness difference was the DEGQS combo (Aspartate (D), Glutamate (E), Glycine (G), Glutamine (Q), Serine (S)), Q and S (**Figure 3.4**). To determine which sole amino acids are contributing to the fitness difference in the DEGQS combo, each amino acid was tested by itself as the sole nitrogen source, and each was taken out one by one from the combo. Glutamine (Q)

and Serine (S) as the sole nitrogen source yielded the wildtype to outcompete the knockout strain. When Glutamine (Q) was taken out of the media from the DEGQS combo nitrogen source, each strain returned back to baseline (50%:50% ratio). This return back to baseline trend was also seen with Serine (S) was removed from the media. On the other hand, an opposite effect was observed when Glutamate (E) was used (as also removed) as the sole nitrogen source. These experiments showed that cellular glutamine: glutamate (Q:E) ratio modulates guanidinium production.

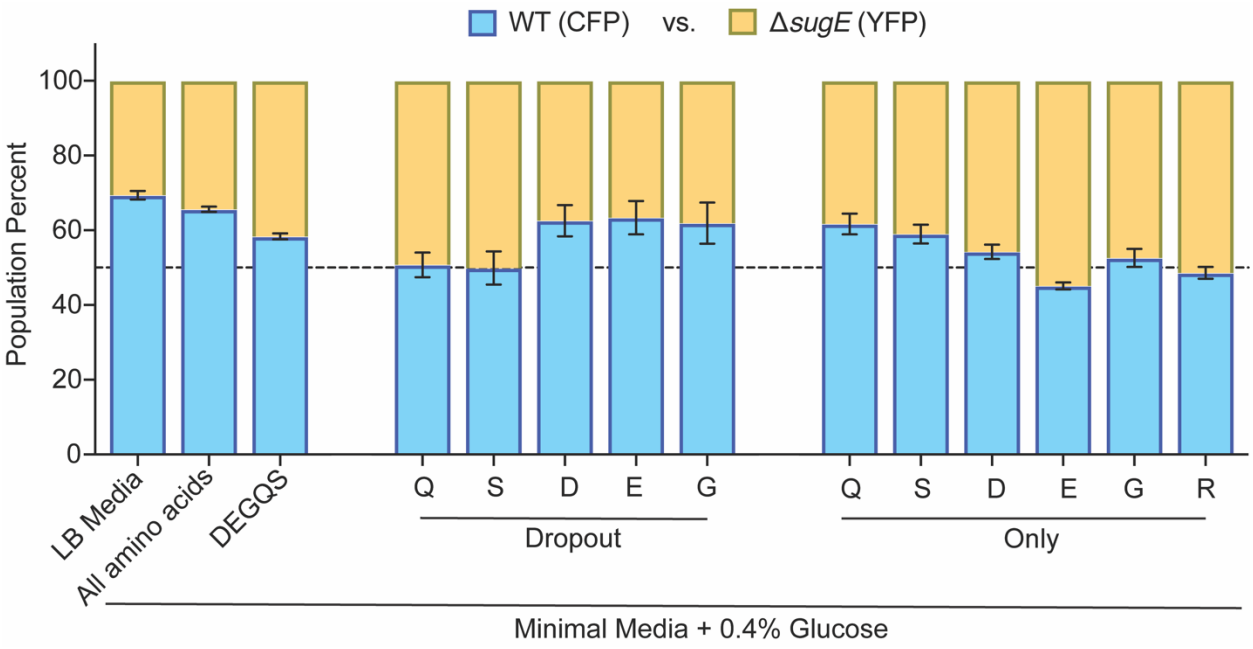

Figure 3.4 Flow cytometry competition assay with DEGQS amino acids as the sole nitrogen source in minimal media with glucose. In the presence of glutamine (Q) and serine (S) the wildtype to knockout ratio is similar to that of rich LB media and minimal media supplemented with all amino acids. 10 mM of individual amino acids were used during the experiment. 2 mM concentration was used when a amino acids were added to the sample. Each amino acid was removed from the combo DEGQS and are indicated as "dropout". The error bars represent the SEM of each replicate of the 24 hour sample. Note that non-fluorescent species (~10-15%) were neglected in the analysis.

Although various nitrogen sources were tested, the carbon source could be the origin of Gdm^+ production or could give insight to how different carbon sources can affect the Gdm^+ production. Bacterial cells exhibit a preference for glucose as their primary carbon source due to

its efficient metabolic conversion pathways (Brückner & Titgemeyer, 2002). While glucose is abundant, bacteria prioritize its uptake and utilization before metabolizing other available carbon sources. However, in the absence of glucose, glycerol can serve as a viable alternative carbon source, with bacteria employing specialized pathways for its catabolism into usable energy (Bren et al., 2016; Hoskisson et al., 2003; Wang et al., 2019). Glucose and glycerol as the primary carbon source was used and a significant difference between the two was observed (**Figure 3.5**). With glycerol, the wildtype strain became more fit compared to the preferred carbon source, glucose. When varying the carbon-source, resulted in a phenotypic trend that seems to be independent of the nitrogen source. While glucose remains the primary carbon source, many bacteria will also preferentially utilize amino acids when available, as they can be directly integrated into central metabolic pathways. Only when the preferred carbon source is limited, would bacteria more extensively metabolize an alternative carbon source, like glycerol. The difference in fitness when glycerol is used could be due to the amino acid being prioritized as the primary carbon source over glycerol. Glucose conditions may alleviate the use of amino acids as a carbon source therefore reducing the potential pathway for Gdm^+ production indicated by the reduced fitness differences. The Δ*sugE* knockout is sensitive to high nitrogen/carbon ratio.

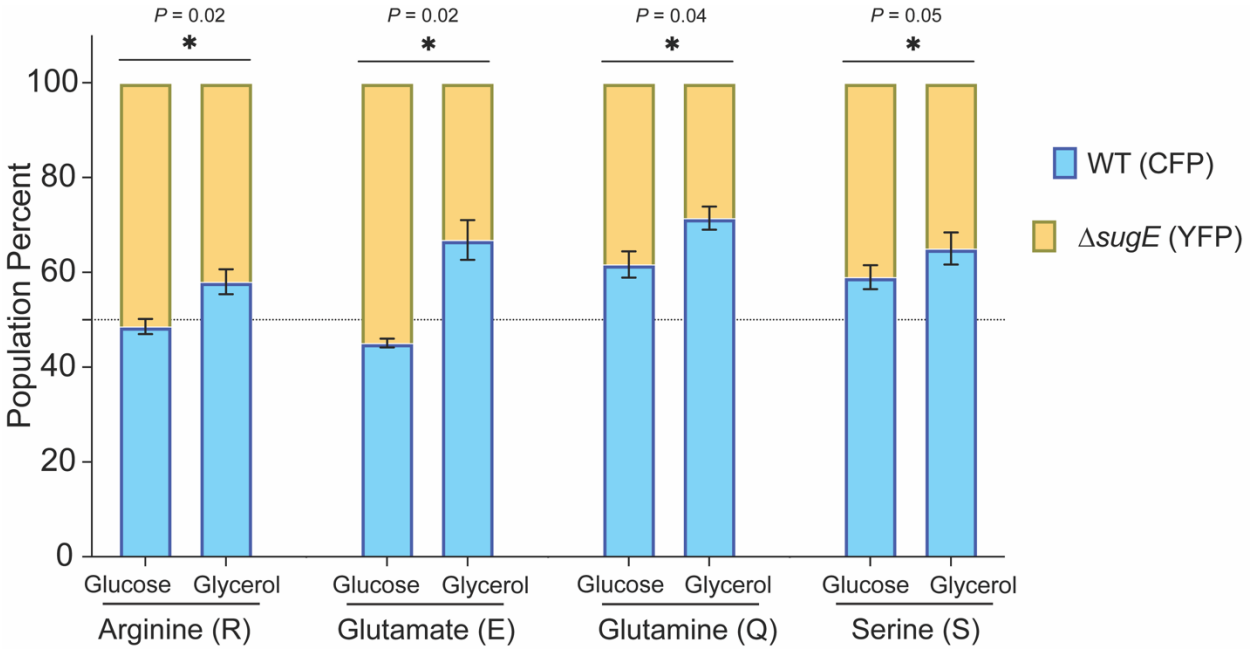

Figure 3.5 Supplemented glucose shows rescue-like affects. Each carbon source was supplemented at 0.4% with 10 mM amino acid. The use of glycerol, wildtype is more fit. With the use of glucose, there is a rescue-like affect which wildtype is almost equally fit. Unpaired t-test was used to determine significance.

3.3 Discussion

It is evident that maintaining Gdm^+ homeostasis is a crucial aspect of bacterial physiology, however, the pathways involving production of Gdm^+ are extremely limited. The only known enzymatic biological pathway for Gdm^+ production has been identified, involving an ethylene-forming enzyme (EFE) that converts arginine and alpha-ketoglutarate to ammonium (Eckert et al., 2014; Wang et al., 2021). This enzyme is absent in bacteria carrying SMR genes and is only in plants and fungi (Biale, 1940; Eckert et al., 2014; Nagahama et al., 1991; Wang et al., 2021). Exploring these homeostatic mechanisms could provide foundational insights into how bacteria manage this specific metabolite and reveal its biological importance.

In this chapter we investigated the biological origin of Gdm^+ while trying to understand the physiological impacts on bacteria. Utilizing a non-pathogenic model system, we determined

the buildup of Gdm^+ ions in a strain lacking the SMR_{Gdx} gene results in diminished growth compared to the wildtype strain. We capitalized on this distinctive phenotype by conducting a competition assay between a strain with the SMR_{Gdx} gene and one without it. Prior evidence suggested that Gdm^+ might be linked to nitrogen metabolism pathways, therefore our competition screen included a variety of simple compounds and precursors, aiming to pinpoint the metabolic pathways where Gdm^+ production might be involved.

Surprisingly, arginine, which contains a guanidinyl group as part of its side chain, did not yield significant fitness disparities between the strains under investigation. Our findings suggest a potential interplay between Gdm^+ production and the cell's balance of carbon and nitrogen. An inverse relationship in fitness distribution between the two strains was observed, emphasizing the role of glutamine and glutamate in monitoring nitrogen homeostasis using the glutamine synthetase (GS) and glutamine oxoglutarate aminotransferase/glutamate synthase (GOGAT) pathway (Hassanov et al., 2018; Helling, 1998; Yan, 2007). Changes in glutamate concentrations also occur when the carbon source is limited or when there are shifts in osmolarity or membrane potential, specifically related to potassium ions (Helling, 1998; Yan, 2007), factors that Gdm^+ may influence. While our technique serves as a valuable screening tool to identify potential pathways for further study, additional experiments are needed to pinpoint the exact metabolic route leading to Gdm^+ production. When glucose, the preferred carbon source, is added to the cultures as the sole carbon source, the observed fitness differences become less pronounced compared to when glycerol is used. In the absence of glucose, cells appear to depend more on amino acids as a carbon source, potentially leading to Gdm^+ production during amino acid catabolism for energy (Bren et al., 2016; Hoskisson et al., 2003; Wang et al., 2019). However, the precise role of Gdm^+ in this context remains elusive. The question remains if Gdm^+ is being

produced during the GS/GOGAT pathway or if it plays a role in the cell's perception of nitrogen and carbon availability.

It is interesting that the result of serine "dropout" closely resembles that of glutamine "dropout", essentially restoring near-equivalent ratios of each strain. Serine is known to participate in purine synthesis, which notably includes structural elements containing guanindinyl groups (Fan et al., 2019). While we haven't explored the connection between serine and guanidinium production, it's worth noting that serine may potentially be related to Bis-(3'-5')-cyclic dimeric guanosine monophosphate (c-di-GMP) second messenger system, which is critically involved in modulating bacterial virulence pathways (Hengge, 2009; Jenal et al., 2017; Miller et al., 2021; Nolan et al., 2023). The c-di-GMP signal acts as regulatory switch for bacterial motility. Elevated levels of this molecule activate genes responsible for biofilm formation, while reduced levels promote biofilm dispersal and bacterial swimming (Hengge, 2009; Jenal et al., 2017; Miller et al., 2021; Nolan et al., 2023). Given that a variety of pathogenic bacterial strains demonstrated sensitivity to Gdm^+ in swimming analysis, it is plausible that this metabolite may intersect with the c-di-GMP synthesis pathway, thereby influencing bacterial virulence states. Interestingly, another nitrogen-based compound, nitrate, has also been shown to alter c-di-GMP signaling, favoring the swimming behavior (Miller et al., 2021). If this relationship is validated, it could present a candidate target for inhibition, as promoting bacterial swimming behavior would render the bacteria more susceptible to antimicrobials agents compared to their biofilm-encased, more resilient counterparts.

3.4 Methods

3.4.1 Bacterial growth curves and resistance assays

Prior to any bacterial growth, competition, biofilm, or resistance assay, overnight cultures were made in LB media with the appropriate antibiotic and were grown at 37°C shaking at 240rpm for 12-18 hours. The following day, precultures were made prior to beginning the assay. The overnight was diluted to OD_{600nm} of 0.1 in fresh LB media supplemented with the appropriate antibiotic and incubated at 37°C until OD_{600nm} reached 0.5 for all assays except for the rugose biofilm assays which the OD_{600nm} was 1.0. During the precultures, rescue plasmid constructs in a pET21 vector, that was transformed into the knockout strain, was expressed as the culture was supplemented with 0.2mM Isopropyl β-D-1-thiogalactopyranoside (IPTG). Sequences of rescue constructs are listed in **Table 3.2**.

Non-pathogenic *E.coli* cell line called the "Keio collection" (wildtype, Δ*sugE*, Δ*emrE*) (Baba 2006) was used for planktonic growth curve analysis, resistance assays, and competition assays. Growth curves were monitored in sterile 250 mL baffled Erlenmeyer flasks containing 100 mL of LB Media at 37°C. Precultures were diluted to an OD_{600nm} of 0.01 and once the cultures reached the log phase (OD_{600nm} 0.5) a range of Gdm^+ concentrations (0, 1, 3, 10, and 30 mM) was added to the cultures and monitored for ten hours. Additionally, 0.2 mM ITPG was added to the cultures that contained the rescue plasmid. Resistance LB agar plates were made with Gdm^+ (0, 1, 3, 10, and 30 mM) and 0.2 mM IPTG. With the OD_{600nm} normalized to 0.5, a series dilution (1:10) was made using sterile 0.9% (*w/v*) NaCl. For each strain, each serial dilution was spotted (5 μL) on each concentration of Gdm^+ plate. Plates were incubated at 37°C overnight and imaged.

3.4.2 UTI89 knockout strain for pellicle and rugose biofilms

Pathogenic UIT89 *E.coli* cell line was used for virulence assays. A SMR_{Gdx} knockout, in frame deletion was made in the UTI89 cell line through lamba red-mediated homologous recombination (Murphy & Campellone, 2003). In brief, primers were designed so that excision of the resistance cassette with the flippase recombinase (FLP) to create an in-frame deletion of the chromosomal gene. To make the lamba red recombinerring system, using the pKD13 plasmid as a template, a PCR product containing a Kanamycin cassette flanked by FLP recognition target (FRT) sites was purified. The product was transformed in UTI89 wildtype cells harboring a temperature sensitive pSIM6 plasmid to induce recombination. Successful knockout and incorporation of the Kanamycin cassette were checked and confirmed through colony PCR. Primers used are listed in **Table 3.1**.

Table 3.1 Primer sequence used to create the Gdx knockout strain in UTI89. Yellow highlights adjacent homologous chromosomal sequences. Red corresponds to *sugE* sequence. Blue highlights sequence homologous to the pKD13 plasmid.

UTI Δ*sugE*	**Primer Sequence**
FWD	5' - AAACGCGTCTTTTCACCGGGGACGGCCCCAATTTTCCGGAGCCTGATATGATTCCGGGGATCCGTCGACC - 3'
REV	5' - AAGTTTATTTGGGTACAGCAGCCCGGTAG**TTA**ATGAGTGCTGAGTTTCAGGTGTAGGCTGGAGCTGCTTCG - 3'

Biofilm assays were conducted as described previously (Evans et al., 2018; Zhou et al., 2012). Sterile YESCA (1 g/L yeast extract, 10 g/L casamino acids, and 20 g/L agar) supplemented with 50 μg/mL Congo Red (CR) plates were made for rugose biofilm plates. For rugose biofilm assay, preculture OD_{600nm} was normalized (1.0) and 4 μL was spotted onto plates and grew at 26°C for 3 days. For the pellicle assay, precultures that were grown in LB media

were diluted to an $OD600_{nm}$ of 1.0 with YESCA media. The cultures were washed two times by pelleting the cells (4,000xg 12 mins) and rinsing the cell pellets with fresh YESCA. In a 24-well plate (2 mL total volume), 2 µL of the washed cultures were added followed by a range of Gdm^+ (0, 1, 3, 10, and 30 mM). Culture plates were incubated at 26°C for two days and then quantitatively analyzed with crystal violet staining as described previously (O'Toole et al., 1999). The pellicle layer was carefully separated from the media and stained with an equal volume of 0.1% (*w/v*) crystal violet. After removing excess dye and washing the biofilms, acetic acid (33%) was added to dissolve the biofilm to read the absorbance of crystal violet at 595nm. Statistical significance was determine using an unpaired t test or one-way ANOVA.

3.4.3 Monitoring swimming behavior

A series of pathogenic and non-pathogenic bacteria models were used to monitor swimming behaviors (Keio *E.coli*, UTI89 *E.coli*, and *Pseudomonas aeruginosa*). Sterile Tryptone (10 g/L tryptone, 5g/L sodium chloride) media with low percentage agar (0.2%) were made for these assays. Following the preculture, the OD_{600nm} was normalized to 0.5 where 4 µL was stabbed in the middle of the agar plate. Each strain had its own designated plate. Plates were incubated at 30°C where the concentric ring diameters were measured and monitored until the diameter reached 6 cm which indicated the end of the assay. Statistical significance was determine using an unpaired t test or one-way ANOVA.

3.4.4 Genomic fluorophore labeling and competition assay

Genomic labeling was conducted as previously described (Crépin et al., 2012; McKenzie & Craig, 2006). The current plasmid used in preliminary trials of plasmid fluorophore expression (pGRG36-Kn-PA1-GFP; Addgene plasmid number 79088 (Yang et al., 2020)), contains the

necessary elements to use Tn7 transposition. Prior to transforming into the knockout strain, the Kanamycin resistance gene that was inserted in the place of the gene, was removed, or "cured". Curing was accomplished using FPL recombination in *E.coli* from the protocol from Barrick lab. The temperature induced plasmid was transformed into wildtype and knockout cells. Using UV light, single colonies were selected and incubated overnight at high temperature (42°C). This temperature induced transposition at the conserved chromosomal attTn7 site. Candidates were selected my "patching" a single colony on a series of LB, LB (with antibiotic selection), and LB agar plates. Successful candidates only grow on the LB plates without selection, indicating the plasmid is no longer in the cell.

Competition assays as were conducted as described in (Stannek et al., 2014). Cultures were grown in sterile 125 mL baffled Erlenmeyer flasks containing 25 mL of unique media at 37°C. Media compositions included LB, Tryptone, and Minimal Media (1X M9 salts (6 g/L Na_2HPO_4; 3 g/L KH_2PO_4; 0.5 g/L NaCl), 100 µM $CaCl_2$, 2 mM $MgSO_4$, 1X vitamins), supplemented with either 19 mM NH_4Cl, "EZ" supplement with all amino acids (Cat #M2014), a combo amino acids at 2 mM, 10 mM individual amino acids or 10 mM of precursors as the nitrogen source. Each condition was supplemented with 0.4% (*w/v*) glucose or glycerol as the carbon source. Overnight cultures were diluted to an OD_{600nm} of 0.05 for each fluorophore strain (WT/CFP and Δ*sugE*/YFP). Each strain was added at a 1:1 (OD 0.05:OD 0.05) ratio. Before incubating, half of the inoculated media (12.5 mL) was pelleted (10 minutes 4,000 x g). Pellet was resuspended and 500 µL of fresh media and 50 µL of 50% glycerol (*v/v*) in a cryotube to be store in -80°C until ready to analyze. At each time point, the OD was measured and a sample with an OD of 1.0 (total volume of 1mL) was collected for each culture (10^9 cells/mL). Time points at 7 and 24 hours were taken from the cultures that were incubated at 37°C, 240 rpm. To

prepare for analyzing the samples on the flow cytometer (Thermo Fisher Scientific NxT Attune), samples were diluted 1,000-fold (10^6 cells/mL). YFP (λ_{ex} = 516 and λ_{em} = 529em) and CFP (λ_{ex} = 433 and λ_{em} = 475) lasers were used to sort ~100 µL of the diluted sample yielding ~100,000 cell count. For plating on agar plates, cultures were diluted 100,000-fold (10^4 cells/mL). Statistical significance was determine using an unpaired t test or one-way ANOVA.

3.5 Appendix

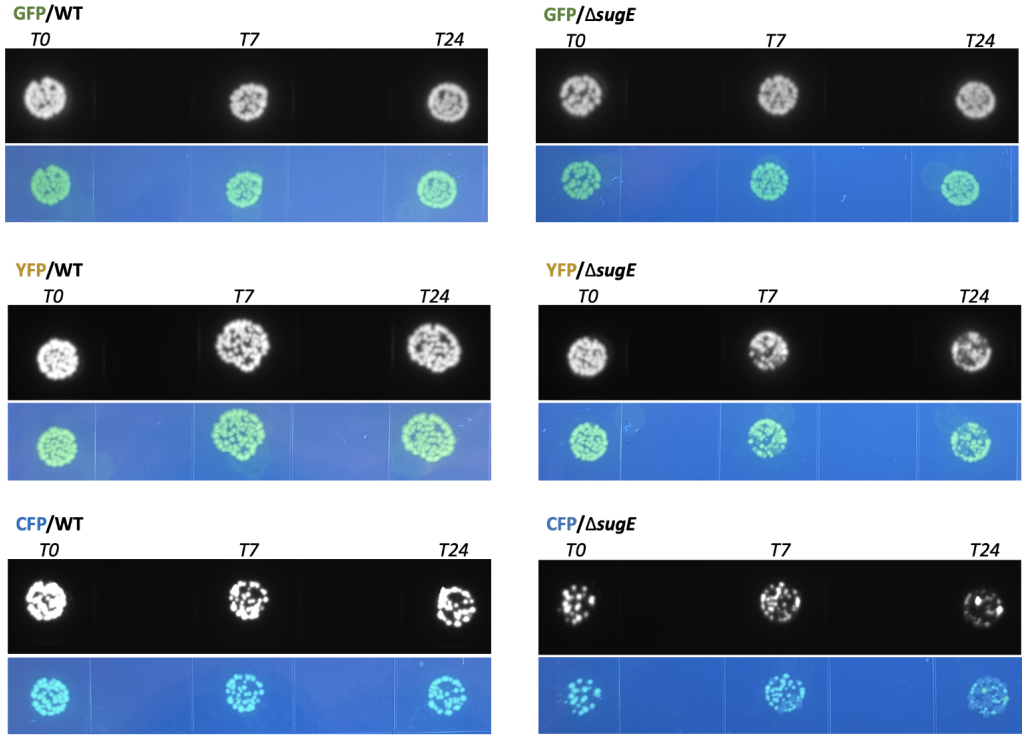

Figure 3.6 Plasmid containing fluorophore expression loss over time. GFP, YFP, and CFP fluorophores expressed in a pGRG36 plasmid in wildtype and knockout strains spotted on LB agar plates. The fluorophores were visualized under UV (λ_{ex} = 280nm – bottom panels) and white light (top panels). Plasmid loss is indicated by the decrease of fluorescence over time.

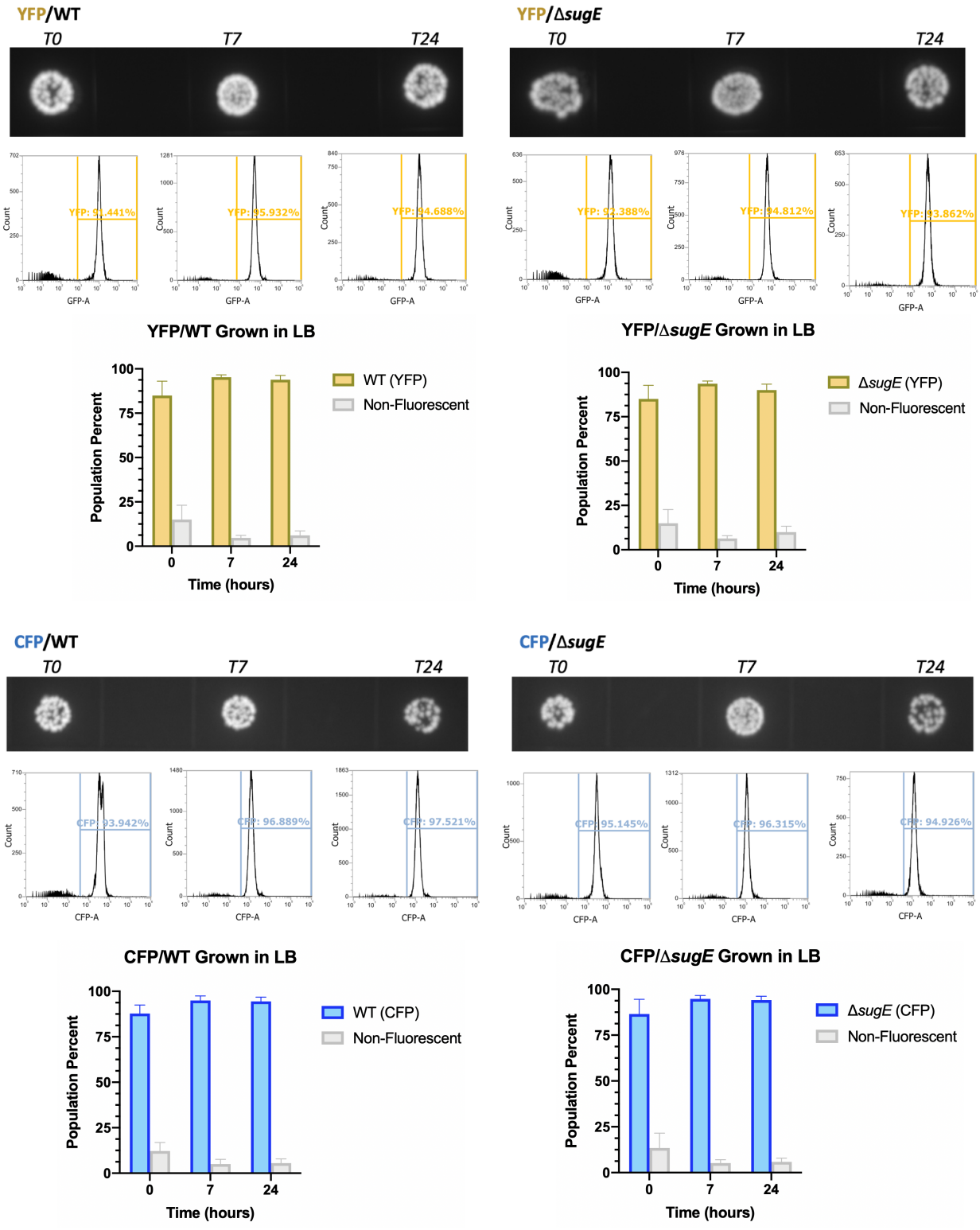

Figure 3.7 Genomic fluorophore labeling in Keio collection cell line is stable. The stability of YFP (top) and CFP (bottom) within the chromosome was spotted on LB agar and quantified using flow cytometry. Fluorophore levels maintained consistency. Note that a population of non-fluorescent species (~10-15%) is present.

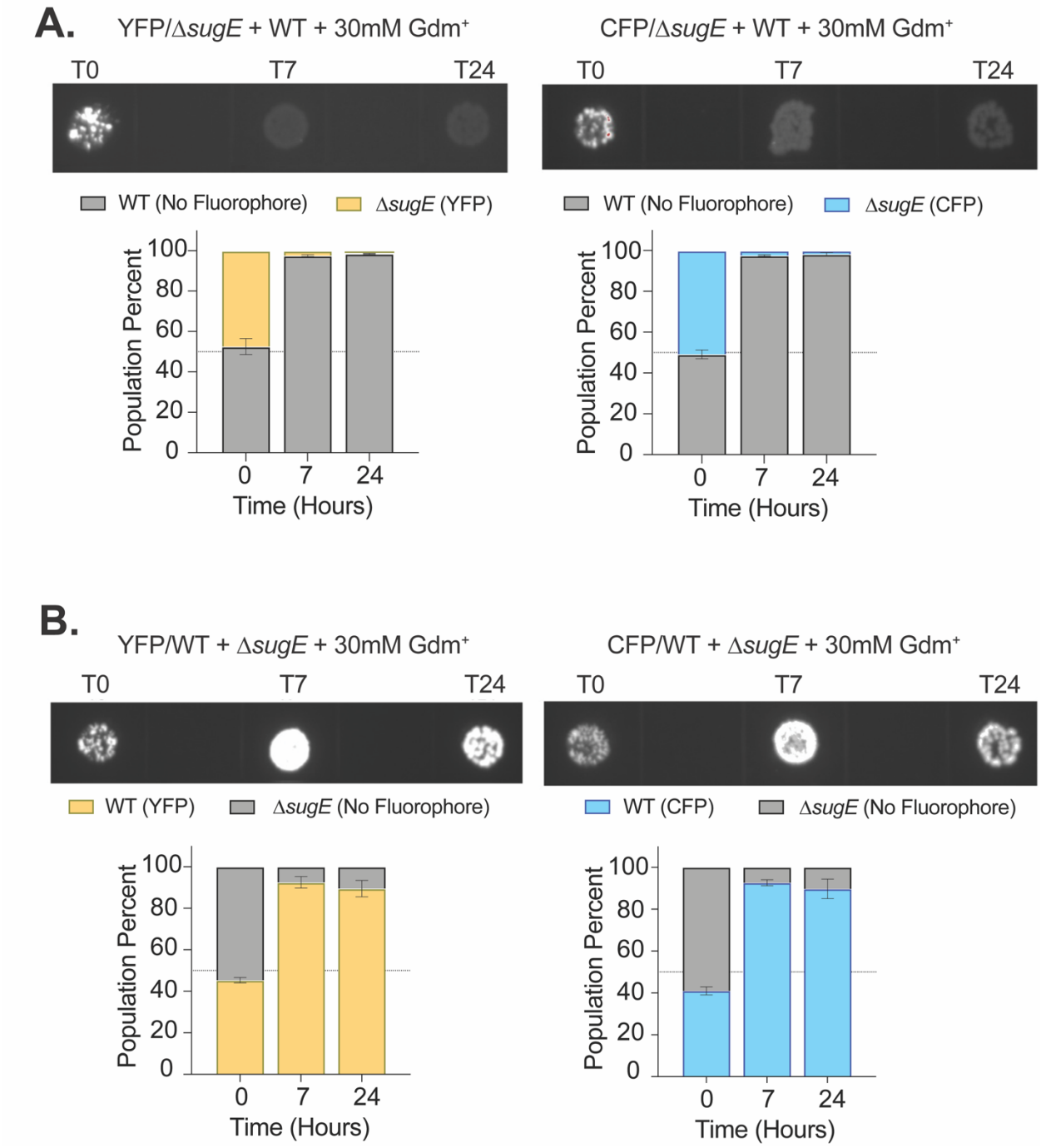

Figure 3.8 Distinction between genomic fluorophore strain labeling can be seen. 30 mM Gdm^+ was added to determine if wildtype is more fit than the knockout as a control. Stability was monitored through plating on agar plates and quantitatively through flow cytometry. No side effects were determined when each isogenic strain was labeled with each fluorophore. Error bars indicate SEM for replicates.

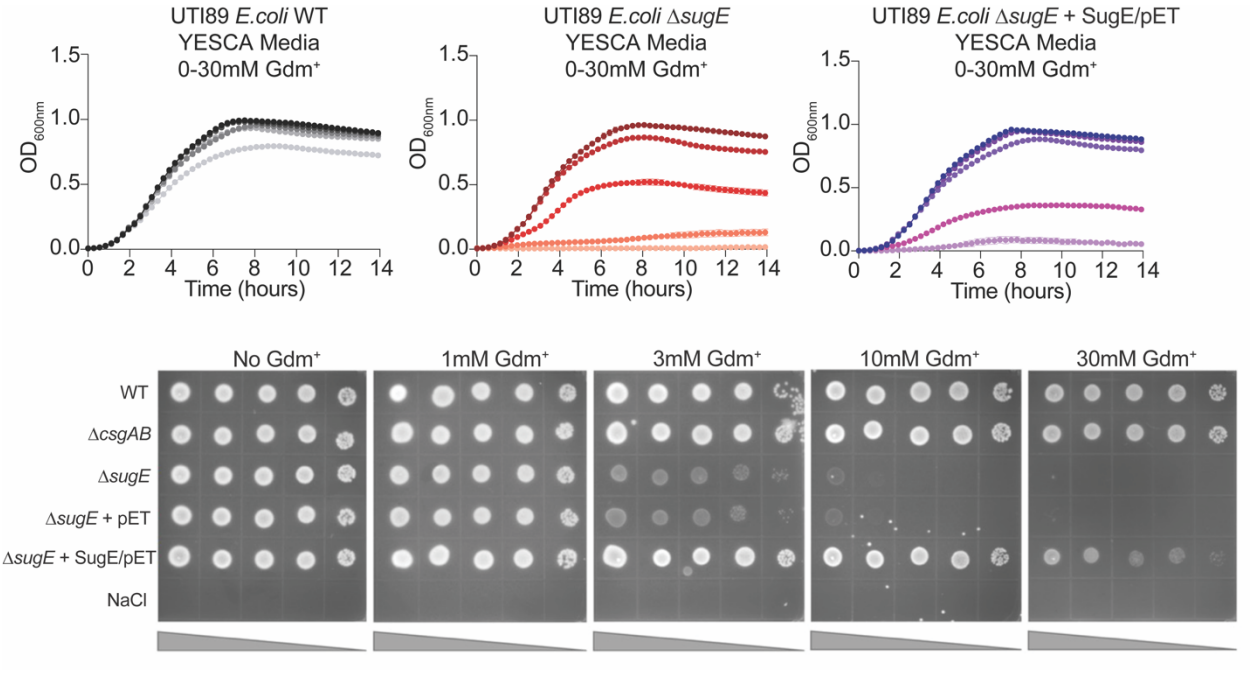

Figure 3.9 UTI89 *E.coli* Gdm^+ resistance in YESCA media. Liquid growth curves (top) with increasing Gdm^+ concentrations (0, 1, 3, 10, 30mM) indicated by the transition from dark (no Gdm^+) to light colors (30mM Gdm^+) and resistance spotting assay (bottom) demonstrating SugE in UTI89 cells confer resistance to Gdm^+. Inserting a plasmid containing UTI SMR_{Gdx} or SugE, can rescue the knockout's decreased fitness.

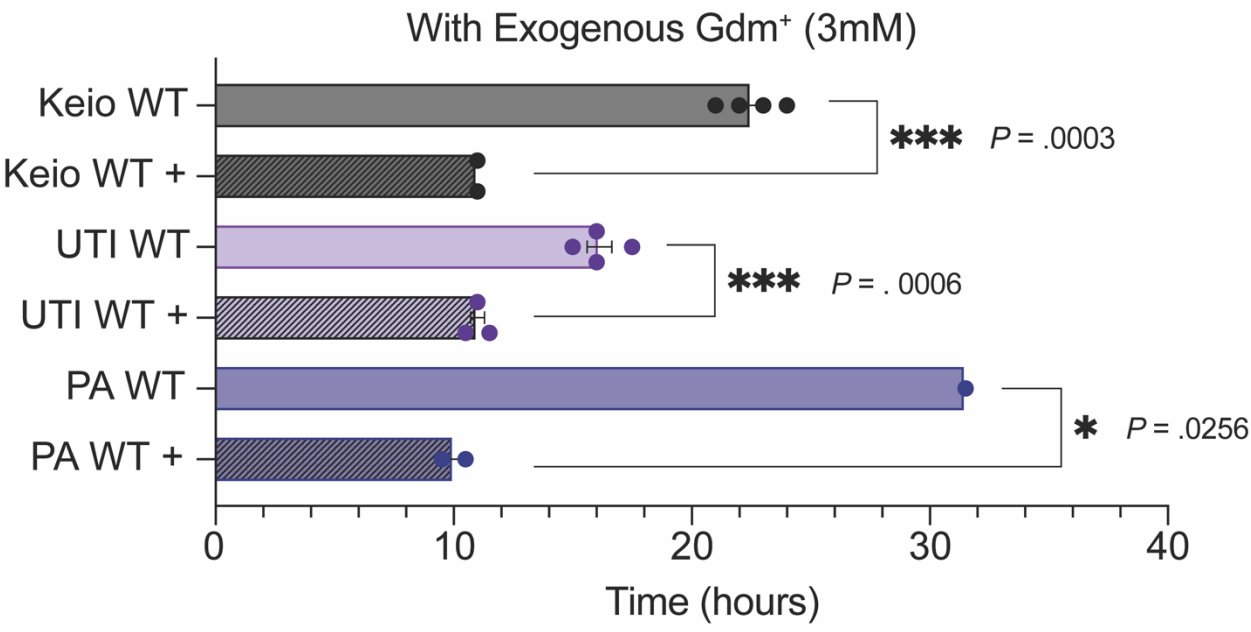

Figure 3.10 Pathogenic strains used to determine swimming rates with 3 mM Gdm^+. Strains include: Keio *E.coli*, UTI89 *E.coli*, and *Pseudomonas aeruginosa*. Error bars represent the SEM replicate measurement. Unpaired t-test analysis was used to determine statistical significance.

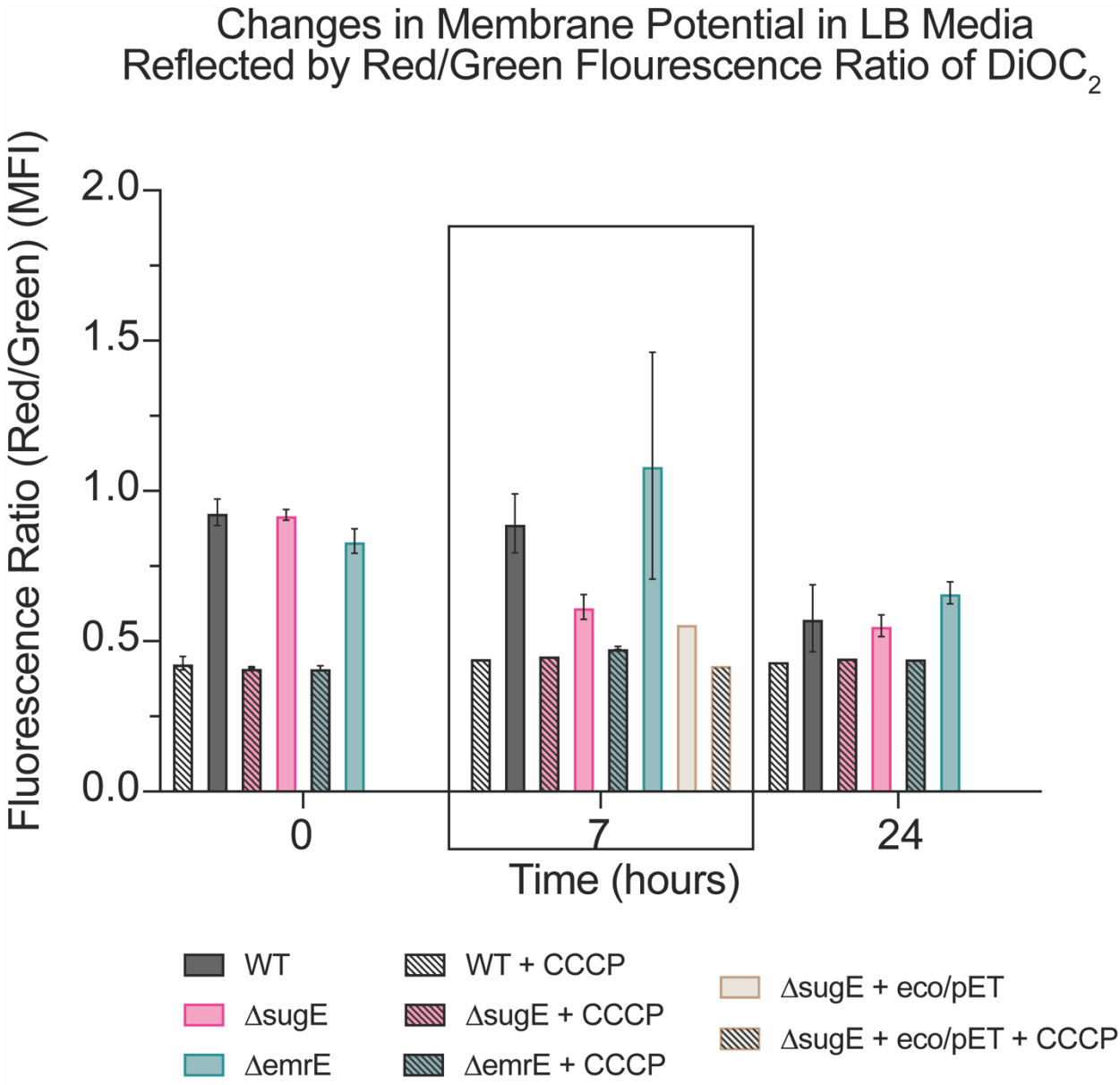

Figure 3.11 Flow cytometry membrane potential determination using BacLight bacterial membrane potential kit. Best determination of membrane potential differences is during log-phase (boxed time point). The buildup of endogenous metabolite alters the membrane potential. Transporter knockout exhibits similar fluorescence as controls using CCCP that eliminate membrane potential in the cell.

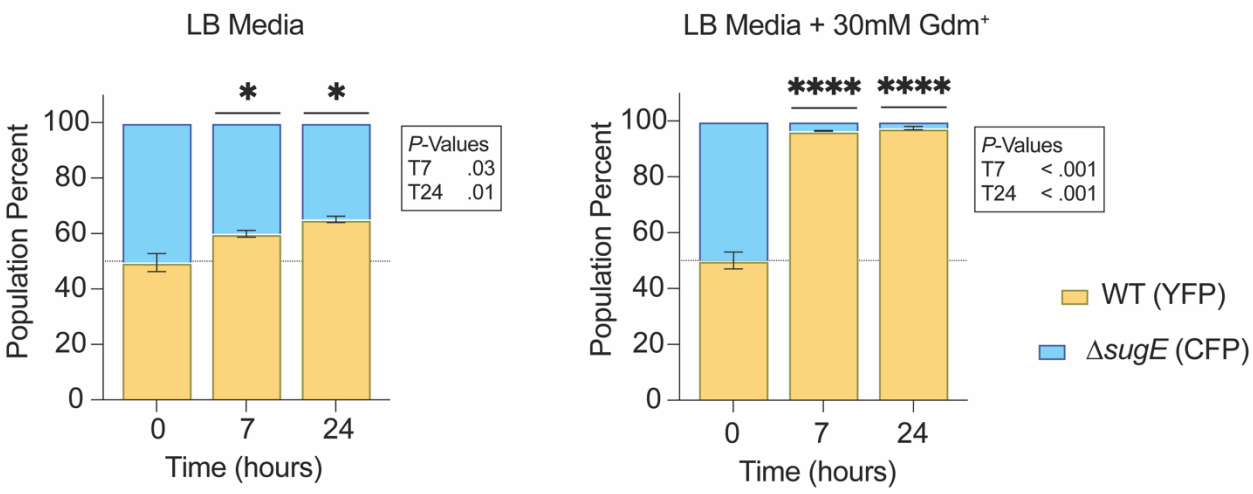

Figure 3.12 Each Keio strain fluorophore label was switched. No indication of major changes in the fluorophore switch.

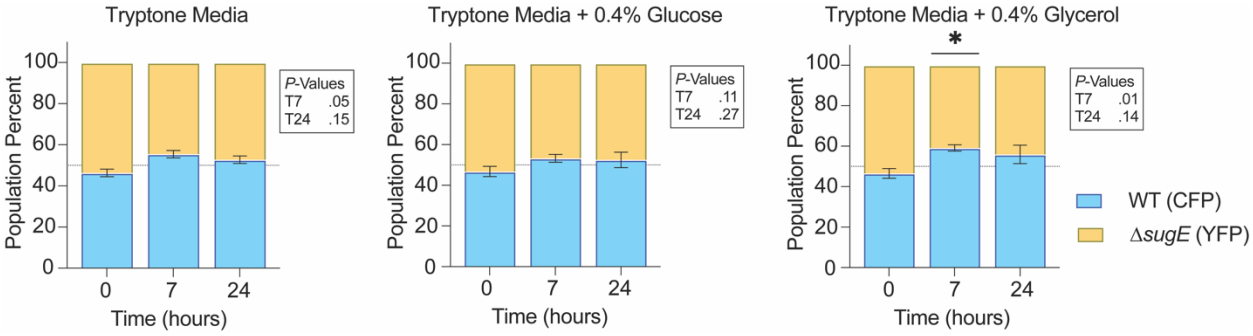

Figure 3.13 Competition assay using various carbon sources in tryptone media.

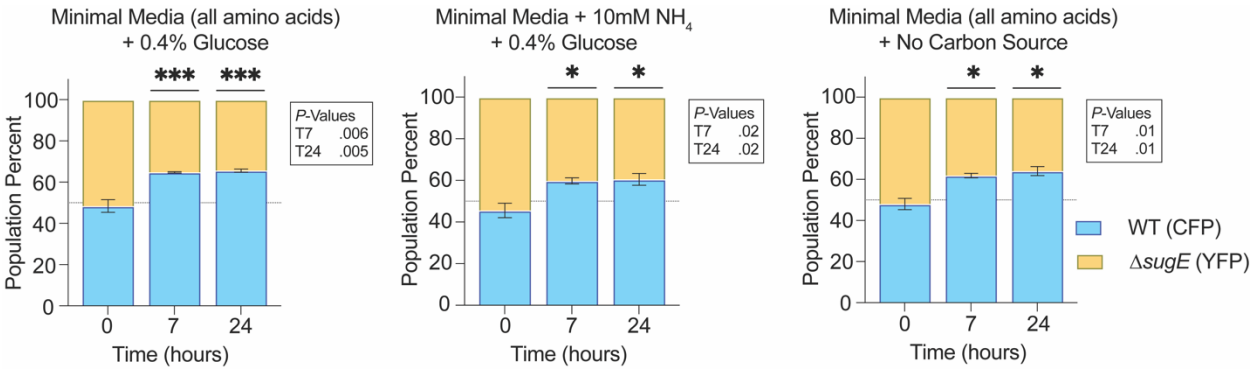

Figure 3.14 Competition assay using various carbon and nitrogen sources in minimal media.

Table 3.2 Coding sequences of rescue constructs in this chapter. Blue indicates predicted promoter region upstream of the Gdx gene.

Construct	Coding Sequence
Keio SugE/pET	ATGAGCTGGATCATTCTGGTGATCGCGGGCCTGCTGGAAGTGGTTTGGGCGGTTGGC CTGAAGTACACCCACGGTTTCAGCCGTCTGACCCCGAGCGTGATTACCGTTACCGCG ATGGTGGTTAGCATGGCGCTGCTGGCGTGGGCGATGAAAAGCCTGCCGGTGGGTACC GCGTATGCGGTTTGGACCGGTATTGGTGCGGTGGGTGCGGCGATCACCGGCATTGTT CTGTTTGGTGAAAGCGCGAACCCGATGCGTCTGGCGAGCCTGGCGCTGATTGTGCTG GGTATCATTGGCCTGAAGCTGAGCACCCATTAATAA
UTI SugE/pET	**GCAATAACGGTACGACAGCTGTGTCGTGCCGTTTGTTTTTTCTGCGATAGTTAC** **ATAGGTAATAGTTGAAATTCCCCTGCCACCTGGCAAAATATCCGTTCAACCATCA** **GCTTTGCAGGACGACCTGCAAACGCGTCTTTTCACCGGGGACGGCCCCAATTTT** **CCGGAGCCTGAT**ATGTCCTGGATTATCTTAGTTATTGCTGGTCTGCTGGAAGTGGTA TGGGCCGTTGGCCTGAAATATACTCACGGCTTTAGTCGTTTGACGCCAAGTGTTATTA CCGTGACGGCGATGATTGTCAGTCTGGCGCTACTTGCCTGGGCGATGAAATCGTTACC AGTAGGGACGGCTTATGCCGTGTGGACGGGTATTGGCGCAGTCGGCGCGGCCATCAC CGGCATTGTGCTGCTCGGTGAGTCCGCTAACCCGATGCGCCTGGCGAGTCTGGCGTTA ATCGTATTGGGGATTATTGGTCTGAAACTCAGCACTCATTAA

3.6 References

Adler, J. (1969). Chemoreceptors in bacteria. *Science*, *166*(3913), 1588-1597. https://doi.org/10.1126/science.166.3913.1588

Andrews, J. S., Rolfe, S. A., Huang, W. E., Scholes, J. D., & Banwart, S. A. (2010). Biofilm formation in environmental bacteria is influenced by different macromolecules depending on genus and species. *Environ Microbiol*, *12*(9), 2496-2507. https://doi.org/10.1111/j.1462-2920.2010.02223.x

Baba, T., Ara, T., Hasegawa, M., Takai, Y., Okumura, Y., Baba, M., Datsenko, K. A., Tomita, M., Wanner, B. L., & Mori, H. (2006). Construction of Escherichia coli K-12 in-frame, single-gene knockout mutants: the Keio collection. *Mol Syst Biol*, *2*, 2006.0008. https://doi.org/10.1038/msb4100050

Berg, H. C., & Anderson, R. A. (1973). Bacteria Swim by Rotating their Flagellar Filaments. *Nature*, *245*(5425), 380-382. https://doi.org/10.1038/245380a0

Biale, J. B. (1940). Effect of Emanations from Several Species of Fungi on Respiration and Color Development of Citrus Fruits. *Science*, *91*(2367), 458-459. https://doi.org/doi:10.1126/science.91.2367.458.b

Biquet-Bisquert, A., Labesse, G., Pedaci, F., & Nord, A. L. (2021). The Dynamic Ion Motive Force Powering the Bacterial Flagellar Motor. *Front Microbiol*, *12*, 659464. https://doi.org/10.3389/fmicb.2021.659464

Bren, A., Park, J. O., Towbin, B. D., Dekel, E., Rabinowitz, J. D., & Alon, U. (2016). Glucose becomes one of the worst carbon sources for E.coli on poor nitrogen sources due to suboptimal levels of cAMP. *Scientific Reports*, *6*(1), 24834. https://doi.org/10.1038/srep24834

Brown, D. A., & Berg, H. C. (1974). Temporal Stimulation of Chemotaxis in Escherichia coli. *Proceedings of the National Academy of Sciences*, *71*(4), 1388-1392. https://doi.org/doi:10.1073/pnas.71.4.1388

Brückner, R., & Titgemeyer, F. (2002). Carbon catabolite repression in bacteria: choice of the carbon source and autoregulatory limitation of sugar utilization. *FEMS Microbiology Letters*, *209*(2), 141-148. https://doi.org/10.1111/j.1574-6968.2002.tb11123.x

Bumann, D., Hueck, C., Aebischer, T., & Meyer, T. F. (2000). Recombinant live Salmonella spp. for human vaccination against heterologous pathogens. *FEMS Immunol Med Microbiol*, *27*(4), 357-364. https://doi.org/10.1111/j.1574-695X.2000.tb01450.x

Cegelski, L., Pinkner, J. S., Hammer, N. D., Cusumano, C. K., Hung, C. S., Chorell, E., Aberg, V., Walker, J. N., Seed, P. C., Almqvist, F., Chapman, M. R., & Hultgren, S. J. (2009). Small-molecule inhibitors target Escherichia coli amyloid biogenesis and biofilm formation. *Nat Chem Biol*, *5*(12), 913-919. https://doi.org/10.1038/nchembio.242

Cho, K. H., Tryon, R. G., & Kim, J.-H. (2020). Screening for Diguanylate Cyclase (DGC) Inhibitors Mitigating Bacterial Biofilm Formation [Review]. *Frontiers in Chemistry*, *8*. https://doi.org/10.3389/fchem.2020.00264

Craig, N. L. (1996). Transposon Tn7. In H. Saedler & A. Gierl (Eds.), *Transposable Elements* (pp. 27-48). Springer Berlin Heidelberg. https://doi.org/10.1007/978-3-642-79795-8_2

Crépin, S., Harel, J., & Dozois, C. M. (2012). Chromosomal complementation using Tn7 transposon vectors in Enterobacteriaceae. *Appl Environ Microbiol*, *78*(17), 6001-6008. https://doi.org/10.1128/aem.00986-12

Eckert, C., Xu, W., Xiong, W., Lynch, S., Ungerer, J., Tao, L., Gill, R., Maness, P. C., & Yu, J. (2014). Ethylene-forming enzyme and bioethylene production. *Biotechnol Biofuels*, *7*(1), 33. https://doi.org/10.1186/1754-6834-7-33

Evans, M. L., Chorell, E., Taylor, J. D., Åden, J., Götheson, A., Li, F., Koch, M., Sefer, L., Matthews, S. J., Wittung-Stafshede, P., Almqvist, F., & Chapman, M. R. (2015). The bacterial curli system possesses a potent and selective inhibitor of amyloid formation. *Mol Cell*, *57*(3), 445-455. https://doi.org/10.1016/j.molcel.2014.12.025

Evans, M. L., Gichana, E., Zhou, Y., & Chapman, M. R. (2018). Bacterial Amyloids. *Methods Mol Biol*, *1779*, 267-288. https://doi.org/10.1007/978-1-4939-7816-8_17

Fan, T. W. M., Bruntz, R. C., Yang, Y., Song, H., Chernyavskaya, Y., Deng, P., Zhang, Y., Shah, P. P., Beverly, L. J., Qi, Z., Mahan, A. L., Higashi, R. M., Dang, C. V., & Lane, A. N. (2019). De novo synthesis of serine and glycine fuels purine nucleotide biosynthesis in human lung cancer tissues. *J Biol Chem*, *294*(36), 13464-13477. https://doi.org/10.1074/jbc.RA119.008743

Grozdanov, L., Zähringer, U., Blum-Oehler, G., Brade, L., Henne, A., Knirel, Y. A., Schombel, U., Schulze, J., Sonnenborn, U., Gottschalk, G., Hacker, J., Rietschel, E. T., & Dobrindt, U. (2002). A single nucleotide exchange in the wzy gene is responsible for the semirough O6 lipopolysaccharide phenotype and serum sensitivity of Escherichia coli strain Nissle 1917. *J Bacteriol*, *184*(21), 5912-5925. https://doi.org/10.1128/jb.184.21.5912-5925.2002

Güthner, T., Mertschenk, B., & Schulz, B. (2006). Guanidine and Derivatives. In *Ullmann's Encyclopedia of Industrial Chemistry*. https://doi.org/https://doi.org/10.1002/14356007.a12_545.pub2

Hassanov, T., Karunker, I., Steinberg, N., Erez, A., & Kolodkin-Gal, I. (2018). Novel antibiofilm chemotherapies target nitrogen from glutamate and glutamine. *Scientific Reports*, *8*(1), 7097. https://doi.org/10.1038/s41598-018-25401-z

Helling, R. B. (1998). Pathway choice in glutamate synthesis in Escherichia coli. *J Bacteriol*, *180*(17), 4571-4575. https://doi.org/10.1128/jb.180.17.4571-4575.1998

Hengge, R. (2009). Principles of c-di-GMP signalling in bacteria. *Nature Reviews Microbiology*, *7*(4), 263-273. https://doi.org/10.1038/nrmicro2109

Hoskisson, P. A., Sharples, G. P., & Hobbs, G. (2003). The importance of amino acids as carbon sources for Micromonospora echinospora (ATCC 15837). *Lett Appl Microbiol*, *36*(5), 268-271. https://doi.org/10.1046/j.1472-765x.2003.01306.x

Hung, C., Zhou, Y., Pinkner, J. S., Dodson, K. W., Crowley, J. R., Heuser, J., Chapman, M. R., Hadjifrangiskou, M., Henderson, J. P., & Hultgren, S. J. (2013). Escherichia coli biofilms have an organized and complex extracellular matrix structure. *mBio*, *4*(5), e00645-00613. https://doi.org/10.1128/mBio.00645-13

Jenal, U., Reinders, A., & Lori, C. (2017). Cyclic di-GMP: second messenger extraordinaire. *Nature Reviews Microbiology*, *15*(5), 271-284. https://doi.org/10.1038/nrmicro.2016.190

Kermani, A. A., Macdonald, C. B., Gundepudi, R., & Stockbridge, R. B. (2018). Guanidinium export is the primal function of SMR family transporters. *Proc Natl Acad Sci U S A*, *115*(12), 3060-3065. https://doi.org/10.1073/pnas.1719187115

McKenzie, G. J., & Craig, N. L. (2006). Fast, easy and efficient: site-specific insertion of transgenes into Enterobacterial chromosomes using Tn7 without need for selection of the insertion event. *BMC Microbiology*, *6*(1), 39. https://doi.org/10.1186/1471-2180-6-39

Miller, A. L., Nicastro, L. K., Bessho, S., Grando, K., White, A. P., Zhang, Y., Queisser, G., Buttaro, B. A., & Tükel, Ç. (2021). Nitrate Is an Environmental Cue in the Gut for

Salmonella enterica Serovar Typhimurium Biofilm Dispersal through Curli Repression and Flagellum Activation via Cyclic-di-GMP Signaling. *mBio*, *13*(1), e0288621. https://doi.org/10.1128/mbio.02886-21

Minamino, T., Morimoto, Y. V., Hara, N., Aldridge, P. D., & Namba, K. (2016). The bacterial flagellar type III export gate complex is a dual fuel engine that can use both H+ and Na+ for flagellar protein export. *PLoS pathogens*, *12*(3), e1005495.

Morales-Soto, N., Anyan, M. E., Mattingly, A. E., Madukoma, C. S., Harvey, C. W., Alber, M., Déziel, E., Kearns, D. B., & Shrout, J. D. (2015). Preparation, imaging, and quantification of bacterial surface motility assays. *J Vis Exp*(98). https://doi.org/10.3791/52338

Mulcahy, H., Charron-Mazenod, L., & Lewenza, S. (2008). Extracellular DNA chelates cations and induces antibiotic resistance in Pseudomonas aeruginosa biofilms. *PLoS Pathog*, *4*(11), e1000213. https://doi.org/10.1371/journal.ppat.1000213

Murphy, K. C., & Campellone, K. G. (2003). Lambda Red-mediated recombinogenic engineering of enterohemorrhagic and enteropathogenic E. coli. *BMC Mol Biol*, *4*, 11. https://doi.org/10.1186/1471-2199-4-11

Naaz, F., Agrawal, M., Chakraborty, S., Tirumkudulu, M. S., & Venkatesh, K. V. (2021). Ligand sensing enhances bacterial flagellar motor output via stator recruitment. *Elife*, *10*, e62848. https://doi.org/10.7554/eLife.62848

Nagahama, K., Ogawa, T., Fujii, T., Tazaki, M., Tanase, S., Morino, Y., & Fukuda, H. (1991). Purification and properties of an ethylene-forming enzyme from Pseudomonas syringae pv. phaseolicola PK2. *Microbiology*, *137*(10), 2281-2286. https://doi.org/https://doi.org/10.1099/00221287-137-10-2281

Nelson, J. W., Atilho, R. M., Sherlock, M. E., Stockbridge, R. B., & Breaker, R. R. (2017). Metabolism of Free Guanidine in Bacteria Is Regulated by a Widespread Riboswitch Class. *Mol Cell*, *65*(2), 220-230. https://doi.org/10.1016/j.molcel.2016.11.019

Nolan, A. C., Zeden, M. S., Kviatkovski, I., Campbell, C., Urwin, L., Corrigan, R. M., Gründling, A., & O'Gara, J. P. (2023). Purine Nucleosides Interfere with c-di-AMP Levels and Act as Adjuvants To Re-Sensitize MRSA To β-Lactam Antibiotics. *mBio*, *14*(1), e0247822. https://doi.org/10.1128/mbio.02478-22

O'Toole, G. A., Pratt, L. A., Watnick, P. I., Newman, D. K., Weaver, V. B., & Kolter, R. (1999). Genetic approaches to study of biofilms. In *Methods in Enzymology* (Vol. 310, pp. 91-109). Academic Press. https://doi.org/https://doi.org/10.1016/S0076-6879(99)10008-9

Peters, J. E., & Craig, N. L. (2001). Tn7: smarter than we thought. *Nat Rev Mol Cell Biol*, *2*(11), 806-814. https://doi.org/10.1038/35099006

Qasim, M. A., & Taha, M. (2013). Investigation of the mechanism of protein denaturation by guanidine hydrochloride-induced dissociation of inhibitor-protease complexes. *Protein Pept Lett*, *20*(2), 187-191. https://doi.org/10.2174/092986613804725217

Sherlock, M. E., & Breaker, R. R. (2017). Biochemical Validation of a Third Guanidine Riboswitch Class in Bacteria. *Biochemistry*, *56*(2), 359-363. https://doi.org/10.1021/acs.biochem.6b01271

Sherlock, M. E., Malkowski, S. N., & Breaker, R. R. (2017). Biochemical Validation of a Second Guanidine Riboswitch Class in Bacteria. *Biochemistry*, *56*(2), 352-358. https://doi.org/10.1021/acs.biochem.6b01270

Sinn, M., Hauth, F., Lenkeit, F., Weinberg, Z., & Hartig, J. S. (2021). Widespread bacterial utilization of guanidine as nitrogen source. *Mol Microbiol*, *116*(1), 200-210. https://doi.org/10.1111/mmi.14702

Stannek, L., Egelkamp, R., Gunka, K., & Commichau, F. M. (2014). Monitoring intraspecies competition in a bacterial cell population by cocultivation of fluorescently labelled strains. *J Vis Exp*(83), e51196. https://doi.org/10.3791/51196

Thomas, R. J., Webber, D., Hopkins, R., Frost, A., Laws, T., Jayasekera, P. N., & Atkins, T. (2011). The Cell Membrane as a Major Site of Damage during Aerosolization of Escherichia coli. *Applied and Environmental Microbiology*, *77*(3), 920-925. https://doi.org/doi:10.1128/AEM.01116-10

Wang, B., Xu, Y., Wang, X., Yuan, J. S., Johnson, C. H., Young, J. D., & Yu, J. (2021). A guanidine-degrading enzyme controls genomic stability of ethylene-producing cyanobacteria. *Nature Communications*, *12*(1), 5150. https://doi.org/10.1038/s41467-021-25369-x

Wang, X., Xia, K., Yang, X., & Tang, C. (2019). Growth strategy of microbes on mixed carbon sources. *Nature Communications*, *10*(1), 1279. https://doi.org/10.1038/s41467-019-09261-3

Yan, D. (2007). Protection of the glutamate pool concentration in enteric bacteria. *Proceedings of the National Academy of Sciences*, *104*(22), 9475-9480. https://doi.org/doi:10.1073/pnas.0703360104

Yan, J., Monaco, H., & Xavier, J. B. (2019). The Ultimate Guide to Bacterial Swarming: An Experimental Model to Study the Evolution of Cooperative Behavior. *Annual Review of Microbiology*, *73*(1), 293-312. https://doi.org/10.1146/annurev-micro-020518-120033

Yang, D. D., Alexander, A., Kinnersley, M., Cook, E., Caudy, A., Rosebrock, A., & Rosenzweig, F. (2020). Fitness and Productivity Increase with Ecotypic Diversity among Escherichia coli Strains That Coevolved in a Simple, Constant Environment. *Appl Environ Microbiol*, *86*(8). https://doi.org/10.1128/aem.00051-20

Zhou, Y., Blanco, L. P., Smith, D. R., & Chapman, M. R. (2012). Bacterial amyloids. *Methods Mol Biol*, *849*, 303-320. https://doi.org/10.1007/978-1-61779-551-0_21

Chapter 4 Conclusions and Future Directions

4.1 Conclusions

Efflux pumps act as essential mediators between the intracellular and extracellular environments, significantly contributing to the mechanisms of microbial pathogenesis. They function in adaptive responses to external stimuli through signaling pathways and are key to maintaining cellular homeostasis. This regulation is especially pertinent in the context of challenging microbial resistance pathways that are often driven by horizontal gene transfer (HGT). Within the framework of the Small Multidrug Resistance (SMR) transporter family, my research uses these simple proteins to explore key questions surrounding the significance and dynamic behavior of this once overlooked metabolite, guanidinium (Gdm^+).

I have explored the reasons behind the widespread dissemination of SMR transporters through HGT (**Chapter 2**). While the transported substrates initially offered no clues, we discovered that xenobiotic guanidinylated substrates, such as guanylurea, were very robustly transported. Intriguingly, not all metformin metabolites, despite having guanidinylated side chains, showed the same transport efficiency. This points to the remarkable specificity and selectivity of SMR_{Gdx} homologues. Within environments rich in anthropogenic pollutants, we found evidence supporting our hypothesis that bacterial consortia contribute to metformin degradation (**Chapter 2**). Yet, the question persists regarding the fitness advantage of carrying a Gdx gene for species not exposed to such conditions. To address this, I explored the physiological impacts of Gdm^+ by comparing strains with and without the Gdx exporter

(**Chapter 3**). Our findings suggest that the absence of Gdx leads to reduced fitness in the presence of Gdm^+, corroborating the idea that Gdx serves to alleviate Gdm^+ toxicity. Further, we investigated the cellular processes potentially disrupted by this under-studied metabolite. The accumulation specifically affected biofilm formation and bacterial motility, whereas general growth and resistance assays were not similarly impacted. This differential sensitivity may offer foundational insight into the mechanistic interactions between Gdm^+ and cellular processes, shedding light on a potential toxicity mechanism requiring Gdm^+ removal. Simultaneously, my findings exposed a potential microbial vulnerability that could be capitalized on as an alternative strategy for combating antimicrobial resistance.

Finally, one of the pressing questions in the field concerns the biosynthesis of Gdm^+: specifically, how and why cells produce the metabolite. Considering the intricate regulatory mechanisms in place – namely, riboswitches that control the expression of SMR_{Gdx} transporters for Gdm^+ removal – it begs the question, why would the cell expend energy to synthesize a metabolite only to subsequently export it. The prevailing assumption is that Gdm^+ is a byproduct of some nitrogen metabolism pathway, and its export is necessitated by its toxicity. However, neither the precise biosynthetic nor the nature of its "toxicity" has been well defined. In an attempt to shed light on this, **Chapter 3** includes competition assays aimed at indirectly determining under which conditions Gdm^+ is produced by assessing the fitness of the knockout strain relative to the wildtype. While our insights are still preliminary, we observed a potential link between Gdm^+ and the cell's nitrogen availability pathways. This was evidenced by an inverse fitness relationship when glutamate and glutamine served as the sole nitrogen source. These observations offer an initial direction for more targeted investigations into the various pathways potentially implicated in Gdm^+ biosynthesis and toxicity.

4.2 Exploring bacterial evolutionary and co-opt native physiologies

Continuing with the SMR_{Gdx} proteins as a model system allows us to scrutinize the ongoing evolutionary shifts possibly related to adaptation to metformin pollution. One intriguing avenue for future research is revisiting the study of ligand for riboswitches that regulate SMRs. Given the structural and transport similarities between Gdm^+ and guanylurea, it remains to be tested if it can also sense guanylurea or metformin. Adopting a similar experimental strategy as previously developed (Nelson et al., 2017), we can use a riboswitch fluorescent reporter construct to monitor ligand-induced gene expression changes in quantifiable β-galactosidase activity from the fused *lacZ* gene. This provides insights into the evolutionary flexibility of these regulatory elements in adapting to the everchanging environmental conditions.

There is a sequence divergence between the wastewater plasmid associated Gdx-pAmi and the genomic Gdx-Clo (**Figure 4.1).** Structurally characterizing Gdx-pAmi in complex with guanylurea and Gdm^+ could give insight to the observed variations in transport kinetics when comparing to Gdx-Clo. Moreover, it could offer a nuanced understanding of how genes evolve following genomic to plasmid transfer to adapt to specific environmental changes. To explore the differing residues, such as the suspected phenylalanine at position 43 in Gdx-Clo (F43) and its glycine counterpart in Gdx-pAmi, which could be key in coordinating the urea group of guanylurea. Another potential position to explore would be methionine at position 39 (M39) in Gdx-Clo, part of the hydrophobic portal previously seen to accommodate long hydrophobic tails (Kermani et al., 2020). Considering the environmental burden of metformin and guanylurea pollutants in wastewater, these findings could lay the groundwork for synthetic biology efforts aimed at engineering more efficient, or specific degradation pathways to mitigate these problematic pollutants.

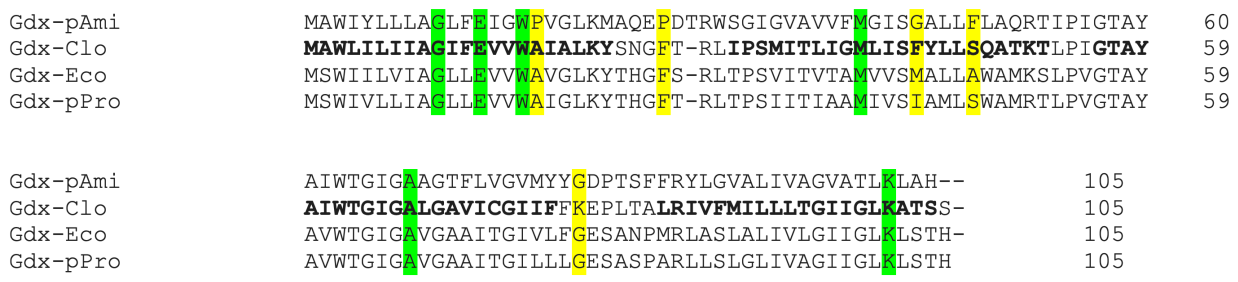

Figure 4.1 Sequence alignment of SMR_{Gdx} representatives in Chapter 2. Highlighted in green are conserved residues while in yellow are residues of divergence.

Another avenue for future study is to substantiate the putative symbiotic relationship between microbial species in wastewater that metabolize metformin. By utilizing rational mutagenesis or targeted genome knockouts, we could empirically assess whether these species are interdependent for optimal metformin degradation and the inter-species dependency on guanylurea export for effective pollutant removal. Additionally, we can explore whether mutations in SMR_{Gdx} transport could enhance the efficacy of guanylurea export, a crucial parameter for future synthetic bioengineering efforts targeting metformin pollution. Expanding on this, mutations could also be introduced in the metabolic pathways of the counter species involved in the bacterial consortia. Based on an outlined metformin degradation pathway (Martinez-Vaz et al., 2022) (**Figure 4.2**), we could specifically target the enzyme responsible for converting biguanide to guanylurea (once it is known). A knockout that enzyme would allow tracking of the flow of guanylurea between cells, thus confirming its export from Gdx. Essential controls must be established to rule out the presence of residual guanylurea in the cells, and if necessary, heavy isotope labeling could be employed to precisely map the compound's route within the microbial consortia. Alternatively, a complementary indirect approach could involve media supplemented with metformin, wherein a Gdx knockout strain would be unable to export the metabolite. The ensuing differences in microbial fitness could be assessed using competition

assays similar to those discussed in **Chapter 3**, with each strain being genomically labeled with a fluorophore. Should guanylurea export prove to be a critical factor, we would anticipate a decline in fitness in the species reliant on guanylurea.

On a separate note, the impact of metformin on human microbiome has recently come under scientific scrutiny. It is crucial to explore the effects of drug usage both in wastewater systems and within patients who are prescribed these medications. The gut microbiome, in particular, may be modulated by metformin, offering a potential avenue for drug repurposing if such changes prove beneficial to the host. Notably, research has indicated that metformin may inhibit biofilm formation in certain bacterial species, such as *Pseudomonas aeruginosa*, potentially through the induction of elevated oxidative stress (Abbas et al., 2017; Shafik et al., 2023). The decline in biofilm formation, with the use of metformin, may serve as an alternative antimicrobial strategy of invasive biofilm forming microbes. The inhibition may be attributed to metformin's interference with cellular metabolism or specific signaling pathways essential for biofilm development.

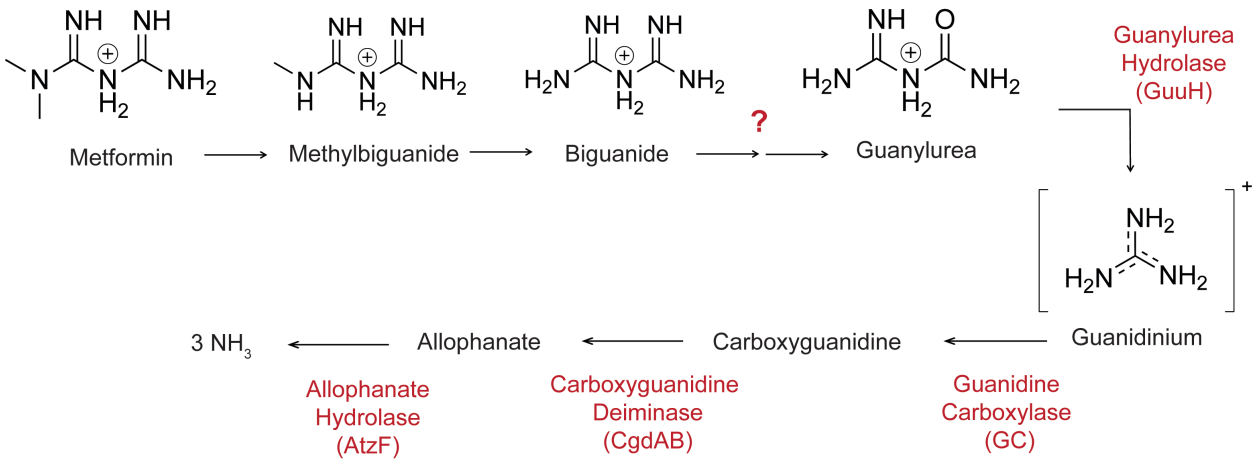

Figure 4.2 Proposed metformin degradation pathway from *Pseudomonas mendocina* GU.

4.3 Investigating how Gdm^+ leaves virulence mechanisms vulnerable

We observed accelerated swimming in the absence of adding exogenous Gdm^+ and heightened sensitivity of biofilms to Gdm^+. Both of these phenomena appear to be regulated by c-di-GMP. To determine whether Gdm^+ directly interferes with this signaling pathway or exerts its effects indirectly, further investigations into c-di-GMP levels, membrane potential, and flagella protein expression are needed. Studying c-di-GMP can be challenging due to its ubiquity within the cell. Various methods exist for examining its levels and activity. For an indirect assessment, Congo red dye that binds to biofilm compositions, can be used quantitatively to measure biofilm formation, which in turn reflects levels of c-di-GMP. For a more direct readout, a group used the Spinach technology (Strack et al., 2013) in which a riboswitch with a fluorescence aptamer region that when binds to a ligand, causes a conformational change in which then the fluorescent dye 5-difluoro-4-hydroxybenzylidene imidazolinone (DFHBI) can bind and be quantitively monitored (Kellenberger et al., 2013; Manna et al., 2021; Okuda et al., 2017; Porter et al., 2017). The construct has been tested *in vivo* cell samples to monitoring the fluorescence (λ_{ex} = 482 nm and λ_{em} = 505 nm). Using a c-di-GMP sensing riboswitch, the fluorescent high throughput readout allows to determine c-di-GMP levels over time. Lastly, another alternative for direct measurement of c-di-GMP, labeled Gdm^+ can be used to track interactions with c-di-GMP related pathways such as diguanylate cyclases (Dgc). Inhibition of Dgc activity has been shown to prevent biofilm formation by curtailing c-di-GMP (Cho et al., 2020).

Microfluidic devices offer a platform for observing fluorescently labeled swimming patterns under varying conditions. This allows a closer examination of features such as flagellar function. If Gdm^+ accumulation leads to an indirect effect on flagellar synthesis pathways,

changes in Flic protein expression can be examined. High-resolution microscopy can also assess whether there is an increase in the amount of flagella or modifications in their rotational patterns that could explain the observed enhancement in swimming speed. Knockouts targeting flagellar genes may provide additional insights into the mechanism.

Another line of inquiry involves examining whether serine, when employed as a sole nitrogen source, disrupts c-di-GMP synthesis or signaling. The riboswitch fluorescent measurement or mass spectrometry could be utilized for this purpose. It is worth noting that serine plays a role in purine synthesis, which encompasses structural elements that include guanindinyl groups (Fan et al., 2019). Moreover, serine is a key component in the pyruvate production pathway, which subsequently feeds into the tricarboxylic acid (TCA) cycle (Kohlmeier, 2003). Through the cycle, molecules such as nicotinamide adenine dinucleotide (NADH) and guanosine triphosphate (GTP) are produced potentially influencing membrane potential (Fink et al., 2022). To determine possible connects between Gdm^+ and serine within metabolic pathway that could result in changes of membrane potential, we could continue employing existing membrane potential kits. This line of investigation could elucidate why faster swimming has been observed in knockout cells. Additionally, we could examine the membrane potential affects when adding 3 mM exogenous Gdm^+ to swimming conditions and determine if there are any similarities in the membrane potential read-out between the wildtype with 3 mM Gdm^+ and the knockout providing more evidence membrane potential is affected with Gdm^+ accumulation. If the accumulation of Gdm^+ becomes overwhelming, this could be an indirect effect of membrane potential, especially since Gdm^+ is positively charged. It might not be just one thing that is influencing the phenotypic changes we have seen. It could be a combination of

cascade events. Determining the linkage between all these factors will help determine the influence on these virulence mechanisms.

4.4 Determining the origin of Gdm^+

To confirm that the conditions with fitness disparities are truly because of Gdm^+ production, a guanidine fluorescent biosensor can be used to report endogenous guanidium. As previously mentioned, a group engineered a fluorophore aptamer region called Spinach. Another group developed a *ykkC* guanidine specific riboswitch to detect Gdm^+. The fluorescent marker allows for *in vitro* and *in vivo* analysis by monitoring the fluorescence (λ_{ex} = 448 nm and λ_{em} = 506 nm) on a plate reader or through flow cytometry (Manna et al., 2021; Porter et al., 2017). This could provide a high throughput screen of conditions to determine Gdm^+ production at various time points.

Overall, a cell-wide a dual screen of active genes (transcriptomics) and endogenous metabolites (metabolomics) in specific conditions need to be conducted to understand the metabolic state of the cell in defined media settings. We can screen for specific metabolites for samples to get a snapshot of the state of the metabolic physiology. Time points will be important in this study as it can provide information about the changes of metabolism over time. Transcriptomics can narrow on specific RNA transcripts to give insight of the cell's regulatory system to adapt to the environment. This is providing more specific information about the pathways involved. Together, metabolomics and transcriptomics, progressively unravel the layers of complexity of the origin of Gdm^+ and a more comprehensive understanding of bacterial metabolism. Following the screen, we can label carbon and nitrogen with heavy isotopes to monitor how the substrate is up taken and degraded by mass spectrometry analysis (Gevaert et

al., 2008). This will allow us to identify the metabolic pathway the labeled metabolite is involved in and how quickly it is processed.

Lastly, to investigate the hypothesis that Gdm^+ is a connected to the cell's monitoring of nitrogen budget, the hypothesis can be investigated through the *E.coli* ammonia transporter (AmtB). This transporter sits in the membrane and is part of the regulation of ammonium (NH_4^+). When extracellular ammonium concentrations are less than 5 μM, AmtB imports ammonium in the cell to be directed directly into the GS pathway. When the external ammonium increases by 10-fold or more, a protein called GlnK binds and blocks entry of ammonium from AmtB (Javelle et al., 2004). Looking closer at the protein-protein binding interaction, GlnK possesses a loop region with an arginine side chain residue, or a guanidinyl group, that is nestled in the pore of AmtB (Gruswitz et al., 2007). The buried Gdm^+ side chain hydrogen bonds with surrounding residues from AmtB, potentially being a binding spot for Gdm^+ ions to bind. A competition binding assay between ammonium and Gdm^+ can be conducted to see if one would outcompete the other. Additionally, binding assays with Gdm^+ alone to determine if Gdm^+ is a plausible ligand or influences the binding partnership of AmtB and GlnK. This could provide insight as to how Gdm^+ and the balance of nitrogen availability is communicated within the cell.

My dissertation lays the groundwork for future research aimed at understanding Gdm^+, a previously overlooked microbial metabolite. Ultimately, elucidating the exact mechanism in which answers all the ongoing questions (why the genes frequent occurrence in transferrable elements, the metabolite effects on virulence pathways, and how is it made) will improve our comprehension of bacterial adaption, evolution, and basic antimicrobial physiology. This in turn, has potential to transform medical and environmental strategies.

4.5 References

Abbas, H. A., Elsherbini, A. M., & Shaldam, M. A. (2017). Repurposing metformin as a quorum sensing inhibitor in Pseudomonas aeruginosa. *Afr Health Sci*, *17*(3), 808-819. https://doi.org/10.4314/ahs.v17i3.24

Cho, K. H., Tryon, R. G., & Kim, J.-H. (2020). Screening for Diguanylate Cyclase (DGC) Inhibitors Mitigating Bacterial Biofilm Formation [Review]. *Frontiers in Chemistry*, *8*. https://doi.org/10.3389/fchem.2020.00264

Fan, T. W. M., Bruntz, R. C., Yang, Y., Song, H., Chernyavskaya, Y., Deng, P., Zhang, Y., Shah, P. P., Beverly, L. J., Qi, Z., Mahan, A. L., Higashi, R. M., Dang, C. V., & Lane, A. N. (2019). De novo synthesis of serine and glycine fuels purine nucleotide biosynthesis in human lung cancer tissues. *J Biol Chem*, *294*(36), 13464-13477. https://doi.org/10.1074/jbc.RA119.008743

Fink, B. D., Rauckhorst, A. J., Taylor, E. B., Yu, L., & Sivitz, W. I. (2022). Membrane potential-dependent regulation of mitochondrial complex II by oxaloacetate in interscapular brown adipose tissue. *FASEB Bioadv*, *4*(3), 197-210. https://doi.org/10.1096/fba.2021-00137

Gevaert, K., Impens, F., Ghesquière, B., Van Damme, P., Lambrechts, A., & Vandekerckhove, J. (2008). Stable isotopic labeling in proteomics. *Proteomics*, *8*(23-24), 4873-4885. https://doi.org/10.1002/pmic.200800421

Gruswitz, F., O'Connell, J., 3rd, & Stroud, R. M. (2007). Inhibitory complex of the transmembrane ammonia channel, AmtB, and the cytosolic regulatory protein, GlnK, at 1.96 A. *Proc Natl Acad Sci U S A*, *104*(1), 42-47. https://doi.org/10.1073/pnas.0609796104

Javelle, A., Severi, E., Thornton, J., & Merrick, M. (2004). Ammonium sensing in Escherichia coli. Role of the ammonium transporter AmtB and AmtB-GlnK complex formation. *J Biol Chem*, *279*(10), 8530-8538. https://doi.org/10.1074/jbc.M312399200

Kellenberger, C. A., Wilson, S. C., Sales-Lee, J., & Hammond, M. C. (2013). RNA-Based Fluorescent Biosensors for Live Cell Imaging of Second Messengers Cyclic di-GMP and Cyclic AMP-GMP. *Journal of the American Chemical Society*, *135*(13), 4906-4909. https://doi.org/10.1021/ja311960g

Kermani, A. A., Macdonald, C. B., Burata, O. E., Ben Koff, B., Koide, A., Denbaum, E., Koide, S., & Stockbridge, R. B. (2020). The structural basis of promiscuity in small multidrug resistance transporters. *Nat Commun*, *11*(1), 6064. https://doi.org/10.1038/s41467-020-19820-8

Kohlmeier, M. (2003). Serine. In M. Kohlmeier (Ed.), *Nutrient Metabolism* (pp. 300-308). Academic Press. https://doi.org/https://doi.org/10.1016/B978-012417762-8.50049-1

Manna, S., Truong, J., & Hammond, M. C. (2021). Guanidine Biosensors Enable Comparison of Cellular Turn-on Kinetics of Riboswitch-Based Biosensor and Reporter. *ACS Synthetic Biology*, *10*(3), 566-578. https://doi.org/10.1021/acssynbio.0c00583

Martinez-Vaz, B. M., Dodge, A. G., Lucero, R. M., Stockbridge, R. B., Robinson, A. A., Tassoulas, L. J., & Wackett, L. P. (2022). Wastewater bacteria remediating the pharmaceutical metformin: Genomes, plasmids and products. *Front Bioeng Biotechnol*, *10*, 1086261. https://doi.org/10.3389/fbioe.2022.1086261

Nelson, J. W., Atilho, R. M., Sherlock, M. E., Stockbridge, R. B., & Breaker, R. R. (2017). Metabolism of Free Guanidine in Bacteria Is Regulated by a Widespread Riboswitch Class. *Mol Cell*, *65*(2), 220-230. https://doi.org/10.1016/j.molcel.2016.11.019

Okuda, M., Fourmy, D., & Yoshizawa, S. (2017). Use of Baby Spinach and Broccoli for imaging of structured cellular RNAs. *Nucleic Acids Res*, *45*(3), 1404-1415. https://doi.org/10.1093/nar/gkw794

Porter, E. B., Polaski, J. T., Morck, M. M., & Batey, R. T. (2017). Recurrent RNA motifs as scaffolds for genetically encodable small-molecule biosensors. *Nature Chemical Biology*, *13*(3), 295-301. https://doi.org/10.1038/nchembio.2278

Shafik, S. M., Abbas, H. A., Yousef, N., & Saleh, M. M. (2023). Crippling of Klebsiella pneumoniae virulence by metformin, N-acetylcysteine and secnidazole. *BMC Microbiology*, *23*(1), 229. https://doi.org/10.1186/s12866-023-02969-9

Strack, R. L., Disney, M. D., & Jaffrey, S. R. (2013). A superfolding Spinach2 reveals the dynamic nature of trinucleotide repeat-containing RNA. *Nat Methods*, *10*(12), 1219-1224. https://doi.org/10.1038/nmeth.2701

Appendix

Appendix A: Molecular Mechanism of Potassium (K^+) Ion Sensing Histidine Kinase Involved in Biofilm Formation

The following appendix chapter is adapted from a dissertation proposal prepared for fulfillment of candidacy requirements for the Program of Chemical Biology (PCB) at the University of Michigan.

Eighty percent of human infections are caused from persistent biofilm communities that have become resistant to antibiotics (Römling & Balsalobre, 2012). Pathogenesis as simple as dental plaque buildup to medical device transplant complications is in need of novel antimicrobial endeavors to combat persistent bacterial infections caused by biofilm formation (Donlan, 2001; Lemon et al., 2008; López et al., 2009; Römling & Balsalobre, 2012). Biofilms contain bacterial cells that secrete polysaccharides and functional amyloid fibrils to the extracellular matrix, tightly locking each cell together creating an extremely robust structure (Branda et al., 2005; Lemon et al., 2008; McLoon et al., 2011; Van Gerven et al., 2018). These unique components allow biofilms to adhere to surfaces allowing for colonization of a host. As the biofilm expands, it can protect individual cells from harsh environments. The components that assist in complex biofilm development also allows the biofilm to be resistant to antibiotics, host defenses, protease digestion and chemical denaturants (Cegelski et al., 2009; Evans et al., 2015; Lemon et al., 2008). Many of these infections have resulted in the overuse of antibiotic drugs, leading to antibiotic resistance, which has made it difficult to alleviate common bacterial

infections (Cegelski et al., 2009; Römling & Balsalobre, 2012). Understanding the mechanisms of biofilm formation can assist in development of novel antimicrobial strategies.

Non-pathogenic, biofilm-forming *Bacillus subtilis* is a widely used bacterial model for studying biofilm mechanisms (Lemon et al., 2008). Bacteria can sense external stimuli and enact genetic changes in response using two-component regulatory systems. This system is widely found in prokaryotes and rarely in eukaryotes and has two main components: a sensor histidine kinase and a response regulator (Buschiazzo & Trajtenberg, 2019; Gushchin et al., 2017; Hamon & Lazazzera, 2001; Liu et al., 2015; Prindle et al., 2015) (**Figure A1**). A signal is sensed by the membrane-anchored histidine kinase, which is then propagated through a phosphorelay transfer to a response regulator, Spo0A, a highly conserved protein in bacteria (Fujita et al., 2005; Hamon & Lazazzera, 2001; McLoon et al., 2011). Phosphorylated Spo0A then initiates various cellular responses to regulate biofilm-forming genes (**Figure A1**) (Fujita et al., 2005; González-Pastor, 2011; Hamon & Lazazzera, 2001; Kearns et al., 2005; McLoon et al., 2011). Through knockout studies, it was discovered that Histidine Kinase C (KinC) was required for Spo0A to be phosphorylated and ultimately for biofilms to form, regardless if the other kinases were expressed or not (LeDeaux et al., 1995). However, the exact activation mechanism of KinC remains unknown. There has been multiple debates on how KinC is activated: 1) the direct sensing of potassium ion through binding, 2) sensing a change in membrane potential, or 3) both (Humphries et al., 2017; Liu et al., 2017; Liu et al., 2015; López et al., 2009).

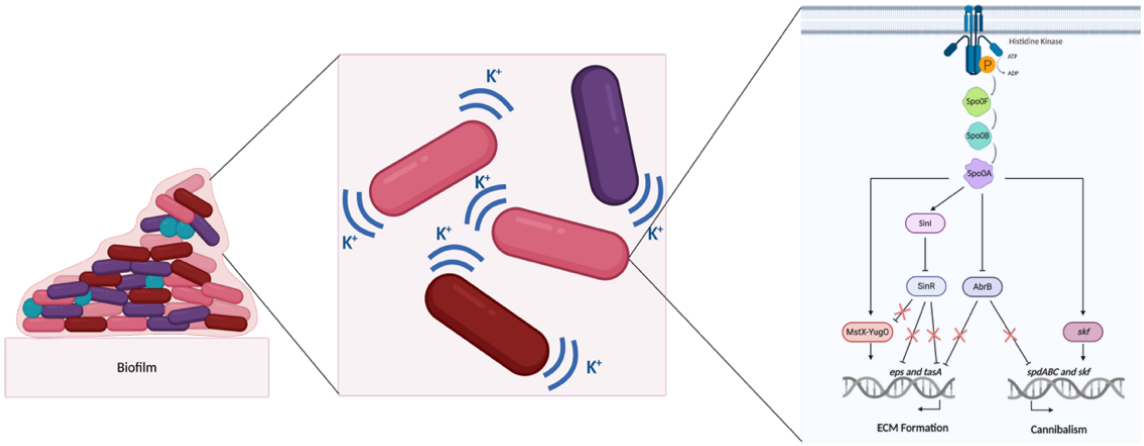

Appendix Figure A 1 Schematic of biofilm communication from the macro (left) to the molecular level (right). An accumulating biofilm (left) will oscillate an electrochemical signal between cells (middle) to initiate the two-component regulatory system (right) for a cellular response to occur to adapt to the changing environment. Image made from BioRender.

It has been suggested that potassium ions may be the signal for KinC activity and are therefore crucial for bacterial biofilm formation (Liu et al., 2017). Lopez *et al*. suggested from their mutational studies of KinC domains, that the K^+ ions interacted with the PAS domain, which is the putative sensing region of KinC. They also observed biofilm formation through pellicle assays with the addition of various natural products (López et al., 2009). Five out of the six compounds that are known to either create pores in the membrane, or insert themselves in the membrane, caused efflux or "leakage" of potassium ions from the interior of the cell that led to biofilm formation (López et al., 2009). These natural products are produced by the bacteria themselves or within the soil where *B. subtilis* is naturally found. On the other hand, Devi *et al*. performed similar pellicle experiments without "leaking" agents and showed that there was no difference in biofilms formation in regards to the presence or absence of K^+. Although the activation mechanism of KinC is unclear, a consensus was reached that a linkage between potassium ions and KinC exists to regulate the expression of biofilm-forming genes (Devi et al., 2015; Humphries et al., 2017; Liu et al., 2017; López et al., 2009; Prindle et al., 2015). The importance of K^+ in biofilm formation has been increasingly recognized. Humphries *et al*. and

Prindle *et al*. used microfluidics and fluorescence microscopy to observe the electrical communication between cells which is facilitated by K^+ ions. They concluded that concentration of potassium ions outside the cells is modulated by ion channels (Prindle et al., 2015), resulting in a change of membrane potential (Stratford et al., 2019). Deletion of a potassium ion channel gene, *yugO*, impairs overall biofilm development in *B. subtilis* (Libby & Dworkin, 2017; Liu et al., 2017; Lundberg et al., 2013). This raises the question of whether KinC is activated by a flow of K^+ ions from a series of ion channel opening and closing events that perturbs membrane potential (Devi et al., 2015; Liu et al., 2015; Prindle et al., 2015).

The uncertainty of KinC's activation mechanism stresses the importance of understanding the overall physiology of histidine kinases in bacteria. Although *in vivo* biofilm screens have established the importance of KinC, the molecular mechanism of KinC activation has not been determined. This proposal will provide the first *in vitro* characterization of KinC's activation, which will allow us to manipulate the environment of KinC and directly determine its relationship with potassium ions. Through this, we can directly characterize KinC's activity which can be quantitatively measured using a radio-labeled substrate. In addition, previous histidine kinase structures only were obtained on truncated versions. The objective of this study is to elucidate the activation mechanism of a bacterial Histidine Kinase from *Bacillus subtilis*, KinC, which initiates a signal transduction cascade leading to biofilm formation.

Wildtype KinC has been successfully recombinantly overexpressed using recombinant, C-terminally His_6-tagged, KinC in OverExpress C43 (DE3), derived BL21 (DE3) chemically competent bacterial cells. and purified along with the first mutant construct targeting the autophosphorylation site to disrupt phosphorylation activity (**Appendix Figure A2** and **A3**). Initial functional assays demonstrate that radiolabeled ATP can be used to study KinC's

phosphorylation activity. To determine the mechanism of activation for KinC, the protein was purified and reconstituted into liposomes allowing for manipulation of external and internal ion concentrations. There are three different possibilities I will test to determine the mechanism of activation of KinC: whether KinC detects 1) potassium ion through direct binding, 2) changes in osmolarity, or 3) changes in membrane potential established by potassium ion gradients. All three of the possibilities can be tested using radioactivity assays with KinC proteoliposomes. Additionally, structural homology-based mutations will be made to identify the autophosphorylation site in KinC and their respective activities will be compared to the wildtype.

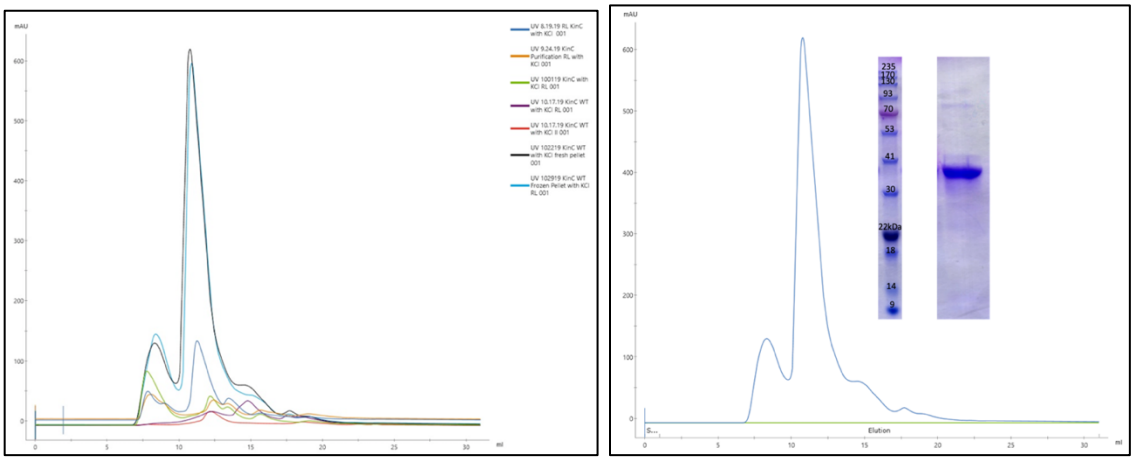

Appendix Figure A 2 SEC FPLC overlay trace of KinC purification optimizations (left) and trace with an SDS-PAGE gel sample of the purified KinC (WT) (right). UV trace of elution of KinC around 11.5mL (1.5mL at [2.4 mg/mL]) confirmed by a sample ran on a gel. A 5 µg sample was ran on a 12% SDS-PAGE gel showing a band in between 41 and 30 kDa molecular weight markers. KinC is 51 kDa with the His_6-Tag but runs at a slightly lower molecular weight due to its membrane properties.

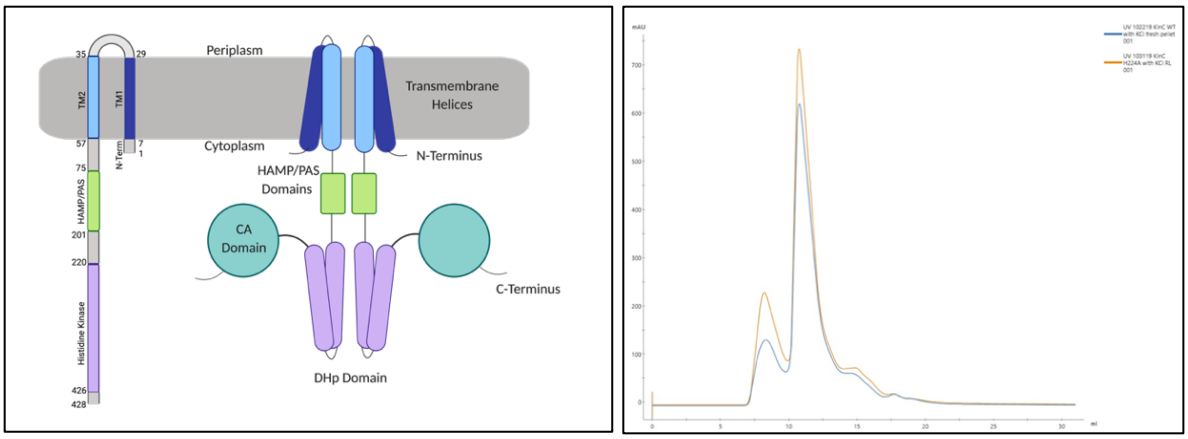

Appendix Figure A 3 Homology prediction model of KinC to design H224A inactive mutant. Using various bioinformatic tools, the predicted orientation and domains are shown (left). Image made from BioRender. SEC FPLC overlay trace (right) of KinC WT and H224A.

Radiolabeled isotopes are very sensitive and specific, but they are expensive and must be handled with care. A safer alternative that could provide the same information would be preferred. Specific antibodies for phosphorylated histidines (p-His) at the N3 position are commercially available that would bind to the KinC p-His species. After initial attempts in using this antibody (**Appendix Figure A4**), both wild type and H224A samples detected KinC p-His species, regardless of ATP was present or not. The appearance of KinC (H224A) phosphorylation is not observed in radioactivity assays, suggesting that the antibody is either non-specifically binding, or binding to endogenous kinases with phosphohistidine that could be a contamination during expression or purification. The antibody for targeting p-His species would have been a good alternative method, but it seems that radioactive ATP is the best method for detection of KinC phosphorylation. Spo0F, the next phosphate acceptor in the phosphorelay system, will be investigated through observing its dephosphorylation effects on KinC through ATPgamma^{32}P. Spo0F has already been successfully purified (**Appendix Figure A5**). This validation will provide another piece in contributing to foundational knowledge of KinC's mechanism.

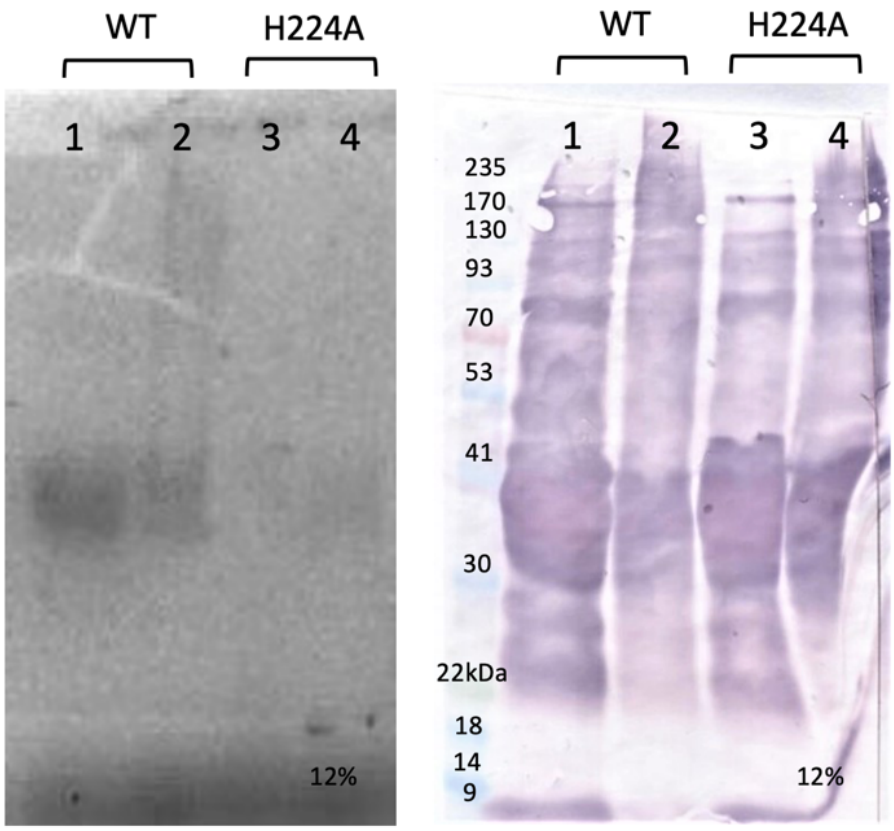

Appendix Figure A 4 Phosphorylation assay using ATPgamma^{32}P with KinC (WT) and H224A liposomes (left) and a Western Blot using an Anti-His antibody (right).

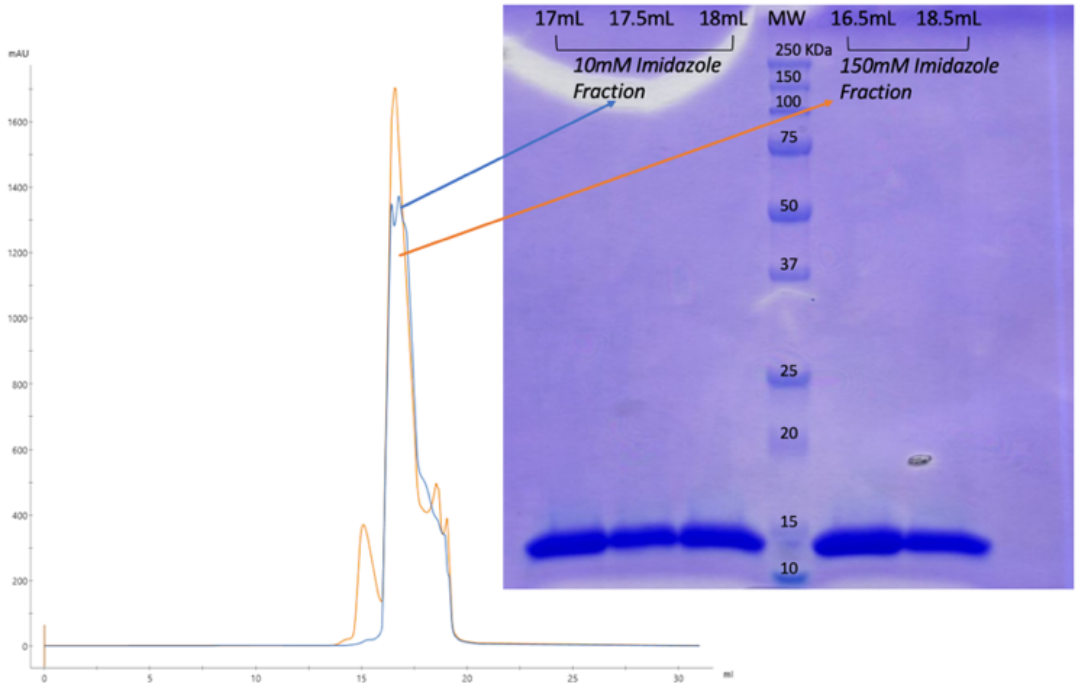

Appendix Figure A 5 SEC FPLC traces and SDS-PAGE of the purified Spo0F. Both overlay traces are two different elution fractions (10 mM and 150 mM Imidazole) from an affinity purification. Both contained Spo0F (16.2 kDa) that eluted at 17 mL from the SEC column at approximately at the 16 kDa molecular weight marker.

A resting cell contains high concentration of potassium ions (150-200 mM) (Ramos et al., 1976), where KinC is thought to be activated when a "leakage" of K^+ ions occurs, establishing that the sensor domain may be sensitive to low internal potassium concentration. We can determine the absolute concentration of K^+ ions detected by the sensor domain of KinC by titrating K^+ ions and observing the respective effects of KinC phosphorylation activity. Each liposome with KinC will be titrated with K^+ ions of concentrations higher and lower than the normal cellular resting potassium concentration from a range of 500 mM to 1 mM. This will allow us to determine whether a relationship exists between the K^+ ions and KinC by providing a concentration of K^+ at which the sensor domain initiates autophosphorylation activity.

KinC may not be responsive to potassium ions directly, but rather to an indirect event that is caused by K^+ ions such as changes in osmolarity or membrane potentials. Determining if osmolarity is contributing to the activation of KinC, a titration of various ions concentrations will be used to establish osmotic changes within the proteoliposome. Naturally abundant ions, such as sodium, or non-ionic osmolytes like sucrose, can be used in comparison to potassium to elucidate the factor for activation. If KinC responses to osmolarity changes, in terms of K^+ ions, we would expect there to be higher phosphorylation activity in hypertonic conditions due to a reduction in solute concentration inside the cell. During hypotonic conditions, we would expect KinC to have lower activity since water is flooding inside the liposome resulting from the high concentration of K^+ ion that would mimic a cell at rest. Nutrient depleted cells tend to have higher osmolarity (high concentration of solutes) therefore would be in a hypotonic state which exhibit lower phosphorylation activity to ensure the cell does not begin to transcribe genes for biofilm-forming genes.

Lastly, to determine if KinC is sensing a change in membrane potential, a series of ion gradients can be generated in the proteoliposomes and screened with radioactive phosphorylation assays. The KinC sensor domain may be sensitive to changing potentials caused by either influx or efflux of ions. In proteoliposomes, a cyclic peptide ionophore, valinomycin, which allows for K^+ transport, can be added to set the membrane potential according to the Nernst potential equation (Berezin, 2015). By setting the internal ion concentration during the reconstitution step, we can then buffer exchange the liposome with conditions of varying external ion concentrations to yield different membrane potentials to observe its effect upon phosphorylation activity with ATPgamma^{32}P. The ion gradients could also be established using other ions such as sodium, which can be transported by the sodium ionophore gramicidin, to eliminate the possibility of KinC responding directly to K^+ ions. These specific membrane potentials represent potentials that are much higher or lower from the bacterial resting potential to determine a change that may be occurring during bacterial cell communication.

Before beginning the assays, it will be crucial to select the orientation of the protein inserted into the liposome that results in functional KinC that can be detected by phosphorylation assays. A protease can be used to cleave off any tagged exposed liposomes. Samples at various time points during the cleavage will be collected and visualized on an SDS-PAGE gel (Tsai et al., 2012) (**Appendix Figure A5**). Both orientation fractions will be tested for KinC functionality to determine if this orientation assay will be necessary in controlling liposomes in functional assays.

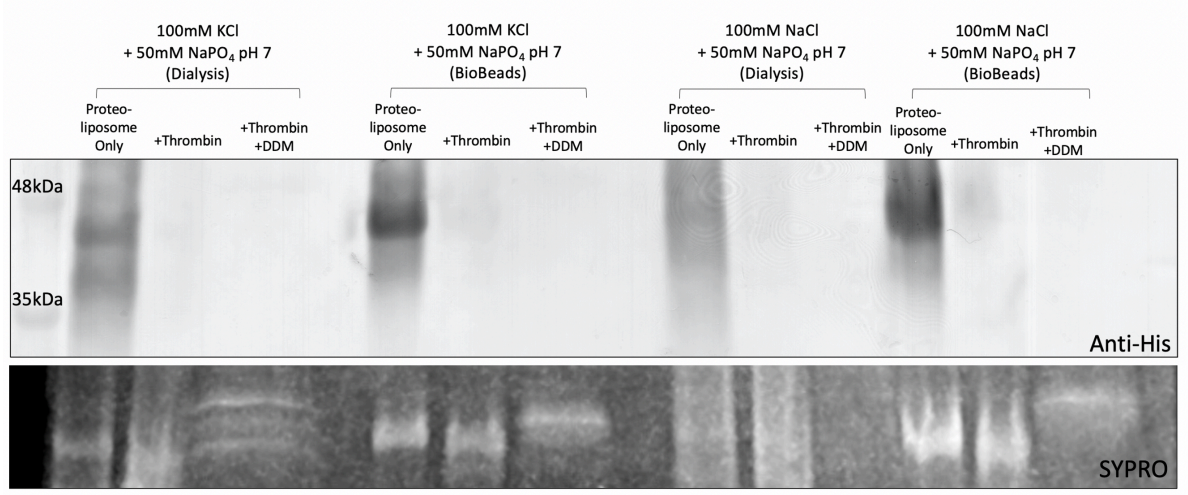

Appendix Figure A 6 KinC Proteolipsome Orientation assay. Using 1ug protein of His_6-tagged protein the cleavage of the tag was monitored. The tag was cleaved by indication of the lack of protein detected in the western blot but appearing still in SYPRO ruby stain.

The oligomerization state of KinC will be investigated using Size Exclusion Chromatography (SEC)-Ultra violet (UV)- Light scattering (LS)-Retractive index (RI) detection and crosslinking agents. We will determine the kinetic parameters of phosphorylation activity by the wild type and mutants. Lastly, we will determine a structure of KinC or mechanistically relevant mutants, which will aid in determining and confirming key structural domains and motifs present in the enzyme. These experiments will provide foundational knowledge and guidance in how biofilm formation can be disrupted by identifying sites that are essential for kinase function. To determine the role of the conserved domains in KinC, truncations or mutations of these domains will be done and the effects on KinC activity will be measured. The TM domains will be truncated (KinC 58-428) followed by the putative sensing region, PAS domain (KinC 201-428) (Taylor & Zhulin, 1999). The function of these truncated forms will be evaluated through K^+ ion titration and ATPgamma^{32}P activity assay. We would expect the KinC 201- 428 truncation to have increased phosphorylation activity indicative of unregulated phosphorylation activity due to the missing sensor domain. Another residue to mutate is the

N335, which is an important residue for ATP binding in the catalytic ATP-binding (CA) domain in other structurally similar histidine kinases. The residue will be mutated to an aspartate (N335D) to hinder ATP from binding to the pocket in the CA domain. ATP binding is essential for autophosphorylation activity and investigating the binding pocket will provide important mechanistic information. Histidine kinase family members contain the conserved HXXXT motif that energetically enables conformational changes to reach the transition state during autophosphorylation (Ji et al., 2020). The threonine residue in this conserved motif is an asparagine in KinC therefore a mutation at this position may yield an interesting effect upon the overall function of KinC.

There are currently no solved structures of KinC in the PDB database. There are structures of a few sensor histidine kinases (CheA from *T.maritima* and PhoQ and EnvZ from *E.coli*) (Marina et al., 2001; Marina et al., 2005; Tanaka et al., 1998) but their structural models only contain the cytoplasmic regions due to the difficulty in crystalizing transmembrane proteins. Through x-ray crystallography, KinC's structure will be solved with molecular replacement by using already solved structures of histidine kinase family members like CheA from *Thermotoga maritima* as a model ((Marina et al., 2005). If there are difficulties in obtaining crystals, we can alternatively attempt to obtain a structure through cryogenic electron microscopy (Cryo-EM). Monomeric KinC including the His_6-tag is 51 kDa, but its dimeric form is 102 kDa which is considered a small protein for Cryo-EM and may be difficult to obtain a structure. Adding a fragment antigen binding (Fab) antibody to the protein will increase the molecular weight which may alleviate the size limitations for Cryo-EM (Wu et al., 2012) and can also help with increasing diffraction and lattice formation in crystallography. We can obtain these Fab molecules through immunogenic synthesis in mouse models, but we can also recombinantly

express and purify the variable region (region that recognizes the Fab epitope) of the Fab protein in bacteria. A structure of KinC or mechanistically relevant mutants will provide a closer look at residues essential for kinase function. This will ultimately provide a platform for us to inhibit the enzymatic activity of KinC, which may help us to potentially combat bacterial biofilm communication networks.

The activation of KinC in *B. substilis* has not been defined but is known to initiate the start of the phosphorelay within the two-component regulatory system (**Appendix Figure A7**) that is important for biofilm formation. Our investigation of the activation mechanism of KinC will provide a clearer understanding of the required components involved in the signal transduction system. A defined mechanism will provide a platform for understanding how biofilms form. Pathogenic homologs could be investigated next as it is crucial in tackling major bacterial infections in humans. The uropathogenic *E. coli* (UPEC) UTI89 strain, known for causing persistent urinary tract infections (UTIs), are resistant to antibiotic treatment or in some cases the antibiotic treatment is effective, but patients relapse from the persisting biofilm (Blango & Mulvey, 2010; Mysorekar & Hultgren, 2006). Using the information that comes out of this research, a development of alternative antimicrobial strategies in combatting pathogenic biofilms will be possible.

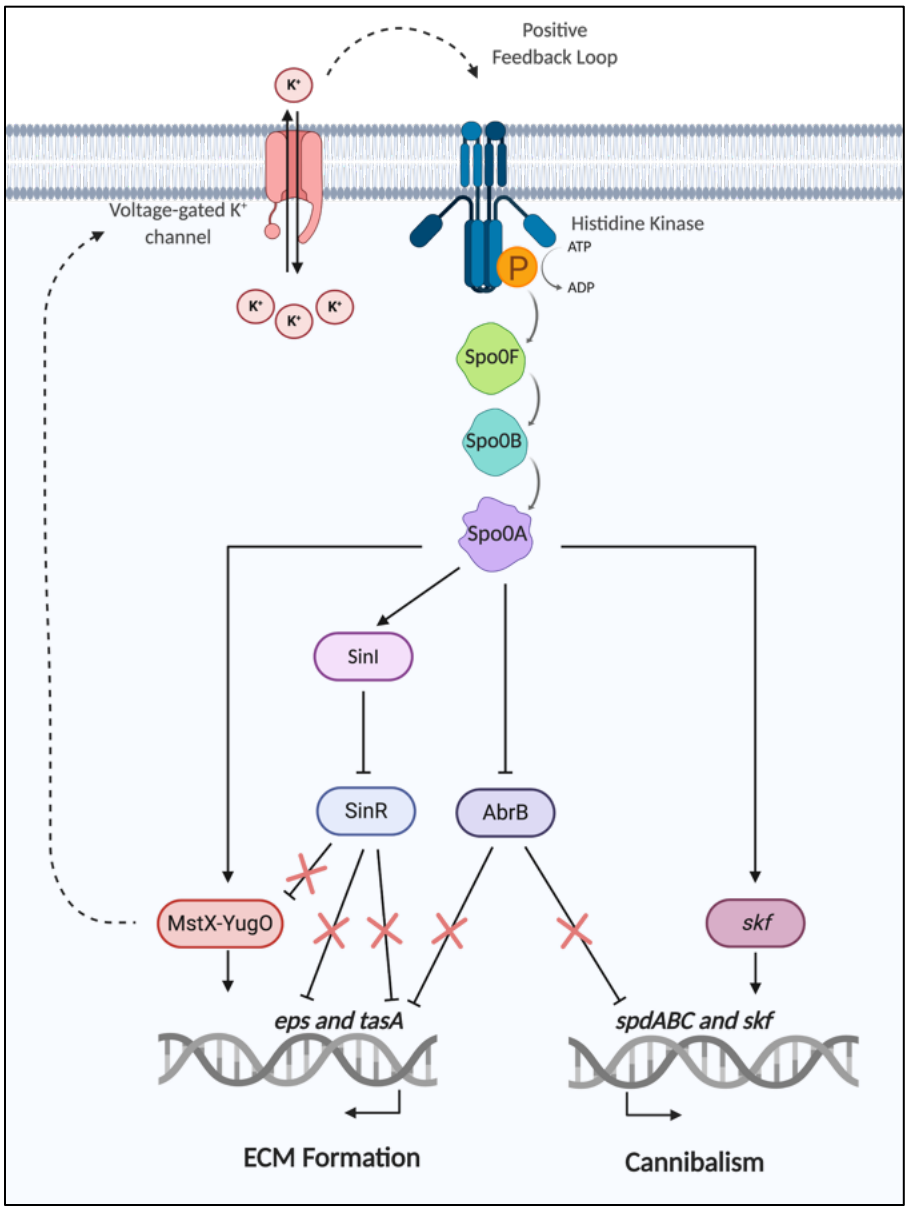

Appendix Figure A 7 Proposed activation mechanism of KinC from *B. subtills*. KinC's activation is hypothesized to be coupled to a potassium channel, YugO. Upon KinC becoming active, there is a positive feedback loop allowing for promotion of more K^+ channel and more efflux of ions. Image made from BioRender.

References

Berezin, S. K. (2015). Valinomycin as a Classical Anionophore: Mechanism and Ion Selectivity. *J Membr Biol*, *248*(4), 713-726. https://doi.org/10.1007/s00232-015-9784-y

Blango, M. G., & Mulvey, M. A. (2010). Persistence of Uropathogenic Escherichia coli in the Face of Multiple Antibiotics. *Antimicrobial Agents and Chemotherapy*, *54*(5), 1855-1863. https://doi.org/doi:10.1128/aac.00014-10

Branda, S. S., Vik, S., Friedman, L., & Kolter, R. (2005). Biofilms: the matrix revisited. *Trends Microbiol*, *13*(1), 20-26. https://doi.org/10.1016/j.tim.2004.11.006

Buschiazzo, A., & Trajtenberg, F. (2019). Two-Component Sensing and Regulation: How Do Histidine Kinases Talk with Response Regulators at the Molecular Level? *Annu Rev Microbiol*, *73*, 507-528. https://doi.org/10.1146/annurev-micro-091018-054627

Cegelski, L., Pinkner, J. S., Hammer, N. D., Cusumano, C. K., Hung, C. S., Chorell, E., Aberg, V., Walker, J. N., Seed, P. C., Almqvist, F., Chapman, M. R., & Hultgren, S. J. (2009). Small-molecule inhibitors target Escherichia coli amyloid biogenesis and biofilm formation. *Nat Chem Biol*, *5*(12), 913-919. https://doi.org/10.1038/nchembio.242

Devi, S. N., Vishnoi, M., Kiehler, B., Haggett, L., & Fujita, M. (2015). In vivo functional characterization of the transmembrane histidine kinase KinC in Bacillus subtilis. *Microbiology (Reading)*, *161*(Pt 5), 1092-1104. https://doi.org/10.1099/mic.0.000054

Donlan, R. M. (2001). Biofilm formation: a clinically relevant microbiological process. *Clin Infect Dis*, *33*(8), 1387-1392. https://doi.org/10.1086/322972

Evans, M. L., Chorell, E., Taylor, J. D., Åden, J., Götheson, A., Li, F., Koch, M., Sefer, L., Matthews, S. J., Wittung-Stafshede, P., Almqvist, F., & Chapman, M. R. (2015). The bacterial curli system possesses a potent and selective inhibitor of amyloid formation. *Mol Cell*, *57*(3), 445-455. https://doi.org/10.1016/j.molcel.2014.12.025

Fujita, M., González-Pastor, J. E., & Losick, R. (2005). High- and low-threshold genes in the Spo0A regulon of Bacillus subtilis. *J Bacteriol*, *187*(4), 1357-1368. https://doi.org/10.1128/jb.187.4.1357-1368.2005

González-Pastor, J. E. (2011). Cannibalism: a social behavior in sporulating Bacillus subtilis. *FEMS Microbiol Rev*, *35*(3), 415-424. https://doi.org/10.1111/j.1574-6976.2010.00253.x

Gushchin, I., Melnikov, I., Polovinkin, V., Ishchenko, A., Yuzhakova, A., Buslaev, P., Bourenkov, G., Grudinin, S., Round, E., Balandin, T., Borshchevskiy, V., Willbold, D., Leonard, G., Büldt, G., Popov, A., & Gordeliy, V. (2017). Mechanism of transmembrane signaling by sensor histidine kinases. *Science*, *356*(6342). https://doi.org/10.1126/science.aah6345

Hamon, M. A., & Lazazzera, B. A. (2001). The sporulation transcription factor Spo0A is required for biofilm development in Bacillus subtilis. *Mol Microbiol*, *42*(5), 1199-1209. https://doi.org/10.1046/j.1365-2958.2001.02709.x

Humphries, J., Xiong, L., Liu, J., Prindle, A., Yuan, F., Arjes, H. A., Tsimring, L., & Süel, G. M. (2017). Species-Independent Attraction to Biofilms through Electrical Signaling. *Cell*, *168*(1-2), 200-209.e212. https://doi.org/10.1016/j.cell.2016.12.014

Ji, S., Luo, L., Li, C., Liu, M., Liu, Y., & Jiang, L. (2020). Rational modulation of the enzymatic intermediates for tuning the phosphatase activity of histidine kinase HK853. *Biochemical*

and Biophysical Research Communications, *523*(3), 733-738. https://doi.org/https://doi.org/10.1016/j.bbrc.2020.01.036

Kearns, D. B., Chu, F., Branda, S. S., Kolter, R., & Losick, R. (2005). A master regulator for biofilm formation by Bacillus subtilis. *Mol Microbiol*, *55*(3), 739-749. https://doi.org/10.1111/j.1365-2958.2004.04440.x

LeDeaux, J. R., Yu, N., & Grossman, A. D. (1995). Different roles for KinA, KinB, and KinC in the initiation of sporulation in Bacillus subtilis. *J Bacteriol*, *177*(3), 861-863. https://doi.org/10.1128/jb.177.3.861-863.1995

Lemon, K. P., Earl, A. M., Vlamakis, H. C., Aguilar, C., & Kolter, R. (2008). Biofilm development with an emphasis on Bacillus subtilis. *Curr Top Microbiol Immunol*, *322*, 1-16. https://doi.org/10.1007/978-3-540-75418-3_1

Libby, E. A., & Dworkin, J. (2017). Habits of Highly Effective Biofilms: Ion Signaling. *Mol Cell*, *66*(6), 733-734. https://doi.org/10.1016/j.molcel.2017.05.036

Liu, J., Martinez-Corral, R., Prindle, A., Lee, D. D., Larkin, J., Gabalda-Sagarra, M., Garcia-Ojalvo, J., & Süel, G. M. (2017). Coupling between distant biofilms and emergence of nutrient time-sharing. *Science*, *356*(6338), 638-642. https://doi.org/10.1126/science.aah4204

Liu, J., Prindle, A., Humphries, J., Gabalda-Sagarra, M., Asally, M., Lee, D. Y., Ly, S., Garcia-Ojalvo, J., & Süel, G. M. (2015). Metabolic co-dependence gives rise to collective oscillations within biofilms. *Nature*, *523*(7562), 550-554. https://doi.org/10.1038/nature14660

López, D., Fischbach, M. A., Chu, F., Losick, R., & Kolter, R. (2009). Structurally diverse natural products that cause potassium leakage trigger multicellularity in Bacillus subtilis. *Proc Natl Acad Sci U S A*, *106*(1), 280-285. https://doi.org/10.1073/pnas.0810940106

Lundberg, M. E., Becker, E. C., & Choe, S. (2013). MstX and a putative potassium channel facilitate biofilm formation in Bacillus subtilis. *PLoS One*, *8*(5), e60993. https://doi.org/10.1371/journal.pone.0060993

Marina, A., Mott, C., Auyzenberg, A., Hendrickson, W. A., & Waldburger, C. D. (2001). Structural and mutational analysis of the PhoQ histidine kinase catalytic domain. Insight into the reaction mechanism. *J Biol Chem*, *276*(44), 41182-41190. https://doi.org/10.1074/jbc.M106080200

Marina, A., Waldburger, C. D., & Hendrickson, W. A. (2005). Structure of the entire cytoplasmic portion of a sensor histidine-kinase protein. *The EMBO Journal*, *24*(24), 4247-4259. https://doi.org/https://doi.org/10.1038/sj.emboj.7600886

McLoon, A. L., Kolodkin-Gal, I., Rubinstein, S. M., Kolter, R., & Losick, R. (2011). Spatial regulation of histidine kinases governing biofilm formation in Bacillus subtilis. *J Bacteriol*, *193*(3), 679-685. https://doi.org/10.1128/jb.01186-10

Mysorekar, I. U., & Hultgren, S. J. (2006). Mechanisms of uropathogenic Escherichia coli persistence and eradication from the urinary tract. *Proceedings of the National Academy of Sciences*, *103*(38), 14170-14175. https://doi.org/doi:10.1073/pnas.0602136103

Prindle, A., Liu, J., Asally, M., Ly, S., Garcia-Ojalvo, J., & Süel, G. M. (2015). Ion channels enable electrical communication in bacterial communities. *Nature*, *527*(7576), 59-63. https://doi.org/10.1038/nature15709

Ramos, S., Schuldiner, S., & Kaback, H. R. (1976). The electrochemical gradient of protons and its relationship to active transport in Escherichia coli membrane vesicles. *Proc Natl Acad Sci U S A*, *73*(6), 1892-1896. https://doi.org/10.1073/pnas.73.6.1892

Römling, U., & Balsalobre, C. (2012). Biofilm infections, their resilience to therapy and innovative treatment strategies. *J Intern Med*, *272*(6), 541-561. https://doi.org/10.1111/joim.12004

Stratford, J. P., Edwards, C. L. A., Ghanshyam, M. J., Malyshev, D., Delise, M. A., Hayashi, Y., & Asally, M. (2019). Electrically induced bacterial membrane-potential dynamics correspond to cellular proliferation capacity. *Proceedings of the National Academy of Sciences*, *116*(19), 9552-9557. https://doi.org/doi:10.1073/pnas.1901788116

Tanaka, T., Saha, S. K., Tomomori, C., Ishima, R., Liu, D., Tong, K. I., Park, H., Dutta, R., Qin, L., Swindells, M. B., Yamazaki, T., Ono, A. M., Kainosho, M., Inouye, M., & Ikura, M. (1998). NMR structure of the histidine kinase domain of the E. coli osmosensor EnvZ. *Nature*, *396*(6706), 88-92. https://doi.org/10.1038/23968

Taylor, B. L., & Zhulin, I. B. (1999). PAS domains: internal sensors of oxygen, redox potential, and light. *Microbiol Mol Biol Rev*, *63*(2), 479-506. https://doi.org/10.1128/mmbr.63.2.479-506.1999

Tsai, M.-F., Fang, Y., & Miller, C. (2012). Sided Functions of an Arginine–Agmatine Antiporter Oriented in Liposomes. *Biochemistry*, *51*(8), 1577-1585. https://doi.org/10.1021/bi201897t

Van Gerven, N., Van der Verren, S. E., Reiter, D. M., & Remaut, H. (2018). The Role of Functional Amyloids in Bacterial Virulence. *J Mol Biol*, *430*(20), 3657-3684. https://doi.org/10.1016/j.jmb.2018.07.010

Wu, S., Avila-Sakar, A., Kim, J., Booth, D. S., Greenberg, C. H., Rossi, A., Liao, M., Li, X., Alian, A., Griner, S. L., Juge, N., Yu, Y., Mergel, C. M., Chaparro-Riggers, J., Strop, P., Tampé, R., Edwards, R. H., Stroud, R. M., Craik, C. S., & Cheng, Y. (2012). Fabs enable single particle cryoEM studies of small proteins. *Structure*, *20*(4), 582-592. https://doi.org/10.1016/j.str.2012.02.017